Exploring a Formulation of Lattice Quantum Gravity

Author:
D.N. Coumbe

Supervisor:
Dr. Jack Laiho

Presented as a thesis for the degree of Ph.D. to the Department of Physics and Astronomy, Glasgow University

May 2013

Abstract

We report on a nonperturbative formulation of quantum gravity defined via Euclidean dynamical triangulations (EDT) with a non-trivial measure term in the path integral. We search the parameter space of EDT for a second-order critical point, whose divergent correlation length would at least in principle allow one to define a continuum limit, whereas the vanishing correlation length of a first-order critical point makes it unsuitable for this purpose. We also search the parameter space of EDT for a physical phase with 4-dimensional semiclassical geometry.

We find that the parameter space contains three phases which we call the branched polymer phase, the collapsed phase, and the crinkled phase. We determine the order of the phase transition dividing the branched polymer phase from the collapsed phase to be first-order. The transition dividing the collapsed phase from the crinkled phase appears to be an analytic cross-over, or a third or higher-order transition. The effective dimension of each phase in the parameter space is studied. We report that EDT with a nontrivial measure term does not appear to contain a phase with 4-dimensional semiclassical geometry.

We argue that within a physical 4-dimensional semiclassical phase, such as that found in causal dynamical triangulations (CDT), a dynamical dimensional reduction from 4 on macroscopic scales to 3/2 on microscopic scales may resolve the tension between asymptotic safety and the holographic principle.

Acknowledgements

First and foremost, I wish to thank my PhD advisor Jack Laiho for a very productive collaboration on a very interesting subject. His work ethic, enthusiasm, and attitude have been most inspiring.

I would like to extend my gratitude to all the staff and students in the particle physics theory group at the University of Glasgow. I wish to thank Christine Davies for acting as my interim advisor after Jack left for Syracuse, her encouragement and advice during the writing up period was much appreciated. Thanks to Chris White, David Miller, Jack Laiho, Jonna Koponen, Rachel Dowdall, Tania Robens, and all the other PhD students for humorous Wednesday lunchtimes at Ichiban. Thanks also to Andrew Davies for his time and effort in working through Peskin and Schroeder with me during the first year.

I am very grateful to have travelled to many conferences during my PhD studies. Thank you to everybody in the MILC collaboration, and in particular Carlton DeTar, for a wonderful stay at the University of Utah. Thanks to the organisers and participants of Lattice '11, hosted in the beautiful Squaw Valley, California. I appreciated the opportunity to present my work and to listen to some genuinely thought provoking presentations. Thanks also to the organisers of the 13th Marcell Grossman meeting in Stockholm, Sweden. This conference allowed me to meet some very interesting and influential people in the field of quantum gravity. To Renate Loll, and the other organisers of *CDT and Friends*, I extend my appreciation for organising and inviting me to a wonderful conference in the Netherlands. Each and every talk was relevant to my work.

And to the students of room 538, thanks for making the long hours more enjoyable. The *points game* and the *would you rather game* created memories that will stay with me until the day I die. Particular highlights include Brian eating bread from a dirty puddle, Kate wearing a tea-towel on her head all day, and António publicly admitting to having Rabies. Thanks also to Gordon for making me laugh at his flippant attitude, especially when it comes to giving presentations at the University of Durham!

The three and a half years I have spent in Glasgow will stay with me for the rest of my life. Thank you to Isabel Gonçalves, António Morais, Gordon Donald, Kate Elliott, Brian Colquhoun, Danilo Ferreira de Lima, Philipp von Weitershausen, Tracey Bowen, Nayomi Tuominen, Ben Galloway, Liam Moore, Stacey Melville, Bipasha Chakraborty, Mary Buchanan, Chris Wormald, Nick Crowe, Ben Cabot, and Adam Coumbe for punctuating the years of hard work with unforgettable moments of fun.

The numerical simulations presented in this thesis were performed on Scotgrid and on the DiRAC facility jointly funded by STFC and BIS, to whom I am grateful. A limited number of simulations were also performed on the network machines in the particle physics theory group at Glasgow University, I greatly appreciate the fact that almost everyone in the group allowed me to run simulations on their already struggling machines.

I would also like to thank the wider scientific community, especially those that have worked on related approaches to quantum gravity. The foundations they have laid through unrelenting hard work have made this thesis possible. I hope that, at least in some small way, the work presented in this thesis will contribute to the effort of formulating a successful theory of quantum gravity.

And finally to my family, a system that is greater than the sum of its parts, I dedicate this thesis to you.

Declaration

I declare that none of the material presented in this thesis has previously been presented for a degree at this or any other university.

Chapter 1 presents a general introduction to the theoretical concepts relevant to my research. Chapter 2 introduces the approach of dynamical triangulations, a particular version of which is used in this thesis, in the general context of simplicial quantum gravity. Chapter 3 details the numerical implementation of our model. J. Laiho is the author of the Monte Carlo evolution code, but the rest of Chapter 3 is my work. Chapters 4 and 5 are my work. Chapter 6 is based on work done in collaboration with J. Laiho. My work described here has appeared in the following publications and proceedings:

- J. Laiho, D. Coumbe,
  "Evidence for Asymptotic Safety from Lattice Quantum Gravity,"
  Phys.Rev.Lett. **107** (2011) 161301 [arXiv:1104.5505 [hep-lat]]

- Daniel Coumbe, Jack Laiho,
  "Exploring the Phase Diagram of Lattice Quantum,"
  PoS Conf. Proc. LATTICE2011 (2011) **334** [arXiv:1201.2864 [hep-lat]]

- Jack Laiho, Daniel Coumbe,
  "Asymptotic safety and lattice quantum gravity,"
  PoS Conf. Proc. LATTICE2011 (2011) **005**

Contents

List of Figures

List of Tables

1 Introduction

1.1 Overview

Our current understanding of the Universe is based on two theories; quantum mechanics and general relativity. Quantum mechanics describes three of the four fundamental interactions of nature, with general relativity describing the fourth, gravity. At short distances quantum mechanical effects typically dominate, whereas general relativistic effects dominate over large distances and for strong gravitational fields. The vast majority of physical phenomena can be described independently by either general relativity or quantum mechanics, without the need for both. However, when strong gravitational fields interact over short distances, such as in the vicinity of the big-bang singularity or near black holes, the description of such phenomena demand a unification of quantum mechanics and general relativity. Such a unification would be a theory of quantum gravity.

Newtonian gravity attempted to explain the gravitational force via the inverse square law of gravitation, claiming that gravity was a universal property that acted instantaneously and on all massive bodies. This was an important mathematical step, but it did not fully explain the mechanism behind gravity. After publishing his special theory of relativity in 1905, Einstein wanted to generalise his theory such that all motion is relative. Einstein's realisation of the equivalence of inertial and gravitational mass is called the equivalence principle, and ultimately led to our current understanding of gravity known as the general theory of relativity. General relativity was not only able to reproduce the results of Newtonian gravity in appropriate limits but it also gave an intuitive explanation for the mechanism behind gravitation.

In general relativity [9] spacetime is represented by a four-dimensional manifold M on which there exists a metric $g_{\mu\nu}$ [10]. The metric $g_{\mu\nu}$ is a set of numbers describing the distance to neighbouring points on the manifold. The field equations of general relativity constrain the possible values that the curvature of spacetime can take. Introducing no additional geometrical structure into spacetime apart from the metric itself and requiring that the field equations contain no derivatives higher than second-order [10], one is uniquely led to the equations,

$$G_{\mu\nu} = 8\pi G_N T_{\mu\nu}. \tag{1}$$

Where $T_{\mu\nu}$ is the stress-energy-momentum tensor describing the amount and distribution of energy in spacetime, and $G_{\mu\nu}$ is the Einstein tensor describing how spacetime is

curved by the presence of matter, and is a function of the metric $g_{\mu\nu}$,

$$G_{\mu\nu} = R_{\mu\nu} - \frac{1}{2} g_{\mu\nu} R. \tag{2}$$

$R_{\mu\nu}$ is the Ricci tensor acting on the metric $g_{\mu\nu}$, and R is the Ricci scalar.[1] The Ricci scalar quantifies the curvature at each point on a Riemannian manifold, and represents the difference in the volume of a ball embedded in curved spacetime with that in flat Euclidean spacetime. Mathematically, the Ricci scalar is defined by the product of the metric with the Ricci tensor,

$$R = R_{\mu\nu} g^{\mu\nu}. \tag{3}$$

In order to obtain exact solutions of the Einstein equations one must impose certain symmetry constraints. For example, imposing spherical symmetry on a non-rotating massive body leads to the Schwarzschild solution. In this way the number of coupled partial non-linear differential equations one obtains when writing Eq. (2) in full are reduced, and exact analytical solutions can be found.

The explanation of the gravitational force as a result of matter following the path of shortest distance in curved spacetimes is an elegant theoretical explanation that has been experimentally verified to high precision. The perihelion of Mercury's orbit, gravitational lensing, and high-precision measurements of the decay of the orbital period of binary pulsars all agree well with general relativistic predictions [11].

Just as general relativity must replace Newtonian gravity in the large mass limit, quantum mechanics must also replace Newtonian mechanics in the small distance limit. For example, until the development of quantum mechanics physicists did not even have a satisfactory explanation for the stability of the atom. In classical mechanics atoms are composed of electrons orbiting along well defined paths about a central nucleus. Classical electromagnetism says that a charged particle with acceleration a and charge e will radiate energy with power P given by Larmor's equation,

$$P = \frac{e^2 a^2}{6\pi\varepsilon_0 c^3}. \tag{4}$$

According to classical physics an electron, therefore, must radiate away all its energy and spiral in towards the nucleus. However, this is not observed in nature.

Max Planck's earlier radical solution to the so-called ultraviolet catastrophe of black-body radiation – in which he posited that electromagnetic energy is not a continuous

[1] Eq. (2) is for pure gravity (vanishing cosmological constant), however for a non-zero cosmological constant one would obtain $G_{\mu\nu} = R_{\mu\nu} - \frac{1}{2} g_{\mu\nu} R + \Lambda g_{\mu\nu}$.

variable, but can only take discrete values, or quanta – also helped to resolve the problem of the apparent instability of the atom. Niels Bohr realised that if an electron's energy was also quantised then the atom could not collapse, because electrons must have a non-zero minimum energy.

Our understanding of the atom was further developed by de Broglie who proposed that particles also have a wave-like nature. In this picture only integer wavelengths will be admitted by the electron's orbit, thereby explaining the particular values of the allowed energy levels of the electron within the atom. Heisenberg and Schrödinger developed these concepts further to give a complete description of a particle's quantum state at any instant of time in terms of the wavefunction Ψ. The evolution of the non-relativistic wavefunction is governed by the Schrödinger equation,

$$i\hbar\frac{\partial}{\partial t}\Psi\left(\mathbf{r},t\right)=\left[-\frac{\hbar^{2}}{2m}\bigtriangledown^{2}+V\left(\mathbf{r},t\right)\right]\Psi\left(\mathbf{r},t\right), \tag{5}$$

where $|\Psi\left(\mathbf{r},t\right)|^{2}$ is interpreted as the probability density of finding the particle of mass m at a given location $\mathbf{r}$ at a time t. A wave-like description automatically introduces an uncertainty relation, for example between the position x and the momentum p_x, known as Heisenberg's uncertainty principle,

$$\triangle x\,\triangle\,p_{x}\geq\frac{\hbar}{2}. \tag{6}$$

A reformulation of quantum mechanics based on a path integral approach was developed by Wiener, Dirac and Feynman [12, 13, 14]. In this interpretation the probability amplitude A for a particle initially located at x_i at time t_i, to be found at some later time t_f at position x_f is calculated by taking a weighted sum over all possible ways in which this can happen,

$$A\left(x_{i},t_{i}\rightarrow x_{f},t_{f}\right)=\int_{path}e^{\frac{i}{\hbar}S_{path}}=\langle x_{f}|e^{-\frac{iS_{path}}{\hbar}}|x_{i}\rangle. \tag{7}$$

The path integral approach to quantum mechanics has a number of advantages over the traditional Hamiltonian approach. Firstly, the path integral approach is intrinsically symmetric with regard to space and time and so provides a manifestly covariant version of quantum mechanics, therefore admitting the possibility of coordinate change in a straightforward manner [14]. Secondly, the path integral approach can be used to study nonperturbative quantum amplitudes using stochastic importance sampling which is important in the development of many physical theories (e.g. Ref. [15]), including the theory that forms the main subject of this thesis.

Quantum mechanics has been subjected to high precision measurements for several decades, and no significant discrepancy between theory and experiment has ever been found. For example, the anomalous magnetic moment of the electron a given in terms of the $g-$factor is experimentally determined to be, [16]

$$a = \frac{g-2}{2} = 0.00115965218073(28), \tag{8}$$

which is in agreement with the value calculated using QED [17] to 10 significant figures.

General relativity and quantum mechanics, in their respective domains of applicability, are extremely accurate theories. However, even at a quick glance there exist points of tension that resist a straightforward unification of the two theories. Firstly, the energy-time uncertainty relation coupled with mass-energy equivalence implies that the smaller the region of spacetime under consideration the greater the allowed mass of particle-antiparticle pairs in the quantum vacuum. Hence, a prediction of general relativity in combination with the uncertainty principle is that as one probes spacetime on ever decreasing distance scales the geometry becomes increasingly turbulent; eventually creating infinite energy fluctuations as the distance scale is taken to zero. Secondly, the notion of time has fundamentally different meanings in general relativity and ordinary quantum mechanics. In ordinary quantum mechanics time is an absolute quantity, the passage of which is completely independent of the state of the physical system. In general relativity, however, time is a purely relational concept whose passage is dependent on the particular configuration of the system.

Nature does not appear to encounter any such problems; after all atoms do fall down in a gravitational field. Physicists tend to think, therefore, that the seeming incompatibility of general relativity and quantum mechanics necessitates the alteration of one or both theories, rather than that nature does not conform to a singular description.

Attempts at unifying general relativity and quantum mechanics have a long history (see Ref. [18] for an excellent overview). As early as 1916, Einstein recognised that his theory of general relativity must be modified to accommodate quantum effects [19] after realising that general relativity predicts that an electron in an atom will radiate away all of its energy in the form of gravitational waves, and eventually collapse on to the nucleus. In 1927, Oscar Klein realised a theory of quantum gravity must lead to a modification of space and time [20]. Technical publications on quantum gravity began appearing in the 1930's, most notably by Fierz and Pauli [21, 22], and by Blokhinstev and Gal'perin [23], whose work first recognised the spin-2 quantum of the gravitational field. In 1938, Heisenberg had the insight that the dimensionality of the gravitational

coupling constant is likely to cause problems with a quantum theory of gravity [24].

The 1950's and 60's saw the application of tools recently developed in quantum field theory to the problem of quantum gravity, mainly because of the success in applying these techniques to the quantisation of the other fundamental interactions. Charles Misner introduced the concepts developed in Feynman's path integral approach to quantum mechanics to develop a weighted sum over geometries [25], which was further developed by Feynman [14]. The Wheeler-DeWitt equation, first published in 1967 [26], describes the wavefunction of the Universe by expressing the quantum mechanical Hamiltonian constraint using variables that are dependent on the metric. By the end of the 60's a complete set of Feynman rules for general relativity were known, thus paving the way for 't Hooft and Veltman to apply perturbative quantisation techniques to the gravitational field, eventually showing that the theory is perturbatively nonrenormalizable.

Although gravity was conclusively shown to be perturbatively nonrenormalizable by power counting in the early 70's, several advances were still made by using an approximation to the full theory of quantum gravity, known as semiclassical gravity. Semiclassical gravity is the quantum mechanical treatment of matter content on curved, but still classical, background geometries. In semiclassical gravity the stress-energy-momentum tensor takes on a quantum mechanical expectation value $\langle T_{\mu\nu} \rangle$ giving field equations for semiclassical general relativity,

$$8\pi G_N \langle T_{\mu\nu} \rangle = R_{\mu\nu} - \frac{1}{2} g_{\mu\nu} R. \tag{9}$$

Hawking used semiclassical gravity to study the effect of particle-antiparticle pair production near a black hole horizon. Because particles can be viewed as positive energy solutions to Dirac's equation, and antiparticles as negative energy solutions, Hawking was able to calculate the effect of antiparticles quantum mechanically tunnelling inwards through the horizon, or conversely particles tunnelling outwards through the horizon and escaping to infinity [27]. The result is that a black hole of mass M emits a thermal shower of particles with Hawking temperature T_H, given by

$$T_H = \frac{\hbar c^3}{8\pi k_B M G_N}. \tag{10}$$

This equation implies that the entropy of a black hole S_{BH} is proportional to its surface area and not its volume,

$$S_{BH} = \frac{A}{4 l_P^2}. \tag{11}$$

This so-called Hawking-Bekenstein entropy formula will prove to be important in later discussions.

A similar phenomena that can be derived using semiclassical gravity is the Unruh effect, first described in its full mathematical form by Bill Unruh in 1976 [28, 29, 30], whereby an observer with non-zero acceleration a in a Minkowski vacuum will measure a non-zero temperature T_U to be

$$T_U = \frac{\hbar a}{2\pi k_B c}. \tag{12}$$

This result, which has not yet been experimentally confirmed, implies that the definition of what constitutes a vacuum is dependent on the state of motion of the observer. Semiclassical results such as Hawking radiation, the black hole entropy formula, and the Unruh effect show the range of new phenomena that arise when combining quantum mechanics with classical general relativity, and may act as a guiding principle in the formulation of a full theory of quantum gravity.

General relativity has been successfully formulated as an effective quantum field theory that is valid up to some low-energy cut-off scale, usually taken to be the Planck scale. For example, the work of Donoghue [31] uses an effective field theory formulation of gravity to calculate quantum corrections to the gravitational potential between two heavy masses, finding that gravity actually forms the best perturbative theory in nature [31]. However, as one increases the energy scale beyond the cut-off in a perturbative expansion new divergences appear that require an infinite number of counterterm coefficients to define the theory [32]. Since an infinite number of counterterm coefficients cannot be measured in a finite number of experiments the theory loses most of its predictive power at high energy scales. When considering small perturbations about flat Minkowski space one observes that the divergences cancel for one-loop diagrams. However, at the two-loop level and higher, such cancellations do not occur and divergences are once again present. The problem is compounded when one includes matter content, with nonrenormalizability occurring at the one-loop level [33].

A more intuitive way of understanding why gravity is perturbatively nonrenormalizable comes from simple dimensional arguments. Gravity is distinguished from the other fundamental interactions of nature by the fact that its coupling constant G_N is dimensionful. In d-dimensional spacetime Newton's gravitational coupling G_N has a mass dimension of $[G_N] = 2 - d$. This means that higher-order loop corrections will generate a divergent number of counterterms of ever increasing dimension. One can clearly see this from the perturbative quantum field theoretic treatment of gravity in d-

dimensional space, where ultraviolet divergencies at loop order L scale with momentum p as

$$\int p^{A-[G_N]L} dp, \tag{13}$$

where A is a process dependent quantity that is independent of L [34]. Equation (13) is clearly divergent for $[G_N] < 0$ because the integral will grow without bound as the loop-order L increases in the perturbative expansion [34]. It is interesting to note that $[G_N] < 0$ is only true when the dimension of spacetime $d > 2$. For $d = 2$ Newton's gravitational coupling in fact becomes dimensionless. Therefore, gravity as a perturbative quantum field theory becomes renormalizable by power counting in 2-dimensions. However, in our 4-dimensional Universe this is clearly not the case.

If one includes higher-order derivative terms in the gravitational action and performs a resummation, such that the higher-order derivative terms are incorporated into the graviton propagator, then gravity is renormalizable by power counting. However, this theory appears to be non-unitary at high energy scales due to the presence of ghost terms containing the wrong sign in the propagator [35]. The ghost poles, however, are of the order of the Planck mass and so the unitarity violations only become significant in the high energy regime where perturbation theory is already known to break down. This further highlights the need for a nonperturbative theory of quantum gravity.

One can still proceed with the standard perturbative approach by finding some mechanism for reducing the infinite number of couplings to a finite set. One attempt is to directly incorporate supersymmetry into general relativity, forming what has become known as supergravity. Supersymmetry postulates the existence of a fundamental symmetry of nature that exists between fermions and bosons, namely that each boson of integer-spin is associated with a fermion whose spin differs by a half-integer [36]. Applying supersymmetry as a local symmetry constraint in combination with the postulates of general relativity leads to the theory of supergravity. In supergravity every bosonic field is associated with a fermionic field with opposite statistics [37], thus the bosonic spin-2 graviton would have a fermionic supersymmetric partner of spin 3/2, the gravitino. It is hoped that supersymmetry can alleviate some of the ultraviolet divergences via the cancellation of divergent quantities in one field with those in the partner field, resulting in milder ultraviolet divergences, or perhaps even their complete elimination [38].

Viewing supergravity as an effective theory of a much larger superstring theory may resolve the issue of nonrenormalizability in quantum gravity all together, at least or-

der by order in perturbation theory [38]. Superstring theory posits that 0-dimensional point-like particles are actually 1-dimensional extended strings whose fundamental degrees of freedom are the vibrational modes of the string. In superstring theory discontinuities in standard Feynman diagrams are smoothed out into two-dimensional sheets, and so the infinite energy limit no longer corresponds to the zero distance limit. Divergences previously associated with the zero distance limit simply do not exist in superstring theory because there is no zero distance. Superstring theory is then perturbatively renormalizable, at least order by order in perturbation theory [38]. Supersymmetric string theory has enjoyed a number of successes, such as the emergence of the spin-2 gravitons as a fundamental mode of string oscillation [39, 40], calculations of the entropy of a special class of black holes that agree with the holographic principle and black hole thermodynamics [41, 42, 43], a calculation of the radiation spectrum emitted from black holes that agrees with Hawking radiation [44], as well as passing several non-trivial self-consistency checks. See Refs. [45, 46] for a comprehensive overview of string theory and its connection to other approaches to quantum gravity.

Another approach to quantum gravity adopts the background independent lessons of general relativity as a fundamental starting point and attempts to construct a quantum theory from it. This approach has resulted in Loop Quantum Gravity, which is background independent and therefore nonperturbative from the outset. The major successes of Loop Quantum Gravity include the agreement with Bekenstein's prediction of black hole entropy up to a constant factor [47], and at least in the low-energy limit the emergence of spin-2 gravitons [48].

An alternative and more conservative candidate for a theory of quantum gravity comes from the asymptotic safety scenario, as first proposed by Weinberg [34]. If the asymptotic safety scenario is correct, gravity is effectively renormalizable when formulated nonperturbatively because the renormalization group flow of couplings end on a non-trivial fixed point in the high energy limit, and therefore remain finite over the entire range of energy scales. Furthermore, the ultraviolet critical surface of the non-trivial fixed point is required to be finite dimensional, and so in principle gravity would be completely determined by a finite number of couplings up to arbitrarily high energies. Under this scenario a perturbative expansion around a fixed background metric corresponds to perturbations about the low energy infrared fixed point, and taking the high energy limit corresponds to following the renormalization group flow towards the ultraviolet fixed point. A lattice formulation of quantum gravity that attempts to make contact with the asymptotic safety scenario forms the central theme

of this thesis.

The remaining sections of chapter 1 will introduce some concepts of lattice regularization, the asymptotic safety scenario and the associated renormalization group methods, thereby providing the necessary theoretical concepts to understand later chapters. This discussion will also naturally motivate the desire for a lattice formulation of quantum gravity.

Chapter 2 focuses on the simplicial approach to quantum gravity as defined via the method of Regge calculus. After detailing the geometric observables that can be computed using simplicial quantum gravity, the scope of the discussion is narrowed to focus on the method of dynamical triangulations. The Euclidean approach to dynamical triangulations (EDT) is introduced before discussing the approach of causal dynamical triangulations (CDT). Possible generalisations beyond 4-dimensional simplicial lattice regularizations are also briefly discussed.

In Chapter 3 I discuss our motivations for resurrecting the original Euclidean theory of dynamical triangulations, detailing how this theory is numerically implemented and tested. Sources of error in lattice calculations, both systematic and statistical, are reviewed.

Details of the phase diagram of EDT are presented in Chapter 4, which are based on numerical calculations I have performed. The order of the phase transition, constraints on the location of the phase transition in parameter space, and geometric properties of the phases of EDT are presented. The various numerical techniques used in studying the geometric properties of each phase, and the location and order of the phase transitions, are given in this section.

In chapter 5 I focus on calculations I have performed within a specific region of the parameter space, known as the crinkled phase. I present a result for the calculation of a quantity known as the volume-volume correlator in order to determine the global Hausdorff dimension of this phase.

Chapter 6 reviews the argument against the asymptotic safety scenario as put forward by Banks and Shomer [49, 50]. I then discuss the behaviour of the short distance spectral dimension in both EDT and CDT, presenting the possibility that a short distance spectral dimension of 3/2 may resolve the tension between asymptotic safety and the holographic principle.

Finally, I present a discussion on what we have learnt about the asymptotic safety scenario from the study of Euclidean dynamical triangulations and outline some future directions for this line of research.

1.2 Lattice regularization

The quantisation of a continuous field theory involves introducing an infinite number of degrees of freedom, which can lead to divergent results. To prevent this, one typically regulates the theory via the introduction of an ultraviolet cut-off. A theory can be regularized by taking a high energy limit, above which the field theory is no longer applicable, or conversely one can impose a minimum length scale. The latter is the approach taken by lattice field theories, which originated from the seminal work of K. Wilson [51]. Lattice field theories replace continuous spacetime with a discrete lattice of points with non-zero spacing a.

The method of lattice regularization allows one to achieve a stable ultraviolet regularization, yielding finite observables. Lattice methods also allow one to recover continuum limit physics by calculating observables at different lattice spacings and extrapolating to the continuum limit, i.e. sending $a \to 0$. In addition to taking $a \to 0$ one must also take the infinite volume limit, so as to eliminate finite-size effects, whilst simultaneously making appropriate adjustments to the bare coupling constants. The existence of a continuum limit requires the presence of a second-order phase transition because the divergent correlation length characteristic of a second-order phase transition allows one to take the lattice spacing to zero whilst simultaneously keeping observable quantities fixed in physical units.

For strongly interacting field theories the applicability of perturbation theory is limited, and nonperturbative lattice methods become essential. Lattice QCD (LQCD), for example, has become the central tool in developing our understanding of the strong interaction, allowing one to calculate the hadronic spectrum and weak matrix elements to high precision [52]. LQCD also contributes to our understanding of confinement, chiral symmetry breaking, and finite temperature QCD. See Refs. [53, 54] for more detailed accounts of the methods and successes of LQCD. Lattice regularization methods have also been applied in Beyond the Standard Model (BSM) physics, most notably in supersymmetric lattice field theories and technicolor theories. See Ref. [55] for an overview of supersymmetric lattice field theory, and Ref. [56] for a more general overview of the application of lattice methods to BSM physics.

Motivated by the successful application of lattice methods to the strong interaction, and their use in studying BSM physics, one is led to ask whether applying similar methods to the gravitational interaction may aid our understanding of nonperturbative quantum gravity. The following section discusses the approach to nonperturbative quantum gravity known as the asymptotic safety scenario.

1.3 Asymptotic Safety

The problems raised by the perturbative nonrenormalizability of gravity have spawned a multitude of competing solutions. A common approach is to assume that the reason quantum mechanics and general relativity cannot be unified in a straightforward manner is because one of the two theories needs to be modified. The most popular notion is to regard quantum mechanics as the more fundamental theory, and that general relativity is just an effective field theory that is only valid up to some high energy cut-off. Typically, this is the route taken by perturbative approaches to quantum gravity such as superstring theory. However, there does exist a possibility of defining a quantum field theory of gravity that is valid over all energy scales despite being perturbatively nonrenormalizable. This is known as the asymptotic safety scenario [34].

When describing phenomena as a function of scale the value of parameters measured on large scales typically differ from those made on small scales. For example, in quantum electrodynamics (QED) the charge of an electron appears to be scale dependent [57, 58]. Since virtual particle pairs permeate the vacuum they become polarised by the presence of the electron's charge. This polarisation tends to screen the strength of the electric charge as measured at large distances. However, at small distances there is less screening, therefore the strength of the electric charge is inversely proportional to distance, or conversely, is proportional to energy. The observation that coupling constants are not in fact constant, but are in general dependent on the energy scale at which they are measured, led to the idea of the renormalization group (RG) [51].

In general relativity the fundamental degrees of freedom are given by the metric field. Fluctuations of space-time would then modify the strength of the gravitational coupling G_N as a function of energy, in an analogous way to the scale dependence of electric charge in QED. We now follow the discussion of asymptotic safety given by Weinberg in [34] in which he considers a generalised set of couplings $g_i(\mu)$ as a function of a renormalization scale μ. If $g_i(\mu)$ has mass dimensions of $[M]^{d_i}$ then we replace $g_i(\mu)$ with a dimensionless coupling $\tilde{g}_i(\mu)$,

$$\tilde{g}_i(\mu) = \mu^{-d_i} g_i(\mu) . \tag{14}$$

The behaviour of the RG flow of the coupling g_i is governed by its β-function, which describes the rate of change of g_i with respect to the scale μ,

$$\beta_i(\tilde{g}(\mu)) = \mu \frac{\mathrm{d}}{\mathrm{d}\mu} \tilde{g}_i(\mu) . \tag{15}$$

To prevent the couplings $\tilde{g}_i(\mu)$ from diverging as $\mu \to \infty$ we can force them to end on a fixed point, g^*, in the limit $\mu \to \infty$. This requires that the beta-function of $\tilde{g}$ vanish at this point,

$$\beta_i(g^*) = 0. \tag{16}$$

Additionally, the couplings must lie on a trajectory $\tilde{g}_i(\mu)$ which actually hits the fixed point. The surface formed from such trajectories is called the ultraviolet critical surface. If the couplings of a particular theory lie on the ultraviolet critical surface of a fixed point then the theory is said to be asymptotically safe.

There exist two types of fixed points, trivial fixed points where $g^* = 0$ and non-trivial fixed points where $g^* \neq 0$. The trivial fixed points are said to be non-interacting because the coupling constant vanishes; the immediate vicinity of this trivial fixed point is described by perturbation theory. This is the construction underlying asymptotic freedom. Conversely, a non-trivial fixed point lies at non-zero values of the coupling constants, and so is said to be an interacting fixed point.

Quantum chromodynamics (QCD) is a special type of asymptotically safe theory because it is also perturbatively renormalizable and asymptotically free. QCD contains a fixed point with only a finite number of attractive renormalization group trajectories in the ultraviolet, namely the Yang-Mills coupling and the quark masses [59]. All other couplings are repelled from the fixed point, and must be set to zero in order to give a well defined ultraviolet limit. QCD is also asymptotically free because colour charge is anti-screened by quark-antiquark pairs, and so at asymptotically high energies quarks become free.

As mentioned in the example of QCD, renormalization group trajectories typically come in two types: trajectories that are attracted to the ultraviolet fixed point, and ones that are repelled from it. As one increases the momentum scale k then the magnitude of an observable under the renormalization group transformation can either increase, decrease, or do neither. Renormalization group trajectories exhibiting such behaviour are said to be relevant, irrelevant or marginal trajectories, respectively. Relevant operators are essential to the description of macroscopic systems, whereas irrelevant ones are not. For a given marginal operator it is unclear whether it contributes to macroscopic physics because it can be ill defined. Macroscopic physics is typically described by only a few observables, whereas microscopic physics is typically characterised by a very large number of variables. This implies that most observables are irrelevant, namely that the microscopic degrees of freedom are not relevant on the macroscopic level.

An important consideration when dealing with a non-trivial ultraviolet fixed point is the dimensionality of its ultraviolet critical surface. The dimensionality of an ultraviolet critical surface is given by the number of renormalization group trajectories that are attracted to the fixed point in the ultraviolet, i.e. the number of relevant trajectories. If an infinite number of such trajectories were attracted to the fixed point then we would be in the same situation as for perturbative renormalization, namely a complete loss of predictive power [34]. The ideal situation is one in which the number of relevant couplings is minimised. For example, if there was just a single trajectory that ended at the fixed point in the ultraviolet then the theory would be maximally predictive.

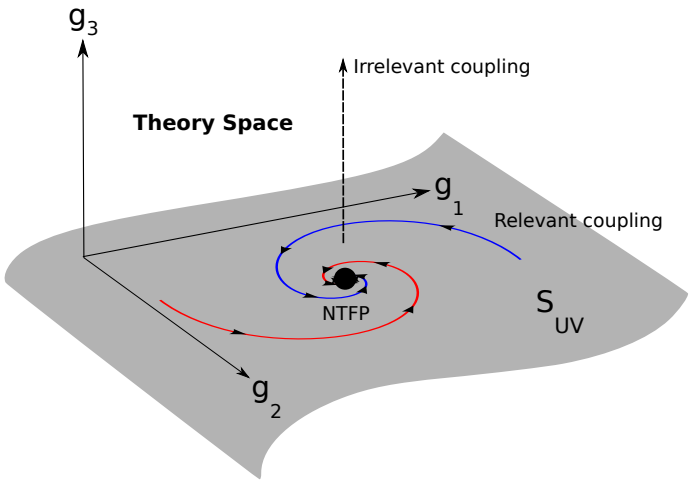

Figure 1: A schematic of the ultraviolet critical surface S_{UV}. Trajectories that are repelled from the non-trivial fixed point (NTFP) are irrelevant couplings. Trajectories that are attracted to the fixed point are relevant couplings. The theory space is defined by the couplings g_i. In the case of the Einstein-Hilbert truncation the couplings are $G_N(k)$ and $\Lambda(k)$. Schematic derived from the work of Refs. [1, 2, 3].

General relativity without matter content is described by the Einstein-Hilbert action

$$S_{EH} = \frac{1}{16\pi G_N} \int d^4x \sqrt{-}g(-2\Lambda + R), \tag{17}$$

where G_N is Newton's gravitational constant, Λ is the cosmological constant, g is the determinant of the metric $g_{\mu\nu}$, and R is the scalar curvature, a function of the metric. If we replace the couplings G_N and Λ by the scale dependent running couplings $G_N(k)$ and $\Lambda(k)$, then recognising that the Einstein-Hilbert action is now a scale dependent functional $\Gamma(k)$ we can write,

$$\Gamma(k) = \frac{1}{16\pi G_N(k)} \int d^4x\sqrt{-}g(-2\Lambda(k) + R + ...). \tag{18}$$

The functional of Eq. (18) in principle contains infinitely many couplings. The renormalization group flow of the functional $\Gamma(k)$ is defined by the exact renormalization group equation (ERGE), and so the ERGE contains the beta-functions of all of the couplings present in the functional. Although exact solutions have been found, e.g. for supersymmetric $O(N)$ theories in the infinite N limit [60, 61], the general form of the ERGE is not exactly solvable, and so one is typically forced to perform truncations of the functional $\Gamma(k)$ such that it contains only a finite number of couplings. The beta-functions can then be extracted from the ERGE without any further approximation [62]. The simplest truncation is the Einstein-Hilbert truncation, in which only the cosmological constant and Newton's constant are retained. The RG flow will typically induce terms quadratic in curvature. However, under the Einstein-Hilbert truncation these contributions are neglected. A more accurate treatment takes the curvature squared terms into account, which is known as the curvature squared truncation. One can then extend this series of truncations up to terms polynomial in the scalar curvature; this has been done up to a polynomial of order eight and higher, demonstrating the existence of a fixed point with a three-dimensional critical surface [63, 64, 65]. Recent RG results have even reported calculations with truncations to a polynomial of order thirty four in the Ricci scalar [66]. See Ref. [67] for an overview of asymptotic safety.

An example of how the ERGE is applied comes from performing a numerical integration of the β-function extracted from the ERGE under the Einstein-Hilbert truncation, i.e for only $G_N(k)$ and $\Lambda(k)$. This gives the following picture [4]:

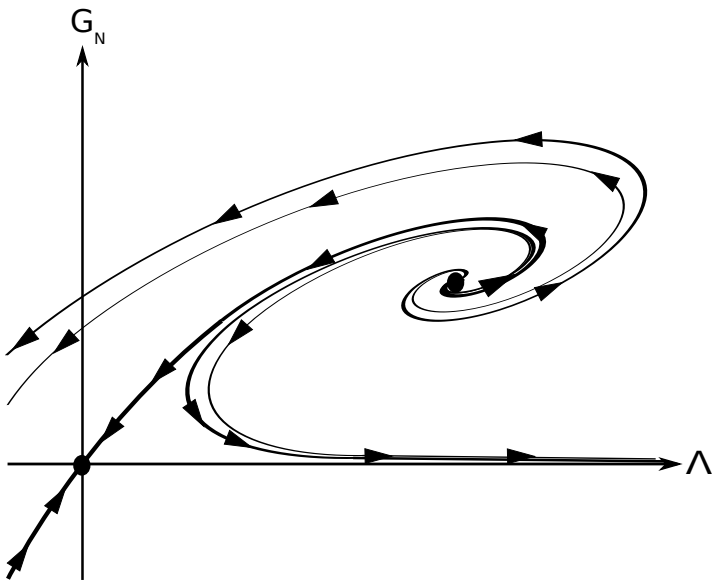

Figure 2: Renormalization group flow of gravity in the Einstein-Hilbert truncation. Arrows indicate RG flow in the direction of increased coarse-graining, or conversely decreasing momentum scale k. Plot adapted from Ref. [4]

At the origin one observes the trivial fixed point (TFP) corresponding to the non-interacting theory. For a non-zero value of Newton's constant and the cosmological constant one may observe a nontrivial fixed point (NTFP) that corresponds to an interacting theory. The fixed point for gravity, if it exists, must be interacting; since gravity is perturbatively nonrenormalizable.

Although the renormalization group studies are suggestive, the truncation of the effective action makes it difficult to systematically assess the reliability of the results obtained using this method[2]. A lattice formulation of gravity is thus desirable and complementary, given the possibility of performing calculations with controlled systematic errors. In a lattice formulation of an asymptotically safe field theory the fixed point would appear as a second order critical point, the approach to which would define a continuum limit [71].

There exists an argument due to Banks [49] (see also Shomer [50]) against the possibility of asymptotic safety. The argument compares the density of states at high energies expected for a theory of gravity to that of a conformal field theory. Since a renormalizable quantum field theory is a perturbation of a conformal field theory by relevant operators, a renormalizable field theory must have the same high energy asymptotic density of states as a conformal field theory. It follows from dimensional

[2] Although systematic error control in ERGE studies is possible and has been exemplified in the work of Refs. [68, 69], for example. Error estimates in quantum gravity in dimensions greater than four have also been studied [70].

analysis, and the extensive scaling of the quantities considered, and the fact that a finite temperature conformal field theory has no dimensionful scales other than the temperature, that the entropy S and energy E scale as

$$S \sim (RT)^{d-1}\,, E \sim R^{d-1}T^d \tag{19}$$

where R is the radius of the spatial volume under consideration and T is the temperature. It follows that the entropy of a renormalizable theory must scale as[3]

$$S \sim E^{\frac{d-1}{d}}. \tag{20}$$

For gravity, however, one expects that the high energy spectrum will be dominated by black holes.[4] The d-dimensional Schwarzschild solution in asymptotically flat spacetime has a black hole with event horizon of radius $r^{d-3} \sim G_N M$, where M is the mass of the black hole. The Bekenstein-Hawking area law tells us that $S \sim r^{d-2}$, so that

$$S \sim E^{\frac{d-2}{d-3}}. \tag{21}$$

This scaling disagrees with that of Eq. (20). If the argument leading to Eq. (21) is valid, then one is led to conclude that gravity cannot be formulated as a renormalizable quantum field theory. This is a potentially serious obstacle that I shall address in Chapter 6.

[3] See Ref. [72] for a critique of the reasoning that leads to this scaling.

[4] Although this assumption has been questioned by Percacci and Vacca [73], among others.

2 Simplicial Quantum Gravity

2.1 Geometric Observables

General relativity describes gravity as the curvature of spacetime, and quantum mechanics describes spacetime on the smallest distance scales. So if we are to unify general relativity and quantum mechanics we must understand what spacetime looks like on the smallest distances. One idea is that spacetime is discrete at the Planck scale, meaning that there exists a smallest possible unit of both space and time, namely the Planck length and the Planck time. A further complication comes from the fact that quantum mechanics describes observables as being in a superposition of all possible states until observation has occurred, and therefore that the geometry of spacetime at the Planck scale could consist of a superposition of all possible geometries. These complications make it very difficult to study the Universe on such small scales. One simplifying approach is to approximate the smooth continuous geometry of spacetime by a lattice of locally flat n-dimensional triangles called simplices. In this way one can numerically generate a large ensemble of configurations that samples all the possibilities of curvature and geometry, allowing one to calculate specific observables by taking the expectation value over the entire set of configurations.

The simplicial approach to quantum gravity, as first proposed by Regge [74], allows one to make use of the considerable number of techniques used in lattice gauge theories. In a similar way to lattice gauge theories, one is not restricted to discrete spacetime, since one can allow the lattice size to approach infinity and take the simplicial edge length to zero. Under these limits one would effectively remove the ultraviolet lattice regulator and recover continuum physics. Regge calculus is not dependent on simplices either; any shape that can be extended into a n-dimensional polytope can be used in the same way. Simplices are chosen because they are essentially the simplest possible polytope that one can use to approximate n-dimensional manifolds.

An n-dimensional simplex is a polytope, where the number of k-dimensional faces N_k is given by

$$N_k = \begin{pmatrix} n+1 \\ k+1 \end{pmatrix} = \frac{(n+1)!}{(k+1)!\,((n+1)-(k+1))!}. \tag{22}$$

A 4-simplex, therefore, has 5 vertices, 10 edges, 10 triangular faces and 5 tetrahedral faces. Simplices are fitted together along their $(n-1)$-dimensional faces creating a simplicial piecewise linear manifold. Simplicial quantum gravity can be subdivided into

two main approaches, Regge calculus and dynamical triangulations. The approach of Regge calculus is to fix the connectivity of the simplices but allow the edge lengths to vary; in this way the dynamics of the geometry is captured. Conversely, dynamical triangulations fixes the simplicial edge lengths but allows the connectivity of the simplices to define the dynamics of the geometry. The main subject of this thesis is that of dynamical triangulations.

The interior geometry of an n-simplex is assumed to be flat, and so in the case of dynamical triangulations the dynamics of a given simplex is entirely contained within the connectivity of the $(n+1)/2$ fixed edge lengths. The curvature in simplicial quantum gravity is defined by the deficit angle around a $(n-2)$-dimensional face at which arrangements of n-simplices converge. If we take the example of a lattice of 2-simplices, or triangles, then the idea becomes clear. Imagine joining 6 such triangles together so that they meet at a single shared vertex, as shown in Fig. 3.

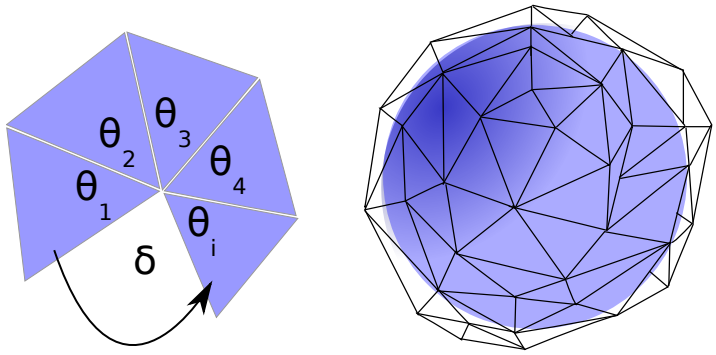

Figure 3: The deficit angle δ for a 2-dimensional lattice (left) and a simplicial approximation to a sphere (right).

One can define a complete angle of 2π radians about this vertex. However, upon removing one of these triangles one now has a deficit angle δ. The remaining simplices can now be joined together along their piecewise linear edges to form a curved geometry. The angle δ is then a measure of the extent to which the geometry is curved. The deficit angle δ is given by

$$\delta = 2\pi - \sum_i \theta_i. \tag{23}$$

The value of the deficit angle defines three different types of curvature. If $\sum_i \theta_i = 2\pi$ the geometry is flat. If $\sum_i \theta_i < 2\pi$ the geometry has positive Gaussian curvature. If $\sum_i \theta_i > 2\pi$ the geometry has negative Gaussian curvature. This idea can be extrapolated

to an arbitrary dimension n, where flat n-dimensional simplices are joined together along their $(n-1)$-dimensional faces, defining the curvature at a hinge of dimension $(n-2)$.

Another geometric observable that can be computed in simplicial quantum gravity is the volume profile. One can calculate the volume profile of a simplicial ensemble in the following way. Firstly, one defines a randomly chosen vertex from the set of triangulations to be the origin o, one then shells radially outwards from this point by hopping to an adjacent vertex. We can thus define a geodesic distance τ from the origin o. By counting the number of simplices within a shell of radius τ one builds up a volume profile for the ensemble of triangulations as a function of geodesic distance from o. Then, just as one sums over all possible paths in the Feynman path integral approach to quantum mechanics to obtain the macroscopic classical path, one should average over all possible geometries to create an expectation value for the macroscopic geometry of the Universe.[5]

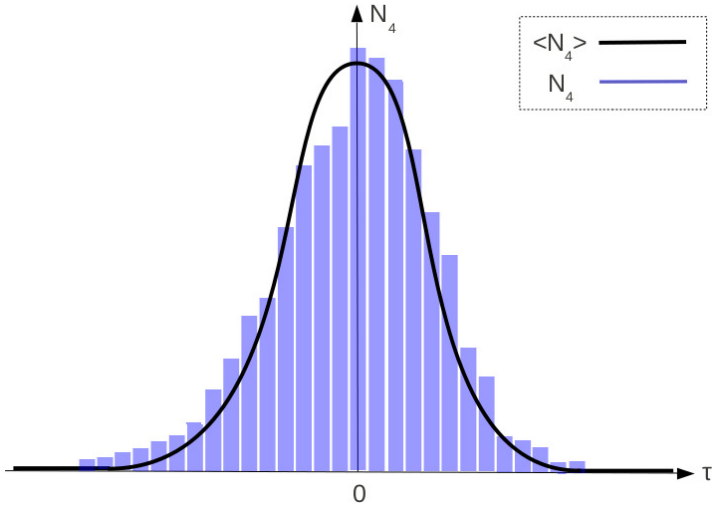

Figure 4: A schematic representing the number of 4-simplices N_4 as a function of geodesic distance τ form an arbitrarily defined origin o. Collectively the blue bars form a single measurement of the volume distribution of N_4. One forms an expectation value $\langle N_4 \rangle$ by making many such measurements and averaging. The centre of volume is located at 0.

Since in appropriate limits a theory of quantum gravity should reduce to general relativity, one would expect that the phase diagram for a theory of quantum gravity should contain a semi-classical phase whose geometry is a solution to general relativity. One such solution is de Sitter space. A de Sitter space is the maximally symmetric

[5]The above description is specific to a model of simplicial quantum gravity with no explicit time direction, although the same principle applies to a theory with an explicit time direction except that in this case one calculates the spatial volume at proper time intervals t.

geometrically flat solution to Einstein's field equations with no matter content and a positive cosmological constant. The de Sitter metric can be written as,

$$ds^2 = dt^2 + a\,(t)\,d\Omega^2_{(3)} = -dt^2 + H_L^2 \cosh^2\left(\frac{\mathrm{t}}{\mathrm{H_L}}\right) \mathrm{d}\Omega^2_{(3)}. \tag{24}$$

Where H_l is the Hubble length given by $H_l = c/H_0 = \sqrt{\frac{3}{\Lambda}}$. $\Omega_{(3)}$ is the 3-dimensional volume element [75],

$$\Omega_{(3)} = d\chi^2 + \sin^2\chi \left(\mathrm{d}\theta^2 + \sin^2\theta \mathrm{d}\phi^2\right). \tag{25}$$

As I shall discuss in Section 2.3 such a de Sitter phase has been shown to exist for a specific model of simplicial quantum gravity, thus verifying that this model has a solution of general relativity as its low energy limit.

One may naively think that a n-dimensional theory of simplicial quantum gravity will always result in a n-dimensional geometry, however, this is not necessarily the case. For dynamical triangulations the dynamics is contained in the connectivity of the n-simplices, where the geometry is updated by a set of local update moves (see Chapter 3.3 for more details). These local update moves can result in the deletion or insertion of vertices within simplices and so it is possible to obtain a geometric structure that has self-similar properties at different scales, meaning the geometry can be a fractal. A fractal geometry admits non-integer dimensions, and so recovering n-dimensional space from n-dimensional fundamental building blocks is a non-trivial result. The approach of simplicial quantum gravity allows the fractal dimension of the ensemble of triangulations to be computed numerically, typically this is done by computing the Hausdorff dimension and the spectral dimension.

The Hausdorff dimension, first proposed by Felix Hausdorff in 1918 [76], generalises the concept of dimension to non-integer values, thereby enabling one to quantify the dimension of a fractal geometry. The standard non-fractal definition of dimension is given by the familiar topological dimension, which can be determined by simply counting the minimum number of coordinates to uniquely specify an event. For example, the topological dimension of a line is one and the topological dimension of a plane is two. However, the validity of the topological dimension comes into question when one considers, for example, a line that undergoes a continuous random walk on a two-dimensional plane. After a sufficiently long period of time the line will essential fill the two-dimensional plane. What then is the dimension of such a geometry? The topological dimension strictly remains one, however, the Hausdorff dimension is a non-integer

D_T	r	V
1	3	3
2	3	9
3	3	27

Table 1: A table showing how the volume of a sphere with topological dimension D_T scales with radius r.

number that is somewhere between one and two, thereby allowing us to quantify the "roughness" of the geometry.

To motivate a mathematical definition of the Hausdorff dimension we consider self-similarity and dimension under scale transformations. Take a line element of length r and perform a scale transformation by a factor of three. The new line element now has a length $3r$. Now take a circle of radius r, and area A, and again apply a factor 3 scale transformation to the radius, the new circle now has an area of $9A$. Now take a sphere of radius r, and volume V, and again scale r by a factor of 3, one now obtains a sphere of volume $27V$. This simple set of scale transformations is depicted in Fig. 5 and the results are tabulated in Table 1.

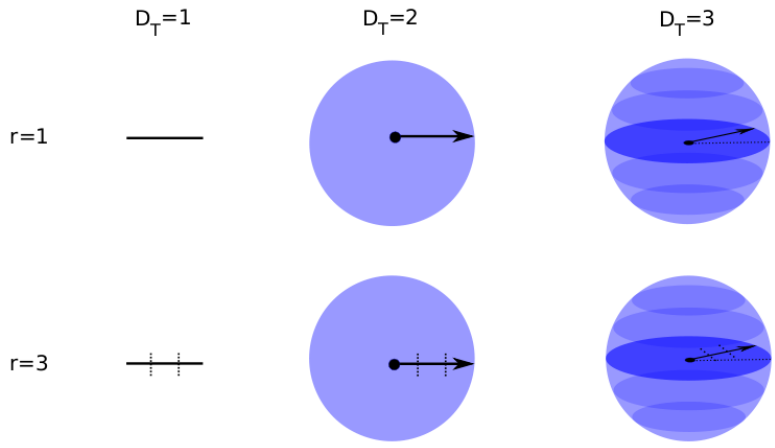

Figure 5: A schematic describing how the Hausdorff dimension is determined. Column 1 shows a line segment with topological dimension 1, the line segment undergoes a scale transformation from $r = 1$ to $r = 3$. Column 2 shows a circle of topological dimension 2 whose area increases by a factor of 9 under such a scale transformation. Column 3 shows a sphere with topological dimension 3, whose volume increases by a factor of 27 under such a scale transformation.

As can be seen from Table 1 the relationship between the D-dimensional volume

and the radius r is given by

$$V \propto r^D. \tag{26}$$

Making D the subject, and taking the limit $r \to 0$, gives us the mathematical definition of the Hausdorff dimension as,

$$D_H = \lim_{r\to 0} \frac{\ln\left(\mathrm{V}\left(\mathrm{r}\right)\right)}{\ln\left(\mathrm{r}\right)}. \tag{27}$$

For volume profiles of the type seen in Fig. 4 one can then determine the Hausdorff dimension of the ensemble of triangulations by simply counting the expectation value for the number of simplices within a given geodesic distance from a randomly chosen vertex. Observing how the number of simplices scales with geodesic distance allows one to measure the fractal Hausdorff dimension.

The large scale geometry of the universe can also be studied via the volume-volume correlator. In a theory with 4-dimensional building blocks the volume-volume correlator gives us a measure of the distribution of the 4-volume as a function of geodesic distance via determining the correlation of adjacent slices of 4-volume. We study the finite volume scaling behaviour of the volume-volume correlator similar to the one introduced in Ref. [77] to study the scaling of CDT,

$$C_{N_4}\left(\delta\right) = \sum_{\tau=1}^{t} \frac{\left\langle N_4^{\mathrm{slice}}(\tau) N_4^{\mathrm{slice}}(\tau+\delta)\right\rangle}{N_4^2}. \tag{28}$$

$N_4^{\mathrm{slice}}(\tau)$ is the total number of 4-simplices in a spherical shell a geodesic distance τ from a randomly chosen simplex. N_4 is the total number of 4-simplices and the normalization of the correlator is chosen such that $\sum_{\delta=0}^{t-1} C_{N_4}\left(\delta\right) = 1$. If we rescale δ and $C_{N_4}\left(\delta\right)$, defining $x = \delta/N_4^{1/D_H}$, then the universal distribution $c_{N_4}(x)$ should be independent of the lattice volume, where $c_{N_4}\left(x\right) = N_4^{1/D_H} C_{N_4}\left(\delta/N_4^{1/D_H}\right)$. One can determine the fractal Hausdorff dimension, D_H, as the value that leaves $c_{N_4}\left(x\right)$ invariant under a change in four-volume N_4.

Another measure of the fractal dimension of a space is the spectral dimension D_S. The spectral dimension D_S defines the effective dimension of a fractal geometry and is related to the probability of return $P_r\left(\sigma\right)$ for a random walk over the ensemble of triangulations after σ diffusion steps.

One can derive the spectral dimension (following Refs. [8, 78]) starting from the d-dimensional diffusion equation,

$$\frac{\partial}{\partial\sigma}K_g\left(\zeta_0,\zeta,\sigma\right)-g^{\mu\nu}\bigtriangledown_\mu\bigtriangledown_\nu K_g\left(\zeta_0,\zeta,\sigma\right)=0. \tag{29}$$

Where K_g is known as the heat kernel describing the probability density of diffusion from ζ_0 to ζ in a fictitious diffusion time σ. $\bigtriangledown$ is the covariant derivative of the metric $g_{\mu\nu}$. The diffusion process is taken over a d-dimensional closed Riemannian manifold M with a smooth metric $g_{\mu\nu}\left(\zeta\right)$.

In the case of an infinite flat Euclidean space, Eq. (29) has the simple solution,

$$K_g\left(\zeta_0,\zeta,\sigma\right)=\frac{\exp\left(-\mathrm{d}_\mathrm{g}^2\left(\zeta,\zeta_0\right)/4\sigma\right)}{\left(4\pi\sigma\right)^{d/2}}. \tag{30}$$

Where $d_g^2\left(\zeta,\zeta_0\right)$ is the geodesic distance between ζ and ζ_0.

The quantity that is measured in the numerical simulations is the probability $P_r\left(\sigma\right)$ that the diffusion process will return to a randomly chosen origin after σ diffusion steps over the spacetime volume $V=\int d^d\zeta\sqrt{\det\left(\mathrm{g}\left(\zeta\right)\right)}$,

$$P_r\left(\sigma\right)=\frac{1}{V}\int d^d\zeta\sqrt{\det\left(\mathrm{g}\left(\zeta\right)\right)}K_g\left(\zeta_0,\zeta,\sigma\right). \tag{31}$$

The probability of return to the origin in the flat infinite space is then just,

$$P_r\left(\sigma\right)=\frac{1}{\sigma^{d/2}}, \tag{32}$$

and so we can extract the spectral dimension D_S by taking the logarithmic derivative with respect to the diffusion time, giving

$$D_S=-2\frac{d\mathrm{log}\langle\mathrm{P_r}\left(\sigma\right)\rangle}{d\mathrm{log}\sigma}. \tag{33}$$

Equation (33) is only strictly valid for an infinitely flat Euclidean space. However, one can still use this definition of the spectral dimension to compute the fractal dimension of a curved, or finite volume, by factoring in the appropriate corrections for large diffusion times σ. Specifically, the probability that the random walk will return to the origin approaches unity as the ratio of the volume and the diffusion time approaches zero, i.e. when the diffusion time is much greater than the volume. This can be intuitively explained by realising that the volume is proportional to the number of vertices, and so as the number of diffusion steps increases relative to the volume, the probability that the random walk will sample all available lattice sites at least once approaches unity. The mathematical explanation is that the zero mode of the Laplacian $-\triangle_g$, which determines the behaviour of $P_r\left(\sigma\right)$ via its eigenvalues λ_n, will dominate

the diffusion in this region, causing $P_r(\sigma) \to 1$ for $\sigma \gg N_4^{2/D_S}$ [8]. One can therefore factor in the appropriate finite volume corrections by ommiting values of $D_S(\sigma)$ for which $\sigma \gg N_4^{2/D_S}$. The curvature of the space on which the diffusion process occurs should also be corrected for due to the fact that it will change the probability that the diffusion process will return to the origin [8].

When numerically computing the spectral dimension one must calculate the expectation value of the return probability $\langle P_r(\sigma) \rangle$ by taking an average over the ensemble of measurements. The diffusion time σ corresponds to the distance scale probed and the dimensionality of the ensemble can be calculated down at the Planck scale if one has fine enough lattices, assuming the lattice theory actually defines a theory of gravity. It is hoped that the ultraviolet divergences encountered in perturbative quantum gravity may be controlled by some as yet unknown property of spacetime on Planckian length scales. Interestingly, a number of recent studies [79, 80, 81, 82, 83, 84, 85, 79, 1] indicate that the number of spacetime dimensions decreases as a function of distance scale. These surprising and exciting results may provide a mechanism to regulate non-perturbative quantum gravity on the shortest distance scales, and therefore eliminate the ultraviolet divergences in a natural way.

2.2 Euclidean Dynamical Triangulations

Euclidean dynamical triangulations (EDT) is a particular implementation of a lattice regularization of quantum gravity. The approach of EDT was originally studied in two-dimensions for the purpose of defining a nonperturbative regularization of bosonic string theory [86, 87]. This two-dimensional approach proved successful; with gravity coupled to conformal matter being shown to correspond to bosonic string theory [88]. Results from lattice calculations agree with continuum calculations in non-critical string theory wherever they are compared [88]. Motivated by the successes of the two-dimensional theory, EDT was generalised to three [89, 90, 91] and four dimensions [92, 93]. This work explores EDT in four-dimensions.

Euclidean dynamical triangulations defines a spacetime of locally flat n-dimensional simplices of fixed edge length. The four-dimensional EDT formalism translates the continuum path integral

$$Z = \int \mathcal{D}g e^{iS_{EH}}, \tag{34}$$

$$S_{EH} = \frac{1}{16\pi G_N} \int d^4x \sqrt{-}g(-2\Lambda + R), \tag{35}$$

into the discrete partition function

$$Z_E = \sum_T \frac{1}{C_T} e^{-S_{EH}}. \tag{36}$$

Where the integration over the metric $g_{\mu\nu}$ is replaced by a sum over all possible triangulations T. C_T is a symmetry factor that divides out the number of equivalent ways of labelling the vertices in the triangulation T. The discretised Einstein-Regge action in the EDT formalism is

$$S_E = -\kappa_2 N_2 + \kappa_4 N_4. \tag{37}$$

Where N_i is the number of simplices of dimension i, and κ_2 and κ_4 are related to the bare Newton's constant G_N and the bare cosmological constant Λ, respectively.

The particularly simple form of Eq. (37) for the discrete Einstein-Regge action S_E is determined via the simplicial geometry, being dependent on the deficit angle θ around a triangular face, where $\theta = \arccos\left(\frac{1}{n}\right)$, and on the n-dimensional simplicial volume V_n, where

$$V_n = \frac{\sqrt{n+1}}{n!\sqrt{2^n}}. \tag{38}$$

The discrete Euclidean-Regge action is then

$$S_E = \kappa \sum 2V_2 \left(2\pi - \sum \theta\right) - \lambda \sum V_4, \tag{39}$$

where $\kappa = (8\pi G_N)^{-1}$ and $\lambda = \kappa\Lambda$. One can rewrite Eq. (39) in terms of the bulk variables N_i, and use Eq. (38) to obtain the simplicial volumes, giving

$$S_E \equiv -\frac{\sqrt{3}}{2}\pi\kappa N_2 + N_4 \left(\kappa \frac{5\sqrt{3}}{2} \arccos\frac{1}{4} + \frac{\sqrt{5}}{96}\lambda\right). \tag{40}$$

Upon substituting $\kappa_2 = \frac{\sqrt{3}}{2}\pi\kappa$ and $\kappa_4 = \kappa\frac{5\sqrt{3}}{2}\arccos\left(\frac{1}{4}\right) + \frac{\sqrt{5}}{96}\lambda$ one recovers the simple form of the discrete Einstein-Regge action in terms of the bulk variables N_2 and N_4, as given by Eq. (37).

Early studies of four-dimensional EDT reported a one-dimensional parameter space containing two phases that were separated by a transition at some critical value of the coupling κ_2^C, but neither of the phases resembled four-dimensional semi-classical general relativity [92, 7, 94, 95, 96]. When $\kappa_2 < \kappa_2^C$, a phase exists in which the simplicial

geometry effectively collapses, and has an infinite fractal dimension [94]. In the regime $\kappa_2 > \kappa_2^C$ the geometry resembles that of thin polymer strands [94]. Measurements of the Hausdorff dimension of these two phases confirm that neither resembles a physical 4-dimensional phase [94].

The work of Catterall et al. in Ref. [95] studied the order of the phase transition between the two phases via an order parameter related to the fluctuation in the number of simplicial nodes and the scaling of the autocorrelation time. Tentatively, Catterall et al. concluded that the transition separating the two phases is continuous, and therefore has the possibility of being second-order. In Ref. [94] Ambjorn and Jurkiewicz measured the critical scaling exponents using numerical simulations in the vicinity of the transition, also concluding that the transition is continuous. However, a more careful study with sufficiently large lattice volumes and with an increased number of lattice configurations showed that the transition was in fact a discontinuous first-order critical point. Specifically, de Bakker in Ref. [97] analysed 32,000 and 64,000 4-simplices and observed a histogram with a double peak in the number of vertices that grows with volume. This behaviour is characteristic of a first-order transition. An independent study by Bialas et al. [98] also reached the same conclusion, showing that for lattice volumes smaller than 16,000 simplices the data was consistent with a continuous transition, but for a lattice volume of 32,000 simplices or greater a bimodal structure in the histogram of the number of vertices emerged.

These studies not only explained why the transition was previously thought to be continuous (because of large finite-size effects) but they also conclusively showed that the transition is first-order. The fact that the transition separating the two phases is first-order makes it unlikely that the theory has a well defined continuum limit, at least in the simplest implementation of the model [98, 97]. This is because a second-order transition, with its diverging correlation length, is needed to define a continuum limit that is independent of the underlying discrete lattice structure.

The sum over triangulations in the original formulation of EDT all used a trivial measure, that is, all triangulations in the sum defining the path integral were weighted equally. The trivial measure is the simplest implementation, but this does not necessarily mean that it is the correct one. Brugmann and Marinari [99], in the early 90's, investigated the effect of adding a non-trivial measure term to the Euclidean path integral by studying the resulting geometric observables. Brugmann and Marinari reported that the inclusion of a non-trivial measure term induced a strong effect, and even suggested that its inclusion may be responsible for a change in the universality

class of the theory. In the late 90's Bilke et al. [100] also investigated the result of introducing a non-trivial measure term in the path integral of 4-dimensional simplicial quantum gravity. Bilke et al. reported the emergence of a new phase for an appropriate choice of couplings. Both the Brugmann and Marinari and Bilke et al. studies were suggestive, but the resulting phase diagram had yet to be explored in any great detail. The present study was partly motivated by the hope that a more thorough study of the phase diagram of EDT with a non-trivial measure could lead to a physical semiclassical phase, and ultimately to a nonperturbative theory of quantum gravity.

In this work we study the partition function,

$$Z_E = \sum_T \frac{1}{C_T} \left[\prod_{j=1}^{N_2} \mathcal{O}\left(t_j\right)^{\beta} \right] e^{-S_E}. \tag{41}$$

The term in square brackets is a non-trivial measure term, which in the continuum corresponds to a nonuniform weighting of the measure by $[\det(g)]^{\beta/2}$. The product in Eq. (41) is over all 2-simplices, and $\mathcal{O}(t_j)$ is the order of the 2-simplex j, i.e. the number of four-simplices to which the triangle belongs. We vary the free parameter β as an additional independent coupling constant in the bare lattice action (after exponentiating the measure term [99]), bringing the total number of couplings to three. Apart from the already mentioned work of Refs. [99] and [100] the vast majority of work on EDT up to now has considered the partition function with $\beta = 0$ only.

The term associated with the non-trivial measure β can be combined into the discrete Einstein-Hilbert action by exponentiating the measure term, giving

$$S_E = -\kappa_2 N_2 + \kappa_4 N_4 - \beta \sum_j \log \mathcal{O}\left(\mathrm{t_j}\right). \tag{42}$$

The partition function of Eq. (41) is implemented via a Monte Carlo integration over the ensemble of 4-dimensional triangulations with fixed topology S^4. The bare cosmological constant, or equivalently κ_4, controls the number of 4-simplices N_4 in the ensemble because they appear as conjugate variables in the action of Eq. (37). One must therefore tune κ_4 such that an infinite volume limit can be taken [101]. It is convenient to ensure that our numerical simulations are performed for a nearly fixed four-volume, and so we introduce a term $\delta\lambda|N_4^f - N_4|$ into the action such that N_4 is kept close to the target value N_4^f, i.e. $N_4^f \approx N_4$. However, this does not change the action for values of $N_4^f = N_4$, about which the volume fluctuates. The purpose of the term $\delta\lambda|N_4^f - N_4|$ is to prevent volume fluctuations about N_4^f from becoming too large to be easily handled in numerical simulations. While the simulation stabilises around the target volume N_4^f

the parameter $\delta\lambda$ is set to 0.08, after stabilisation $\delta\lambda$ is reduced to 0.04. This term permits fluctuations in N_4 of magnitude $\delta N_4 = \left(\langle N_4^2\rangle^2 - \langle N_4\rangle^2\right)^{1/2} = \left(\frac{1}{2\delta\lambda}\right)^{1/2}$. We are then left with a two-dimensional parameter space, which is explored by varying κ_2 and β.

2.3 Causal Dynamical Triangulations

The difficulties encountered in the original EDT model, namely the absence of a physical phase and a second-order critical point, led Ambjorn and Loll [102] to introduce a causality constraint on the set of triangulations over which the path integral is taken, in the hope that it would fix these problems. The method of causal dynamical triangulation (CDT) distinguishes between space-like and time-like links on the lattice so that an explicit foliation of the lattice into space-like hypersurfaces of fixed topology (usually chosen to be S^3) can be introduced. This prevents branching of geometries into "baby universes" along the time direction.

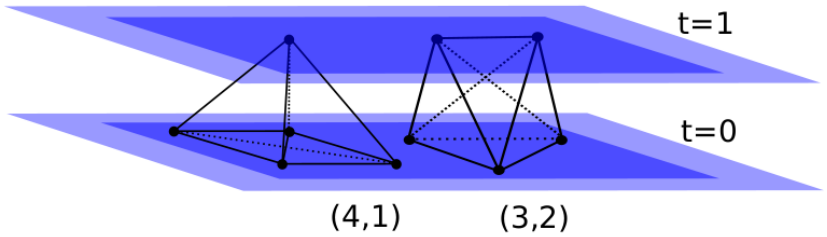

Figure 6: The building blocks of CDT. The $(4,1)$ and $(3,2)$ 4-simplices.

Figure 6 shows the two fundamental building blocks of causal dynamical triangulations. The four-simplex labelled $(4,1)$ has four vertices on the space-like hypersurface of constant time $\tau = 0$ that are connected by space-like links l_s, and one vertex on the hypersurface $\tau = 1$. The space-like hypersurfaces τ and $\tau + 1$ are connected by time-like edges l_t. The two types of simplices can be glued together, along with their time-reversed counterparts, to form a causal slice of spacetime of duration τ. One can then stack t such slices on top of one another, forming a causal spacetime of duration $\tau = t$. The causal structure of spacetime in CDT demands an extra parameter α that describes the ratio of the length of space-like links l_s to time-like links l_t (for Euclidean dynamical triangulations $\alpha = 1$) on the lattice and is given by,

$$\alpha = \frac{l_s^2}{l_t^2}. \tag{43}$$

The metric for CDT has the Lorentzian signature $(-1, 1, 1, 1)$ resulting in a path integral, or partition function, of the type

$$Z = \sum_T \frac{1}{C_T} e^{-\imath S_E(T)}, \tag{44}$$

which contains complex probabilities and is not suitable for numerical integration. CDT must therefore be rotated to Euclidean signature $(1, 1, 1, 1)$, producing a real action that is numerically tractable. It is important to note, however, that although the sum over geometries is performed with Euclidean metric signature the end result is strictly Lorentzian. This is because one starts by restricting the set of possible Euclidean geometries to only include those that meet the conditions of the causality constraint. One then Wick rotates the α parameter in the lower half of the complex plane and performs the Euclidean sum over geometries. At least in principle one can then Wick rotate back to Lorentzian signature. The inverse Wick rotation is not feasible using numerical methods alone, which is a familiar feature of numerical lattice field theory.

Numerical simulations in CDT generate a walk over the ensemble of triangulations based on Monte Carlo importance sampling with time extension t. The local updating algorithm consists of a set of moves that change the geometry of the simplicial manifold locally, without altering its topological properties [77]. CDT appears to obtain the correct macroscopic properties of spacetime from a minimal set of assumptions. Numerical simulations using causally triangulated ensembles have demonstrated the existence of a phase whose ground state turns out to be the maximally symmetric vacuum solution of general relativity, namely de Sitter space [103]. Quantum fluctuations, that are well described by a semiclassical expansion about de Sitter space, have also been reported [104, 103]. The macroscopic dimension of this phase has been non-trivially determined, and is found to be consistent with 4-dimensional spacetime.

On microscopic scales CDT makes a number of non-classical predictions for the geometry of spacetime. Specifically, the approach of CDT reports a reduction in the number of spacetime dimensions as a function of distance scale, predicting that the dimension of spacetime decreases from 4 on macroscopic scales to ≈ 2 on microscopic Planckian scales. This result is found to be in approximate agreement with renormalization group calculations [77].

A recent study by Ambjorn et al. [5] claims the existence of a second-order transition in CDT. They determine the order of the transition in three main ways. Firstly, the histogram of the vertex number is studied, revealing a double peak structure that is found to not increase with simplicial volume in the vicinity of the transition that divides

the de Sitter phase from the unphysical collapsed phase (B-C transition in Fig. 7). This is indicative of a second, or higher-order, transition.

Secondly, they measure the shift in the critical exponent $\tilde{\nu}$ of the asymmetry parameter Δ to be 2.51, which is in clear violation of the prediction $\tilde{\nu} = 1$ known for a first-order transition [105]. The critical parameter Δ scales as a function of volume

$$\Delta^C(N_4) = \Delta^C(\infty) - CN_4^{-1/\tilde{\nu}}, \tag{45}$$

where C is a constant of proportionality and $\Delta^C(N_4)$ is the critical value of the bare parameter Δ at which the transition occurs.

Finally, Ambjorn et al. also report on the measurement of geometric observables $\mathcal{O}$ using a quantity known as Binder's cumulant [105], which is defined by

$$B_{\mathcal{O}} = \frac{1}{3}\left(1 - \frac{\langle \mathcal{O}^4 \rangle}{\langle \mathcal{O}^2 \rangle^2}\right). \tag{46}$$

This quantity will tend to zero in the infinite volume limit if the transition is second-order, and will tend to a non-zero (but possibly very small) constant if the transition is first-order. They report a Binder's cumulant that is consistent with zero in the infinite volume limit, as expected from a second-order transition.

Figure 7 shows the phase diagram of CDT containing three distinct phases A, B, and C. Phase A consists of uncorrelated spatial slices. The volume profile is illustrated by rotating the number of spatial simplices about the time axis, resulting in Fig. 8a. Phase B consists of geometries of simplices with extremely high coordination number such that the vast majority of the volume is concentrated around a single spatial slice, as depicted in Fig. 8b. Phase C is a semi-classical de Sitter phase with extended 4-dimensional geometry. The volume of revolution for phase C is shown in Fig. 8c. Ambjorn et al. in Ref. [5] present strong evidence that the A-C transition is first-order and that the B-C transition is likely second-order.

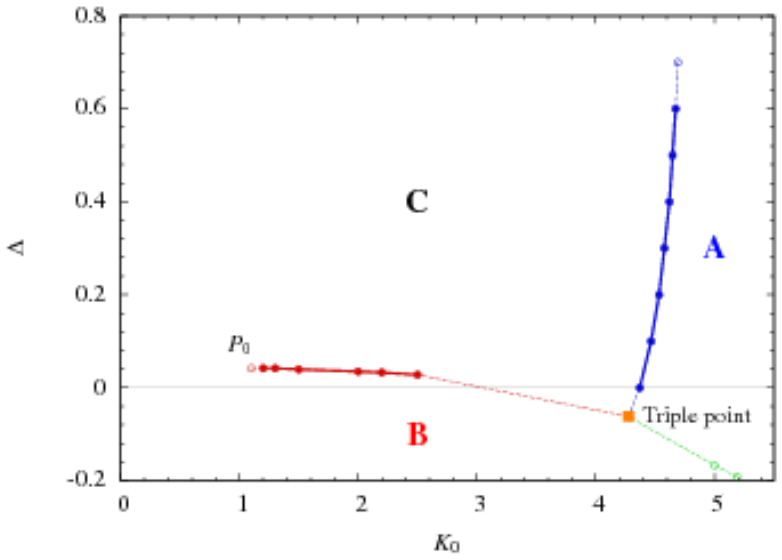

Figure 7: The 2-dimensional phase diagram of CDT as defined via the parameters κ_0 and Δ. Image courtesy of Ambjorn et al. [5]

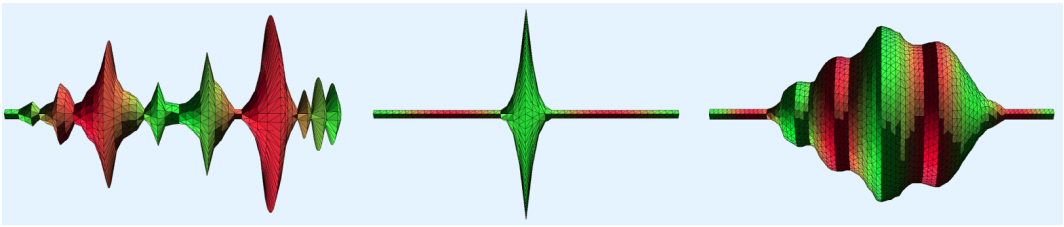

(a) **(b)** **(c)**

Figure 8: The volume profiles of the three distinct phases of CDT. (a) The branched polymer phase of CDT (phase A). This phase primarily consists of a series of uncorrelated spatial slices. (b) The collapsed phase of CDT (phase B), in which a large number of simplices collapse onto a small number of vertices. (c) The extended phase of CDT (phase C). In this phase one obtains an extended 4-dimensional de Sitter geometry. Image courtesy of Ambjorn et al. [6].

The global time foliation that is an inherent feature of CDT and that explicitly breaks the isotropy between space and time is also a defining feature of Hořava-Lifshitz gravity [106]. Hořava-Lifshitz gravity is a proposed theory of quantum gravity that explicitly breaks the four-dimensional diffeomorphism symmetry of general relativity in the high energy regime [106]. Although in Hořava-Lifshitz gravity the symmetry between space and time is explicitly broken at the shortest scales, it is hoped that Lorentz invariance is recovered in the large distance limit. It has been shown that the

phase diagram of CDT is similar to that of the generic phase diagram of Lifshitz gravity, under the validity of a certain assumption.[6] Furthermore, in Ref. [107] Ambjorn et al. show that analytically solvable 2-dimensional CDT is equivalent to Hořava-Lifshitz gravity in 2-dimensions. Thus, CDT might also provide a unifying nonperturbative framework for anisotropic theories of quantum gravity [80].

In this work we revisit the original Euclidean theory for two reasons. Firstly, the CDT restriction to a fixed foliation is potentially at odds with general covariance, though it may amount to a choice of gauge [108]. Even if this is the case it would be interesting to establish whether the same results can be obtained using the explicitly covariant EDT approach. Secondly, the CDT model contains three free parameters in the bare lattice action, whereas the original EDT model typically included only two. Renormalization group studies [64, 65] suggest that the ultraviolet critical surface is 3-dimensional, so it seems worthwhile to revisit EDT with an additional parameter in the bare lattice action [99, 100]. We point out that both the CDT and EDT models include the bare Newton and cosmological constants, but that CDT also includes a third parameter, the ratio of the lengths of space-like and time-like links on the lattice. Thus, we would like to investigate the result of including a third parameter in the bare lattice action of EDT [109, 110, 111].

2.4 Why 4-dimensional simplices?

There exist three main advantages of using simplices over any other geometric construction. Firstly, a simplex is the simplest possible regular polytope that will tessellate to fill an n-dimensional volume. Secondly, a simplicial lattice provides a natural way to define curvature via the counting of n-dimensional simplices that meet at a given $(n-2)$-dimensional hinge. Thirdly, geometric properties of simplices such as volumes and angles allow for fast and easy computation of physical observables.

It should be emphasised, however, that choosing to simulate with simplices is made out of simplicity and not necessity. For example, at least one group has developed similar models using hypercubic lattices (See for example Ref. [112]). A continuum theory of quantum gravity must be independent of the particular choice of lattice regularization, such that as the lattice spacing is taken to zero one obtains a unique theory of continuum physics.

One may also wonder whether there is anything special about using 4-dimensional simplices. At first glance one would expect that constructing a theory out of 4-

[6] The assumption being that the average geometry in CDT can be correctly identified with the Lifshitz field [80].

dimensional building blocks will always yield a four-dimensional spacetime. However, this is not necessarily the case because emergent geometry can exhibit fractal properties. It is therefore a non-trivial test of a theory constructed from 4-dimensional building blocks that it obtain 4 macroscopic dimensions. To numerically simulate with n-dimensional building blocks, where n is some integer greater than four, and obtain a macroscopic dimension of 4 would be a remarkable result as it would non-trivially verify that there is something unique about 4-dimensional spacetime. Very few higher-dimensional studies of dynamical triangulations have been performed (See Ref. [113] for the first detailed account of dynamical triangulations in 5-dimensions).

3 Numerically Implementing EDT

3.1 Overview

Analytical methods in 4-dimensional dynamical triangulations have thus far proved intractable due to the complex nonperturbative sum over geometries. However, with the advent of powerful computational tools, numerical approaches to dynamical triangulations can now be successfully employed via Monte Carlo simulations. In this section we outline our method of numerically implementing Euclidean dynamical triangulations.

Since one wants to sample the path integral, one requires some process of sampling the space of triangulations. This process can locally alter the geometry of the triangulations without causing a change in the global topology.[7] One can generate an ensemble of dynamical triangulations using a set of ergodic local update moves that are implemented via the Metropolis algorithm. A set of moves is said to be ergodic if one can go from any given configuration of triangulations to any other via a repeated application of moves in the set.

In this section I shall review the set of local update moves for the relatively straightforward case of 2-simplices, then extend these concepts to simplicial geometries of three and four dimensions. One can choose different classes of triangulations over which to perform the state sum. Here we consider two such classes of triangulations; combinatorial and degenerate triangulations. I shall define each approach and highlight the computational advantages of degenerate over combinatorial triangulations. The purpose of generating such a set of triangulations is so that we can calculate specific physical observables in our theory. For this purpose I introduce the average Regge curvature as an order parameter, and define its derivative χ_R, so that the phase diagram can be explored. In this section I shall also discuss how we made various tests of our code via a comparison of results obtained using our code with those obtained in the literature. I will then outline the methods used to establish that our ensembles are thermalized, so that calculations using these ensembles are reliable. Finally, I review sources of systematic and statistical error, and how they are estimated using numerical methods.

[7] Although it is possible to have a local topology change. The causal approach to dynamical triangulations in two-dimensions has been generalised to include a limited number of spatial topology changes [114].

3.2 Metropolis Algorithm

Feynman's path integral approach to quantum mechanics teaches us that an individual quantum mechanical path does not constitute a macroscopic observable; one must consider the weighted sum of all possible paths. In the same way, the measurement of a particular observable calculated from a single simplicial configuration is not an observable, one must calculate an expectation value from a weighted sum over all possible configurations.

The expectation value of the observable $\langle O \rangle$ is calculated by summing over all individual measurements of the observable $O(T)$ and weighting each according to a Boltzmann factor $\mathrm{e}^{-\mathrm{S_E(T)}}$, applied over the ensemble of triangulations T.

$$\langle O \rangle \equiv \frac{\sum\limits_{T} O(T)\, \mathrm{e}^{(-\mathrm{S_E(T)})}}{\sum\limits_{T} \mathrm{e}^{(-\mathrm{S_E(T)})}} \sim \frac{1}{N} \sum_{j}^{N} O(C_j)\,, \tag{47}$$

where C_j is a Markov Chain Monte Carlo (MCMC), which in this case is a random walk through the space of possible configurations. The Metropolis algorithm is one particular example of a MCMC algorithm. The probability that one configuration C_N will transition to another configuration C_{N+j} is donated by $P(C_N, C_{N+j})$. One ensures that the random walk converges on an equilibrium probability distribution by use of the so-called detailed balance condition,

$$\frac{P(C_N, C_{N+j})}{P(C_{N+j}, C_N)} = \frac{\mathrm{e}^{\left(-\mathrm{S_E}\left(\mathrm{T_{N+j}}\right)\right)}}{\mathrm{e}^{(-\mathrm{S_E(T_N)})}} = \mathrm{e}^{(-\Delta \mathrm{S_E})}. \tag{48}$$

The number of update moves required for the random walk to reach an equilibrium probability distribution is known as the thermalization time.

The proposed changes to the triangulation T implemented via the ergodic local update moves are accepted or rejected based on the change to the Euclidean Einstein-Hilbert action ΔS_E. If $\Delta S_E > 0$ the proposed update move is accepted with probability X. When this is the case, the probability X is calculated by defining some random number r, where $0 \leq r \leq 1$. If $r \leq X$ the proposed update is accepted, otherwise it is rejected. If $\Delta S_E \leq 0$ the proposed update move is accepted with probability one.

The MCMC begins with a randomly selected configuration C_N. After one update move the ensemble has a new configuration C_{N+1}. One can use configurations C_N and C_{N+1} to calculate the expectation value of the observable $\langle O \rangle$, based on individual measurements O_N and O_{N+1}, respectively. After one such local update move the observables are typically highly correlated, $O_1 \simeq O_2$. To accurately calculate the statistical error

associated with a given observable one must use uncorrelated configurations. The number of update moves required for measurements O_N and O_{N+j} to become uncorrelated is known as the autocorrelation length. The autocorrelation length is dependent on the particular observable, on the simplicial volume, and on the particular value of the parameters in the bare lattice action.

3.3 Local Update Moves

An ensemble is generated using the Metropolis algorithm with a set of five local update moves. The set of moves is chosen to be ergodic. The so-called (p, q) moves consist of either inserting or removing a vertex, or flipping a triangle, or replacing a tetrahedron by an edge, and vice-versa. The set of local update moves are called in random order and it is ensured that the number of accepted moves of each type are approximately equal. Every attempted local update to the geometry of triangulations is accepted or rejected based on its effect on the action.

In order to fully characterise the dynamic ensemble of triangulations we must know two things; the location of every vertex in the configuration space of triangulations at any given instant of Monte Carlo time, and all the possible ways it can evolve to a new configuration at some later instant of Monte Carlo time. The first step is achieved by labelling the vertices of each n-dimensional simplex, so that for example any two vertices are neighbours if they belong to the same n-dimensional simplex. In a similar way, any two n-dimensional simplices are neighbours if they share a $(n-1)$-dimensional simplex, or equivalently d vertices [115]. This vastly simplifies the process of keeping track of the dynamical connectivity, and by constructing such a list one can in principle reconstruct the entire simplicial geometry.

The second step is slightly more involved as we have to define a set of local update moves that result in a topologically invariant geometry. Furthermore, the moves are to be applied randomly to the set of triangulations, and with an approximately even distribution amongst the set of moves. The set of (p, q) moves provide one possible set of ergodic update moves. I will now describe the set of (p, q) moves for the two-dimensional case before extending the concepts to higher dimensions.

In two-dimensions there are just three possible moves. To understand the first move imagine we have two triangles joined together along a common edge, forming a diamond shape. Let's label the vertices of the first triangle as 123, and the vertices belonging to the second triangle as 124. The edge that the two triangles share is then clearly 12. However, one can now flip the common edge length to be 34 instead of 12. One has now

defined two new triangles whose vertices are labelled 134 and 234. Note that one could then perform the inverse of this operation to return to the original configuration. This specific move is ergodic on the space of fixed volumes. This is called the $(2, 2)$ move because one replaces two simplices, in this case triangles, with two completely different simplices. The changes in the triangulation can be kept track of in the following way,

$$123 + 124 \leftrightarrow 134 + 234. \tag{49}$$

The second move in 2-dimensions consists of adding a new vertex 4 to the inside of the triangle 123, thereby creating three new triangles $124, 234$, and 134. This move is referred to as the $(1, 3)$ move, because it changes one triangle into three different triangles. Unlike in the case of the $(2, 2)$ move, which is its own inverse, the inverse of the $(1, 3)$ move defines a separate third move in the set. The vertex 4 that was added to the original triangulation 123 is of order three, meaning that it connects three simplices. So if one is to perform the inverse of the $(1, 3)$ move then one must ensure that a vertex of order three is removed from the triangle; this third move is called the $(3, 1)$ move. Using vertex labelling notation these moves can be expressed as,

$$123 \leftrightarrow 124 + 234 + 134. \tag{50}$$

The (p, q) moves in 2-dimensions are depicted in Fig. 9. This set of moves is ergodic, meaning that one can go from any given configuration to any other via a repeated application of moves from the set. It should be noted that this set of ergodic moves is not unique [116]. A point-splitting method proposed in Ref. [71], a version of which is used in the construction of the ergodic CDT moves, provide an equivalent ergodic construction.

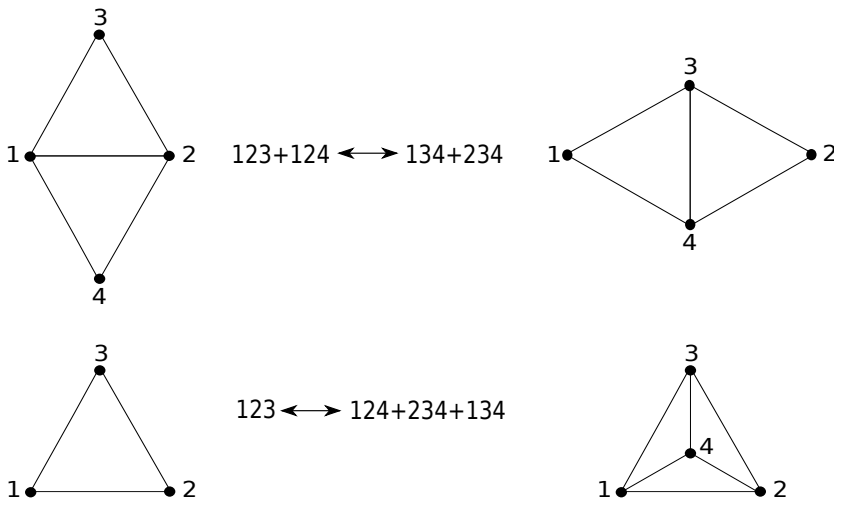

Figure 9: The $(2,2)$ and $(1,3)$ 2-dimensional update moves.

Moving to the case of three dimensions, there are two types of moves, each with an inverse, giving a total of four moves. The first move in three dimensions is the $(1,4)$ move which consists of inserting a new vertex 5, of order four, within the tetrahedron 1234. This creates four separate tetrahedra $1235, 2345, 1245$, and 1345.

$$1234 \leftrightarrow 1246 + 2346 + 1456 + 3456. \tag{51}$$

Second is the $(2,3)$ move which starts out with two tetrahedra 1234 and 1235 sharing a triangle 123 and replaces the triangle with an edge of order three connecting vertices 4 and 5, thus producing three separate tetrahedra $1245, 2345$ and 1345.

$$1234 + 1235 \leftrightarrow 1245 + 2345 + 1345. \tag{52}$$

The three-dimensional moves are shown diagrammatically in Fig. 10.

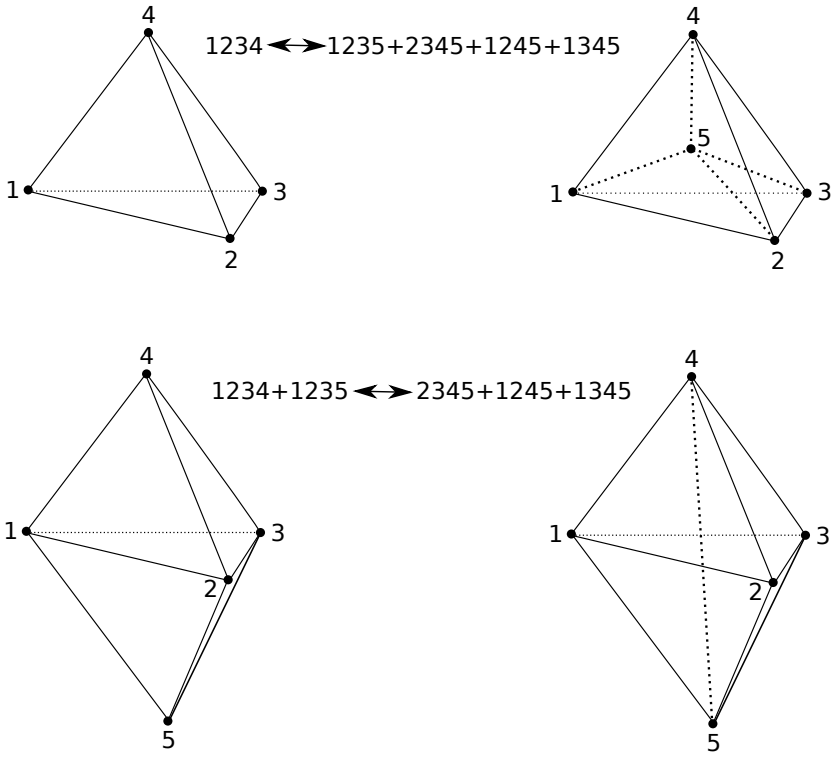

Figure 10: The $(1,4)$ and $(2,3)$ 3-dimensional update moves.

Simplices in 4-dimensions and higher are more difficult to visualise and draw, however, we can simplify this process by using what is known as the triangulation's dual graph. A dual graph is constructed by replacing all simplices by vertices, and connecting them if they share a $(n-1)$-dimensional simplex. Using the dual graph method we can more readily visualise the set of ergodic moves in 4-dimensions. The set of moves in 4-dimensions consists of the $(1,5)\,,(2,4)$ and $(3,3)$ moves. The $(1,5)$ and $(2,4)$ moves have distinct inverses, whereas the $(3,3)$ move is its own inverse. This gives a total of five moves in 4-dimensions.

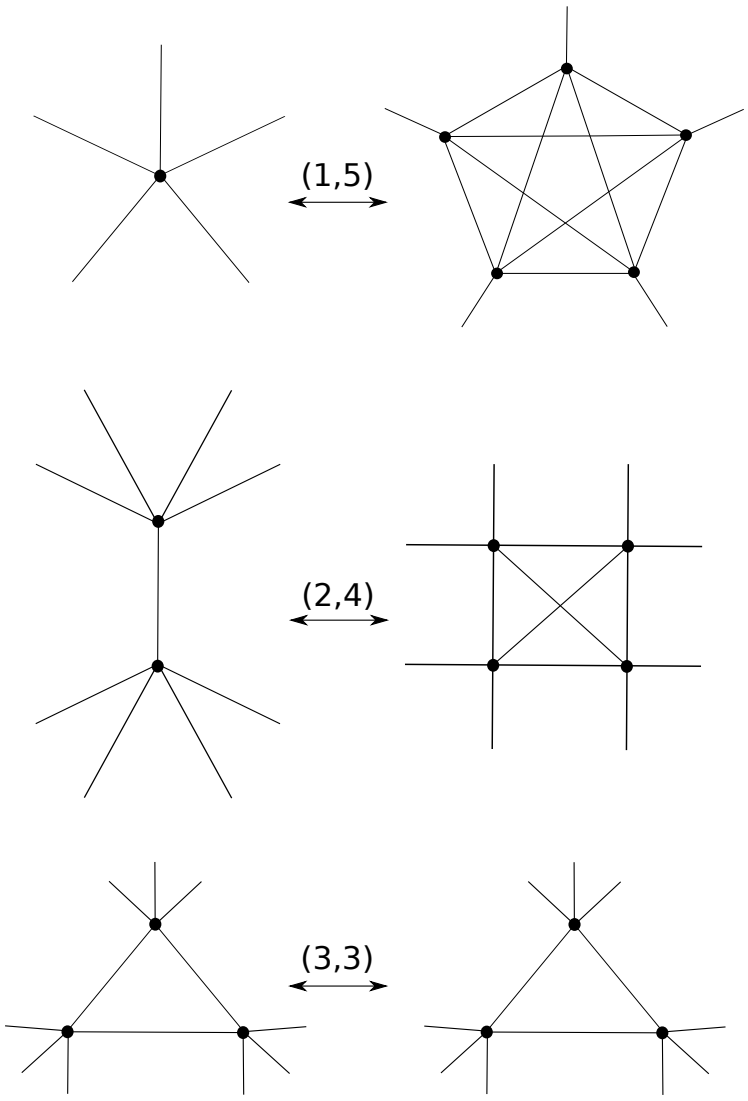

Figure 11: The local update moves of EDT in 4-dimensions.

The partition function of Eq. (41) is implemented via a Monte Carlo integration over the ensemble of 4-dimensional triangulations with fixed topology S^4. As discussed above an ensemble is generated using the Metropolis algorithm with a set of five ergodic local update moves. The set of local update moves are called in random order and it is ensured that the number of accepted moves of each type are approximately equal. Every attempted local update to the geometry of triangulations is accepted or rejected based on its effect on the action. We define a sweep to consist of 10^8 attempted moves, with the computational time for a sweep exhibiting a weak volume dependence.

3.4 Combinatorial and Degenerate Triangulations

A d-dimensional simplicial manifold is constructed by gluing d-simplices together along their $(d-1)$-dimensional faces. To each d-simplex there exists a simplex label and a set of combinatorially unique $(d+1)$ vertex labels. The set of combinatorial triangulations was used in most early simulations of EDT. However, the constraint of combinatorial uniqueness can be relaxed to include the larger set of degenerate triangulations in which the neighbours of a given simplex are no longer unique [100]. However, one retains the restriction that every 4-simplex must be defined by a set of distinct vertices, i.e. we exclude degenerate simplices [100]. Degenerate triangulations don't need combinatorial manifold constraints and are therefore computationally less expensive as compared to combinatorial triangulations. Furthermore, it has been shown numerically that simulations using degenerate triangulations lead to a factor of $\sim$10 reduction in finite-size effects compared to combinatorial triangulations [100]. We have made various checks of our code against the literature using combinatorial triangulations [7], as well as for degenerate triangulations [117], and good agreement was found for both classes of triangulation. I discuss these checks in more detail in Section 3.6.

Simulations are performed by locally manipulating the simplicial geometry via the (p, q) moves. For spacetime dimension $d \leq 4$ the (p, q) moves are known to be ergodic for combinatorial triangulations. The same must be true for the larger degenerate set of triangulations because every set of combinatorially unique simplices can be made distinct by a finite sequence of (p, q) moves. Therefore, one can go from any given degenerate triangulation to any given combinatorial triangulation via the (p, q) moves [117].

3.5 Order Parameters and Phase Transitions

An order parameter is a quantity that characterises the location and order of a phase transition. Previous attempts at Euclidean dynamical triangulations have taught us the importance of quantifying the order of phase transitions. The original EDT model without a non-trivial measure term found two distinct phases that were thought to be separated by a second-order phase transition [92, 95, 94]. This created some excitement because it implied the possibility of taking a continuum limit at the second-order transition. However, upon a more detailed analysis, which included larger simplicial volumes, the phase transition was revealed to be first-order [98, 97].

One must therefore take care when defining an order parameter and when using it

to determine the order of a phase transition. In the infinite-volume limit a first-order transition is characterised by a discontinuity in the first-order derivative of the order parameter at the transition point, whereas second-order transitions are continuous in the first derivative of the order parameter but discontinuous in the second-order derivative [118]. One cannot practically implement simulations in the infinite-volume limit, and so with finite volume studies first-order transitions will only approximate discontinuous behaviour. This can make it difficult to distinguish first-order from higher-order transitions. For both first and second-order transitions the peak height of the susceptibility of the order parameter diverges. However, the susceptibility of the order parameter for first and second-order transitions diverge with different exponents of the volume, thus allowing one to distinguish between the two.

Third and higher-order transitions can be difficult to numerically distinguish from analytic crossovers. This is because as one goes to higher-order transitions the peak of the susceptibility of the order parameter has an increasingly weak dependence on volume, and analytic crossovers have no dependence at all [119], and so they become progressively more difficult to differentiate from one another.

A suitable choice of order parameter for exploring the phase diagram is provided by the expectation value of the Regge curvature.

$$\langle R \rangle \equiv \frac{\langle \int d^4x \sqrt{g} R \rangle}{\langle \int d^4x \sqrt{g} \rangle} \tag{53}$$

The average Regge curvature is relatively easy to determine from the bulk variables N_2 and N_4, and can be numerically determined via the equation

$$\langle R \rangle = \frac{1}{\rho} \langle \frac{N_2}{N_4} \rangle - 1. \tag{54}$$

where $\rho = \frac{10 \arccos(1/4)}{2\pi}$ and N_i is the total number of i-simplices. Taking the derivative of the Regge curvature with respect to κ_2 gives the curvature susceptibility $\chi_R(N_2, N_4)$ as a function of N_2 and N_4. The curvature susceptibility χ_R aids our exploration of the phase diagram and is given by

$$\chi_R(N_2, N_4) = \left[\left\langle \left(\frac{N_2}{N_4} \right)^2 \right\rangle - \left\langle \frac{N_2}{N_4} \right\rangle^2 \right] N_4. \tag{55}$$

3.6 Code Tests

Since the computer code that allows us to simulate EDT with a non-trivial measure term was written independently by us it is important to test it against results ob-

tained in the literature. The original version of our EDT code used combinatorially unique simplices, however, as discussed above relaxing the constraint of combinatorial uniqueness to include the large set of degenerate triangulations leads to a factor of ∼10 reduction in finite-size effects. For this reason we also have a second version of the code using degenerate triangulations. We have therefore made various checks of our code against the literature using combinatorial triangulations [7], as well as for degenerate triangulations [100]. In this section I review the non-trivial quantitative checks I made of our code against the literature.

Using combinatorial triangulations, de Bakker and Smit [7] calculated the average number of simplices $N'(r)$ a geodesic distance r from from a randomly chosen origin in the ensemble of triangulations. They studied three different points in the parameter space of couplings, see Fig. 12, namely $\kappa_2 = 0.8, 1.22$, and 1.5 with β fixed at zero. The points in parameter space were chosen such that one is in each of two distinct phases, with the third in close proximity to the transition between the phases. de Bakker and Smit also calculated the curvature susceptibility, χ_R, for the same three points in parameter space. We obtained agreement for both quantities at all three points in parameter space, within the quoted errors. See Table 2.

	$\kappa_2 = 0.8$	$\kappa_2 = 1.22$	$\kappa_2 = 1.5$
χ_R calculated in Ref. [117]	0.320±0.050	0.595±0.060	0.090±0.001
χ_R calculated in this work	0.297±0.041	0.692±0.066	0.089±0.001

Table 2: A table comparing the curvature susceptibility χ_R calculated in Ref. [7] to our numerical calculations.

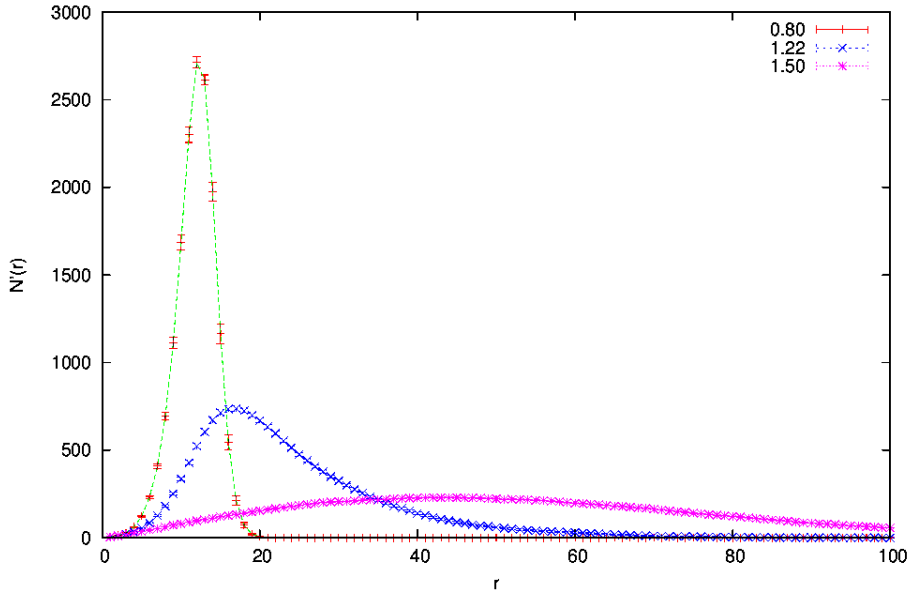

Figure 12: The average number of simplices $N'(r)$ a geodesic distance r from a randomly chosen origin for three values of κ_2 at $\beta = 0.0$. $N'(r)$ values were calculated using an ensemble of 16,000 combinatorial triangulations.

We have also checked our combinatorial code against the work of Ref. [100]. We studied the fluctuations in the order of the three most singular vertices, p_0, p_1 and p_2 when plotted as a function of β for κ_2 held constant at 3.0. Simulations were performed with a lattice volume of 4,000 4-simplices, as in Ref. [100].

The most singular vertex p_0 can be defined as the vertex that belongs to the greatest number of 4-simplices in a given configuration, with p_1 and p_2 the second and third most common vertex, respectively. The susceptibility of the order of the most singular vertex, χ_{p_0}, is defined by the equation,

$$\chi_{p_0} = \left(\left\langle p_0^2 \right\rangle - \left\langle p_0 \right\rangle^2 \right) / N_4. \tag{56}$$

Where N_4 is the total number of four-simplices [100]. The values of χ_{p_0}, χ_{p_1} and χ_{p_2} were calculated using a code written to extract the three most frequent vertices in a given configuration of N_4 simplices, the data was blocked and a jackknife performed to give an estimate of the statistical error.[8] Ten (κ_2, β) coordinates were sampled in total, namely $(3.0, 0.0)$, $(3.0, -0.5)$, $(3.0, -1.5)$, $(3.0, -2.0)$, $(3.0, -3.0)$, $(3.0, -4.0)$, $(3.0, -4.75)$, $(3.0, -5.0)$, $(3.0, -5.75)$, and $(3.0, -6.5)$. The thermalization of the lattices was estimated by choosing an initial sweep number greater than 10000, where a sweep is

[8] This code was written independently by the author and by J. Laiho so as to provide a cross-check; the results obtained were found to be in agreement with one another.

defined as N accepted moves, with N equal to the number of 4-simplices, as suggested by the definition of thermalization in [7].[9] The code used in this comparison was written independently by the author. Agreement was found with Ref. [100] for all ten points in parameter space within errors.

We have also checked our degenerate triangulation code against the work presented in Ref. [117]. The authors of Ref. [117] determine the critical κ_2 value at which a first-order transition is present using degenerate triangulations and for a simplicial volume of 4,000 4-simplices, finding $\kappa_2^C = 1.673$. We obtain a value of $\kappa_2^C = 1.672$ using the same numerical set-up (i.e. the same simplicial volume, using degenerate triangulations, and using the same non-trivial measure). The first-order transition at $\beta = 0$ and $\kappa_2 = 1.672$, for a simplicial volume of 4K, is shown in Figs. 28a and 29.[10]

3.7 Thermalization Checks

If one measures an observable on an ensemble of lattice configurations then there will be fluctuations in this observable as a function of Monte Carlo time. An example of this is shown in Fig. 14. In this context Monte Carlo time is defined as the number of sweeps, where one sweep is 10^8 attempted updates to the geometry. The geometry is updated via a Monte Carlo algorithm, and because the update moves locally alter the geometry by adding or removing vertices, the number of vertices N_0, for example, will fluctuate as a function of Monte Carlo time. If an ensemble is not thermalized, observables will have a strong dependence on Monte Carlo time, rather than exhibiting fluctuations about their equilibrium values. In other words, lattices need to thermalize before measurements can be made. For example, this can be seen in Fig. 13 for Monte Carlo times less than ≈ 13000. The time required for the original lattice configuration to equilibriate is called the thermalization time. For Fig. 13 this occurs for Monte Carlo times ≈ 13000.

If one calculates an observable using a lattice that is not thermalized one will obtain an erroneous result. The aim, therefore, is to determine the point at which the observable fluctuates about some constant value, i.e. when the lattice has thermalized. Once thermalization has been achieved, increasing the number of configurations used in the calculation of the observable will just result in the mean approaching the correct value with an increasingly small statistical error.

[9] This definition, however, was found by us to be somewhat lacking. Our definition of thermalization given in Section 3.7 was found to be more reliable.

[10] Note that we also observe discontinuous behaviour at $\kappa_2 = 1.673$ but the value of $\kappa_2^C = 1.672$ gives us a more symmetric double Gaussian structure, and therefore appears to be the more accurate κ_2^C value.

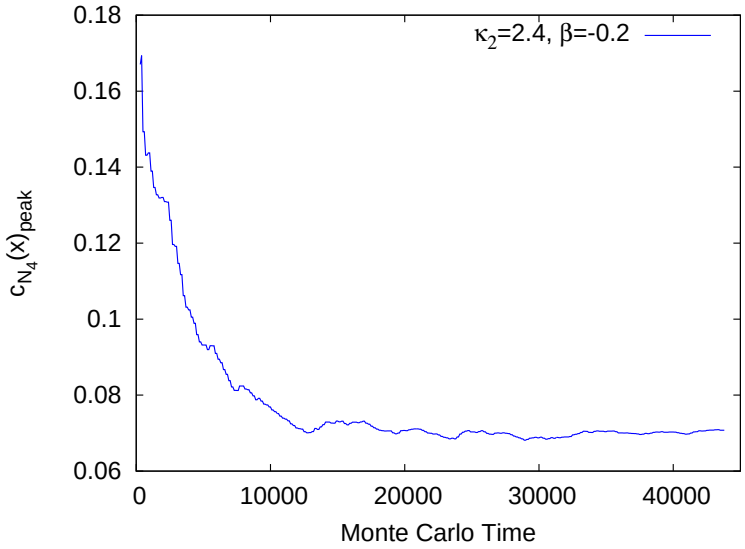

Figure 13: A thermalization check as performed via a plot of the peak in the volume-volume correlator $c_{N_4}(x)$ as a function of Monte Carlo time.

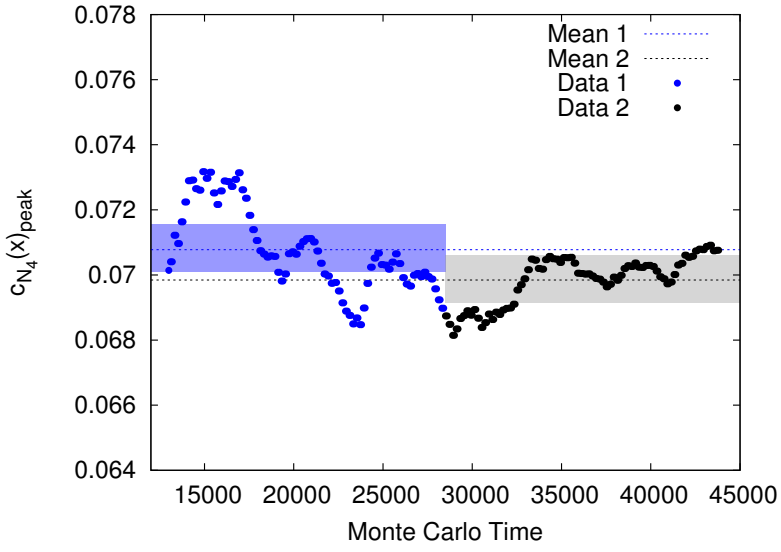

Figure 14: A thermalization check as performed via a plot of the peak in the volume-volume correlator $c_{N_4}(x)$ as a function of Monte Carlo time.

We output a stochastic quantity from the simulation and plot it as a function of Monte Carlo time. Different quantities have different sensitivities to thermalization.

For example, we calculated both the vertex number N_0 and the peak in a quantity called the volume-volume correlator $c_{N_4}(x)$ (which is defined and discussed in more detail in Section 5.2) as a function of Monte Carlo time; finding that $c_{N_4}(x)_{peak}$ is much more sensitive to thermalization than N_0. This is because it is a global large scale quantity, and so is more sensitive to whether the lattice is thermalized. In this work $c_{N_4}(x)_{peak}$ as a function of Monte Carlo time is used as the principle thermalization indicator.

Figure 14 is a zoomed-in version of Fig. 13, focusing on a configuration range we believe to be thermalized, namely 13,000-44,000. The configurations are divided into two equal sets, denoted by Data 1 and Data 2. The reason for dividing the data is to allow a statistical comparison to be made between the first and second half, therefore providing a systematic method for verifying the thermalization of any given lattice. In Fig. 14 the average is calculated for Data 1 and is denoted by the dashed blue line. The light blue band is 1 standard deviation from the mean of data set 1. The average of the second data set is given by the dashed black line, and the light grey band is 1 standard deviation from the mean of data set 2. As can be seen in Fig. 14 there exists no statistical tension between data set 1 and 2, we therefore conclude that there is statistical agreement over this range of configurations, indicating that the lattice is most likely thermalized.

A bounding system is used, whereby thermalization for a point in parameter space with a large value of κ_2 is checked, and if the ensemble is thermalized one can assume that every point in parameter space with a smaller κ_2 value is also thermalized, as long as it has an equal or greater number of configurations and an equal or smaller lattice volume for fixed β. Extensive checks were performed to verify that thermalization times increase with increasing κ_2 and with simplicial volume for a constant value of β. See Figs. 15 and 16 for evidence in support of this claim.

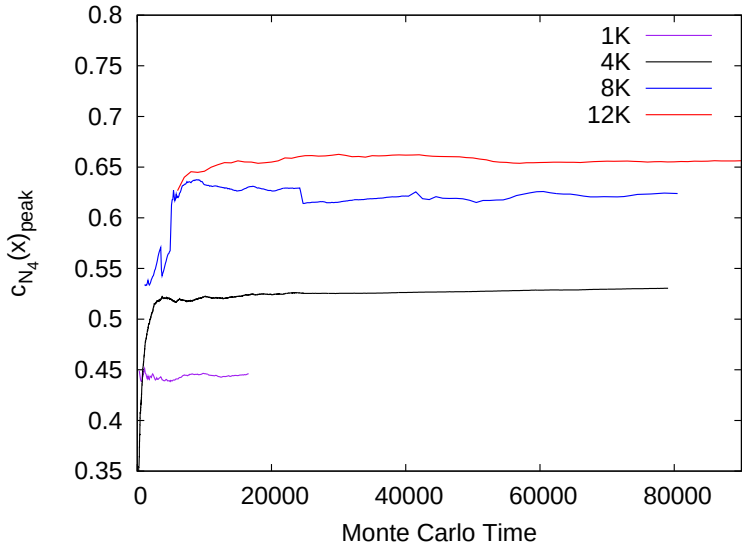

Figure 15: A plot of the peak in the volume-volume correlator $c_{N_4}(x)$ as a function of Monte Carlo time. $c_{N_4}(x)$ is calculated for four different volumes 1K, 4K, 8K, and 12K at $\kappa_2 = 2.1$ and $\beta = -1.0$. This plot provides evidence that the thermalization time increases with increasing volume.

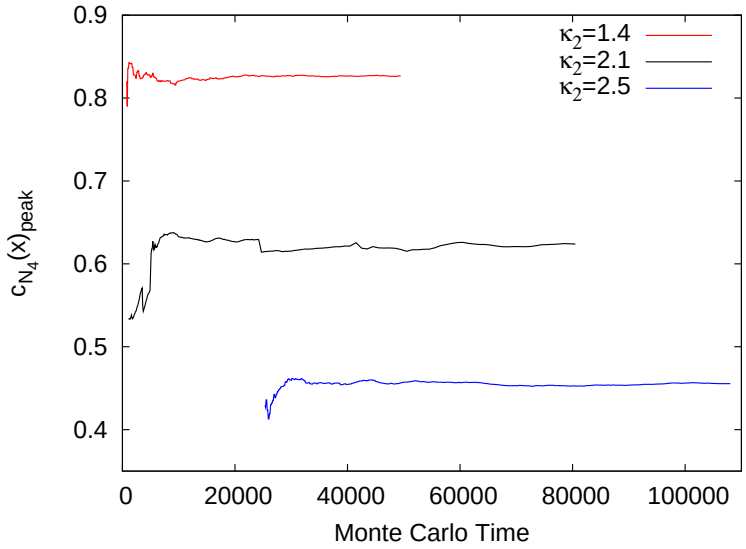

Figure 16: A plot of the peak in the volume-volume correlator $c_{N_4}(x)$ as a function of Monte Carlo time. $c_{N_4}(x)$ is calculated for κ_2=1.4, 2.1, and 2.5 using the 8000 4-simplices. This plot provides evidence that the thermalization time increases with increasing κ_2.

3.8 Systematic Errors

Approximating continuous spacetime with a discrete and finite lattice is inevitably going to introduce systematic errors. In this subsection I shall review the main sources of systematic errors, namely finite-size effects and discretisation errors.

One of the main sources of systematic errors are finite-size effects. Quantifying finite-size effects is of major importance to this work because one of our central aims is to search the phase diagram of EDT for second-order critical points, which would allow for the possibility of defining a continuum limit. Since finite-size scaling can be used to determine the order of the phase transition, estimating systematic errors arising from finite-size effects is essential.

Due to finite computational power one can only ever hope to simulate with finite lattice volumes. One can however both quantify and reduce finite-size effects by simulating on large enough volumes and for several volumes, thus allowing one to extrapolate to the infinite volume limit.

Errors associated with using a discrete lattice to approximate continuum physics, discretisation errors, can be estimated by using an effective field theory and extrapolat-

ing down to the continuum.[11] One can calculate the absolute lattice spacing in physical units via a comparison of simulations with physical results in the classical limit. For example, in the causal approach to dynamical triangulations Ambjorn et al. [103] have estimated an absolute lattice spacing of $a \approx 2.08\ l_P$ via a comparison of the value of G_N inferred from quantum fluctuations about de Sitter space to the physical value. One estimates discretisation errors by performing numerical simulations at successively smaller values of the lattice cut-off a, i.e. taking the limit $a \to 0$. In this way one can estimate discretisation errors associated with the particular lattice regularization via a comparison of results obtained using a finite lattice spacing with those obtained in the continuum.

3.9 Statistical Errors

Statistical errors decrease as $\frac{1}{\sqrt{N}}$, where N is the size of the data set, if each measurement N is statistically independent. Typically, however, stochastic measurements are correlated to some degree and the true statistical error must therefore account for this correlation in some way. A procedure for estimating the statistical error of a correlated data set is provided by the jackknife resampling procedure.

Simulations in EDT will typically output some quantity a number of times N, the idea being that the data set can be used to calculate the expectation value of some observable q. However, this straightforward approach does not give a statistical error associated with the measurement with the correct propagation of errors. To obtain such an error we employ a jackknife re-sampling technique. The single-elimination jackknife procedure starts by discarding the first value from the data set, leaving a set of $N-1$ resampled values. One then calculates the desired quantity q using the reduced sample size of $N-1$, resulting in some observable M_{j1}. A second iteration of resampling is now performed, this time the second value from the data set is discarded and a new value for the observable q is obtained, call it M_{j2}. The process is repeated i times, once for each member of the data set N, resulting in a new set of observables $M_{ji}, i = 1, ..., N$, where the standard error is given by,

$$\sigma_j^2(q) = (N-1)\sum_{i=1}^{N}\left(M_{ji} - M\right)^2/N, \tag{57}$$

where M is the result of sampling over the entire set.

An autocorrelation, as the name suggests, is a measure of the extent to which a signal

[11] Parameters must be tuned to a fixed point for a continuum limit to exist.

is correlated with itself. The ideal situation when performing stochastic simulations is to obtain entirely independent measurements of a certain observable, meaning that each individual measurement is completely uncorrelated with the adjacent measurement in Monte Carlo time. We estimate the effect of autocorrelations on the measurements of observables by grouping individual measurements into larger blocks of data. From this one can estimate the true statistical error for a specific observable accounting for autocorrelations.

The data set of size N can be divided into equally sized blocks of maximum size $N/2$. The block size is increased until the error is maximised such that the correlation between adjacent blocks is eliminated so that one is not underestimating the true statistical error. Blocking is used to estimate errors when there are autocorrelations present.

In our simulations this is done in the following way. A data set comprising N measurements of an observable is divided into blocks of size N/n, where n is an integer, thus giving the factors of N. The value of the observable is calculated for different values of n counting upwards from 2, until the error is maximised. At this point the error originating from the autocorrelations is most accurately reflected in the statistical error. In other words, the block size is systematically increased until adjacent blocks of data become uncorrelated. For example, if each individual measurement of the observable was completely uncorrelated, a block size of one would most accurately reflect the true statistical error.

4 The Phase Diagram of EDT

4.1 Overview

This section explores the parameter space of couplings in EDT with a non-trivial measure term in the gravitational path integral. The parameter κ_4 is adjusted to take the infinite volume limit [101], leaving a two-dimensional parameter space that can be explored by varying κ_2 and β. Results presented in this section are based on calculations I have performed.

The parameter space of EDT is enlarged via the inclusion of the new parameter β that is associated with the non-trivial measure term, as given in the discretised Einstein-Hilbert action of Eq. (37). The result is a phase diagram with three phases; the branched polymer phase, the collapsed phase, and the crinkled phase. The branched polymer phase and the collapsed phase are separated by a first-order phase transition line AB, as shown in Fig. 17. The CD transition, separating the collapsed phase from the crinkled phase, is a softer transition that is consistent with an analytic crossover or higher-order transition.

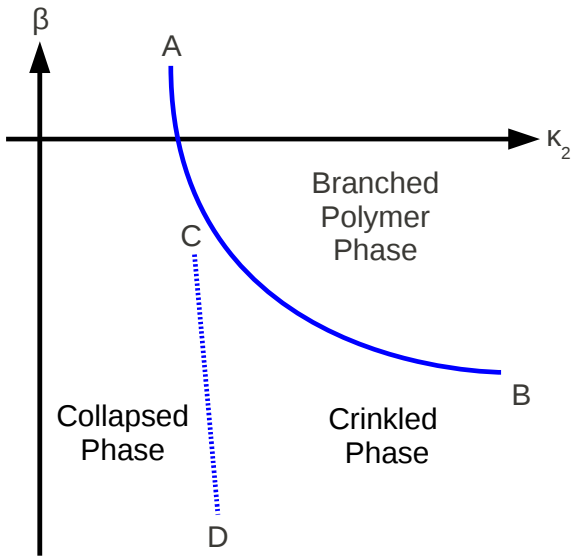

Figure 17: A schematic of the phase diagram of EDT with a non-trivial measure term.

The collapsed phase exists for sufficiently small values of κ_2, or conversely for sufficiently large values of Newton's constant G_N. The collapsed phase is characterised

by a very large, and possibly infinite, fractal Hausdorff dimension D_H. In this phase the spectral dimension D_s also becomes very large, and possibly infinite in the infinite volume limit. The collapsed phase is so-called because simplices tend to collapse on top of one another resulting in a large number of simplices sharing a small number of vertices. In this scenario the vertices are said to have a large coordination number. The volume distribution, as measured by the number of simplices within a given geodesic distance, within the collapsed phase is not well-described by Euclidean de Sitter space. The geometric properties of the collapsed phase mean that it is generally regarded as being unphysical in nature.

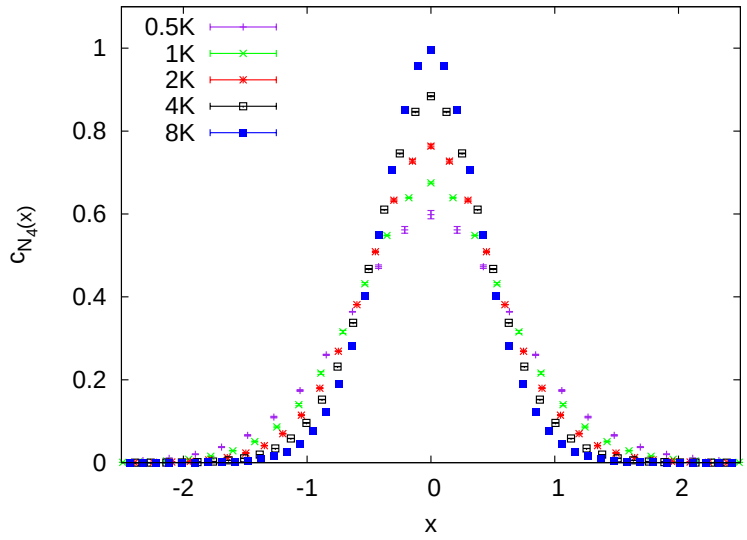

Figure 18: The volume-volume correlator $c_{N_4}(x)$ as a function of x for $\kappa_2 = 1.0$ and $\beta = 0.0$ using five different simplicial volumes. The volume-volume correlator for all volumes is calculated with a Hausdorff dimension of $D_H = 4.0$.

Figure 18 is a plot of the rescaled volume-volume correlator $c_{N_4}(x)$ (previously defined in Section 2.1) as a function of the rescaled time variable x for $k_2 = 1.0$ and $\beta = 0.0$, and for five different simplicial volumes. In Fig. 18 $c_{N_4}(x)$ is calculated with for a scaling dimension $D_H = 4$. Note that in this work a simplicial volume quoted as 4K, for example, is defined to mean a volume of 4000 4-simplices. As discussed in Section 2.1 the quantity $c_{N_4}(x)$ should be volume independent for a constant value of the Hausdorff dimension. However, as can be seen in Fig. 18 the peak of $c_{N_4}(x)$ grows with increasing simplicial volume, thus indicating that the Hausdorff dimension

is inconsistent with the integer 4, as expected within the collapsed phase.

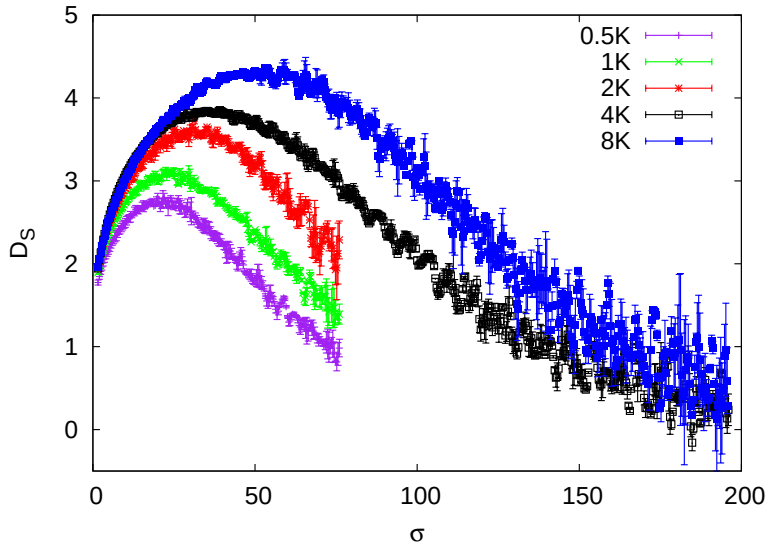

Figure 19: The spectral dimension as a function of diffusion time for $\kappa_2 = 1.0$ and $\beta = 0.0$ using four different simplicial volumes 8K, 4K, 2K, and 1K.

The spectral dimension at the same point in parameter space, namely $k_2 = 1.0$ and $\beta = 0.0$, is shown in Fig. 19. One can see that the spectral dimension increases beyond $D_S = 4$ as the simplicial volume is increased. This behaviour is consistent with the point $\kappa_2 = 1.0$ and $\beta = 0.0$ being in the collapsed phase. As explained in Section 2.1 the probability that a diffusion process returns to the origin after σ diffusion steps approaches unity for $\sigma \gg N_4^{2/D_S}$. Since D_S is typically larger in the collapsed phase than in the two other phases the number of diffusion steps before the condition $\sigma \gg N_4^{2/D_S}$ is met is smaller, resulting in D_S being driven to zero sooner in the collapsed phase.

The branched polymer phase exists for sufficiently large values of κ_2. Within this phase the geometry of triangulations undergoes numerous instances of "pinching" in which the geometry collapses to a minimal neck and branches off into polymer-like baby universes. This phase has a highly irregular geometry, exhibiting a fractal tree-like structure even on macroscopic scales.

The Hausdorff dimension of the branched polymer phase is $D_H = 2$, a result that is confirmed by our calculations, as shown in Fig. 20. Figure 20 is a plot of the rescaled volume-volume correlator $c_{N_4}(x)$ as a function of x for $\kappa_2 = 3.0$ and $\beta = 0.2$, for four different simplicial volumes 8K, 4K, 2K, and 1K. Here $c_{N_4}(x)$ is calculated with

$D_H = 2$, and statistical agreement can be seen over the entire range of x values. This provides strong evidence that the point $\kappa_2 = 3.0$ and $\beta = 0.2$ is within the branched polymer phase because the global Hausdorff dimension is consistent with the theoretical prediction of $D_H = 2$.

The spectral dimension of the branched polymer phase is $D_s = 4/3$, a result that is known analytically [120, 121] and is confirmed by our numerical calculations as shown in Figs. 21a, 21b, 21c, and 21d. The spectral dimension is calculated for the point $\kappa_2 = 3.0$ and $\beta = 0.2$ for the 8K, 4K, 2K, and 1K ensembles, as depicted in Figs. 21a, 21b, 21c, and 21d. The large distance spectral dimension is calculated by taking an average over the range $\sigma = 100 - 200$, the results are presented in Table 3. The results for the spectral dimension at $\kappa_2 = 3.0$ and $\beta = 0.2$ are found to be consistent with the theoretically known value of $D_S = 4/3$ in the branched polymer phase for all four simplicial volumes.

Neither the collapsed nor the branched polymer phase appears consistent with a physical 4-dimensional semiclassical phase.

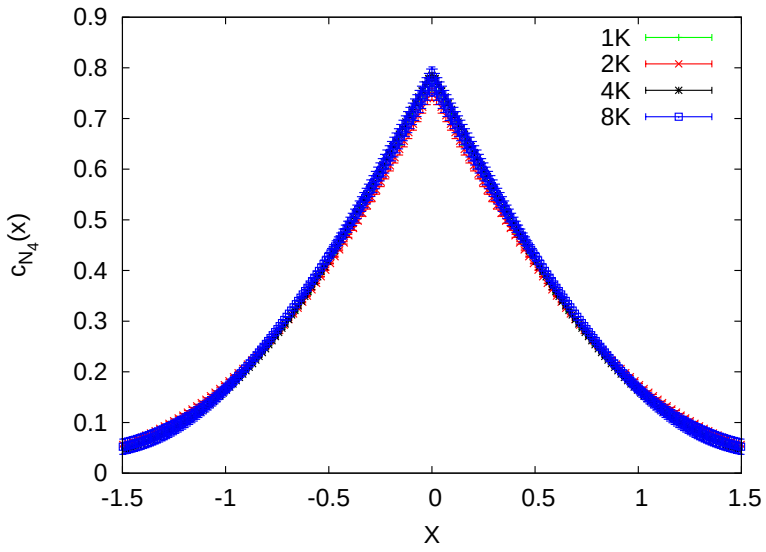

Figure 20: The volume-volume correlator $c_{N_4}(x)$ as a function of x for $\kappa_2 = 3.0$ and $\beta = 0.2$ for 4 different simplicial volumes 8K, 4K, 2K, 1K. The volume-volume correlator is calculated using a Hausdorff dimension of $D_H = 2.0$.

Volume (N_4)	$D_S(\sigma \to \infty)$	Standard deviations from 4/3
8000	1.330 ± 0.015	0.2
4000	1.337 ± 0.005	0.8
2000	1.306 ± 0.008	3.4
1000	1.288 ± 0.022	2.0

Table 3: A table of the simplicial volume N_4, the macroscopic spectral dimension $D_S(\sigma \to \infty)$, and the number of standard deviations from the theoretical prediction of 4/3.

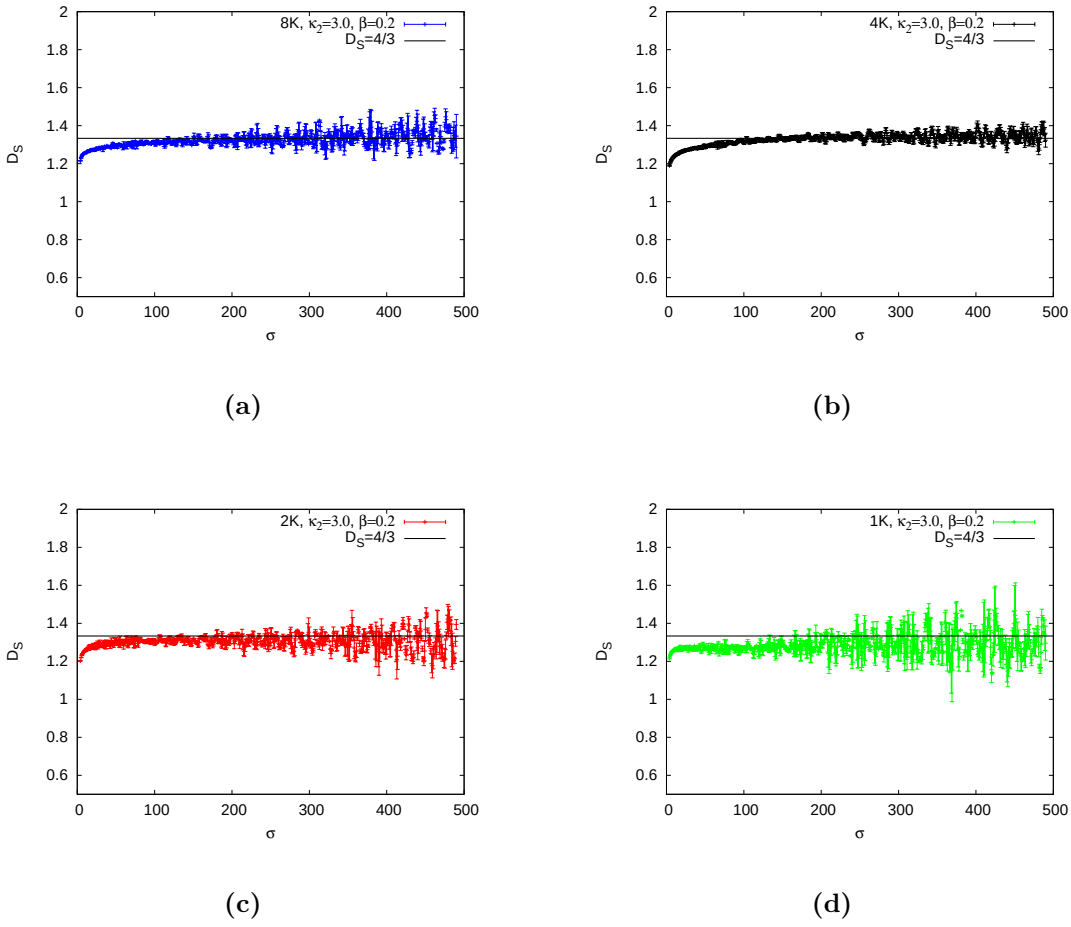

Figure 21: The spectral dimension D_S as a function of diffusion time σ for the bare parameters $\kappa_2 = 3.0$, $\beta = 0.2$. The theoretical prediction of D_S=4/3 is included in each plot for comparison. D_S is calculated as a function of σ for simplicial volumes (a) N_4=8000, (b) N_4=4000, (c) N_4=2000, and (d) N_4=1000.

It is well-established in the literature [97] that at $\beta = 0$ the solid line AB dividing the branched polymer phase from the collapsed phase (see Fig. 17) is a first-order critical point for combinatorial triangulations, and Ref. [117] provides evidence that this is also true for degenerate triangulations. Our simulations support this picture, finding a first-order phase transition at $\beta = 0$ and similar discontinuous behaviour in the curvature susceptibility for β=0.2, -0.2, -0.4, and -0.6, though it is difficult to study the transition for more negative values of β because of large finite size effects. Evidence for the existence of a first-order transition is presented in Section 4.2.

The dashed line CD appears to be a much softer transition than the solid line AB. Studies of the curvature susceptibility and the average Regge curvature at $\beta = -1.0$ show continuous-type behaviour with little or no finite-size scaling, which is indicative of an analytic cross-over, or higher-order transition. The cross-over type transition divides the collapsed phase and the crinkled phase. Within the collapsed phase clear finite-size scaling is observed, suggesting $D_H \to \infty$ as one approaches the infinite volume limit. Within the crinkled phase finite-size effects are much greater, which originally led us to think that this phase possessed a 4-dimensional extended geometry [109, 111, 110]. However, by simulating with larger volumes the finite-size scaling appears to be similar to the collapsed phase.

The crinkled region appears to be just a region within the collapsed phase with very large finite-size effects and long autocorrelation lengths. Thus for small lattice volumes the geometry can appear 4-dimensional and even de Sitter like. However, with increasing lattice volume the geometry seems to depart from a 4-dimensional semi-classical de Sitter-like phase, displaying the usual characteristics of the collapsed phase. Section 5 discusses various aspects of the crinkled phase in detail.

4.2 Phase Transition Line A-B

In this section I use the order parameter $\langle R \rangle$ and its derivative χ_R to locate the position of the transition line A-B in EDT. Once the (κ_2, β) coordinates of the transition have been determined to the required precision, it is possible to determine the order of the phase transition. To do this we plot the number of vertices as a function of Monte Carlo time, histogramming the data for at least two simplicial volumes. A first-order phase transition in the infinite volume limit is discontinuous in the first derivative of the order parameter. Plots of the number of vertices as a function of Monte Carlo time at a first-order transition typically exhibit a number of discontinuous transitions between two meta-stable phases (see e.g. Fig. 24). Histogramming this data should give a

signature double Gaussian distribution if a first order transition is present. Crucially, a double Gaussian distribution for just one simplicial volume is not sufficient to confirm a first-order transition; one must observe such a distribution over at least two volumes and see the peak separation grow with volume. This is because only in the infinite volume limit does one actually observe a discontinuous transition, and so one must study finite volumes and extrapolate the approximate finite volume behaviour to the infinite volume limit.

4.2.1 $\beta = 0.2$

In this section I present evidence that a first-order transition exists when $\beta = 0.2$. This is the first time anyone has confirmed that the transition is first-order for $\beta \neq 0$ using 4-dimensional degenerate EDT with a non-trivial measure.

We study the order parameter $< R >$ and its derivative χ_R as defined in Eqs. (54) and (55), respectively. Figure 22 shows the expectation value of the Regge curvature as a function of κ_2. One observes that the average Regge curvature for $\kappa_2 \leq 0.5$ is a slowly increasing function of κ_2 which then undergoes a rapid, almost discontinuous transition, into another plateau region when $\kappa_2 \geq 2.0$. Since the curvature susceptibility χ_R is defined as the first-order derivative of the Regge curvature with respect to κ_2 one observes a sharp spike at the discontinuous value of κ_2, as shown in Fig. 23.

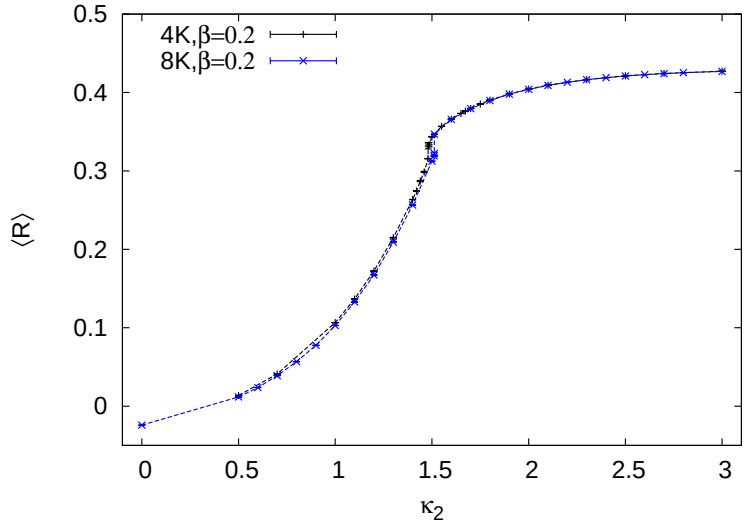

Figure 22: The average Regge curvature $\langle R \rangle$ as a function of κ_2 for 4K and 8K simplicial volumes at $\beta = 0.2$.

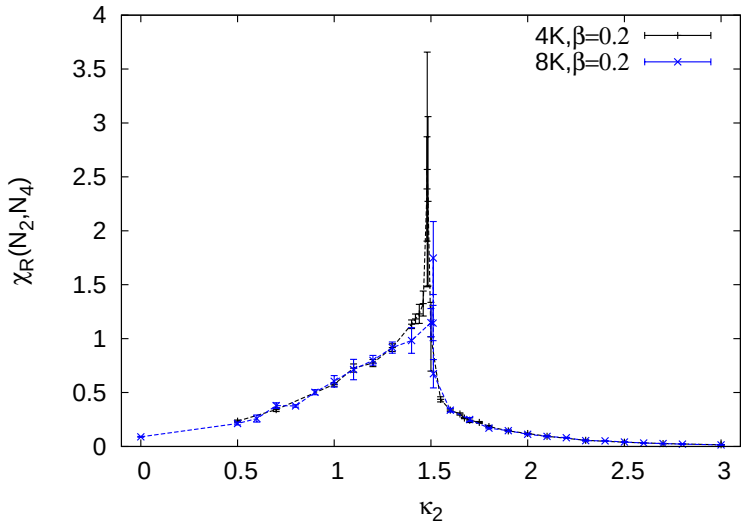

Figure 23: The curvature susceptibility χ_R as a function of κ_2 for 4K and 8K simplicial volumes at $\beta = 0.2$.

The critical value of κ_2 at which χ_R has a peak is located and the Monte Carlo time history of N_0 and the corresponding histogram are produced. A first-order phase transition has a signature double Gaussian peak in the histogram of N_0, with a peak separation that increases with volume.

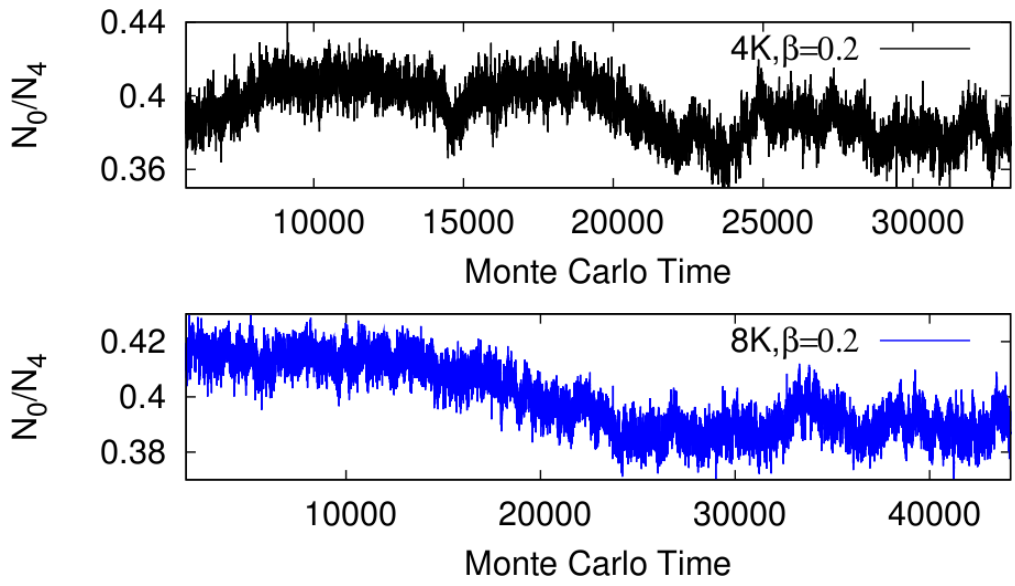

Figure 24: The Monte Carlo time history of N_0/N_4 for two different simplicial volumes at $\beta = 0.2$. The pseudo-critical κ_2 value for the 4K ensemble (top figure) at $\beta = 0.2$ is $\kappa_2 = 1.481$, and for the 8K ensemble (bottom figure) it is $\kappa_2 = 1.513$.

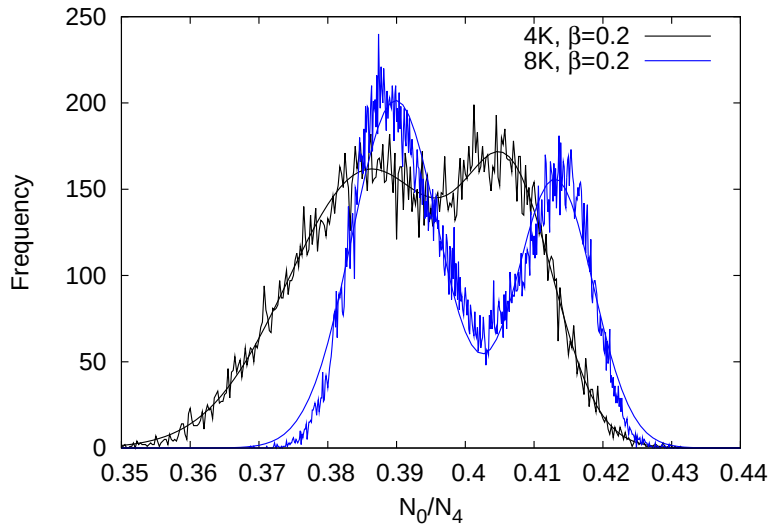

Figure 25: The histogram of N_0/N_4 including double Gaussian fits for 4K and 8K simplicial volumes at $\beta = 0.2$. The pseudo-critical κ_2 value for the 4K ensemble (shown in black) at $\beta = 0.2$ is $\kappa_2 = 1.481$, and for the 8K ensemble (blue) it is $\kappa_2 = 1.513$.

Figure 24 shows evidence for discontinuous-type fluctuations between the two metastable phases for the 4K and 8K ensembles that are characteristic of a discontinuous phase

transition. The transition between the two metastable values of N_0/N_4, however, only becomes truely discontinuous in the infinite volume limit, and so for finite volumes as shown in Figure 24 the transitions will only approximate an actual discontinuity. Figure 25 shows the histogram of N_0 divided by the volume N_4, in which a clear double Gaussian peak is observed for both volumes. The distance between the peaks grows approximately linearly with volume for a first-order transition and so the peak separation for N_0/N_4 should be a constant for a first-order transition. Figure 25 supports this picture. Comparing the peak seperation of the histogram of N_0/N_4 via the fit functions for the 8K and 4K ensembles we find a tension of less than one standard deviation with a constant. From this we are led to conclude that a first-order transition exists when $\beta = 0.2$ on line A-B.

The critical κ_2 values at which the first-order transition occurs are volume dependent, as expected from a first-order transition[12], with $\kappa_2^c(4K) = 1.481$ and $\kappa_2^c(8K) = 1.583$.

4.2.2 $\beta = 0$

It is well established in the literature (see Ref. [97] for combinatorial triangulations and Ref. [124] for degenerate triangulations) that the critical line A-B is a first-order phase transition when $\beta = 0$. The results presented in this section confirm this picture.

[12] As an example consider a temperature-driven phase transition in a $d-$dimensional Ising model with volume $V = L^d$ [122]. From this one finds a power-law behaviour for the transition point p_{crit}, which is given by $|p_{crit}(\infty) - p_{crit}(V)| \propto V^{-1/\tilde{\nu}}$, with $\tilde{\nu} = 1$ for a first-order transition [105, 123].

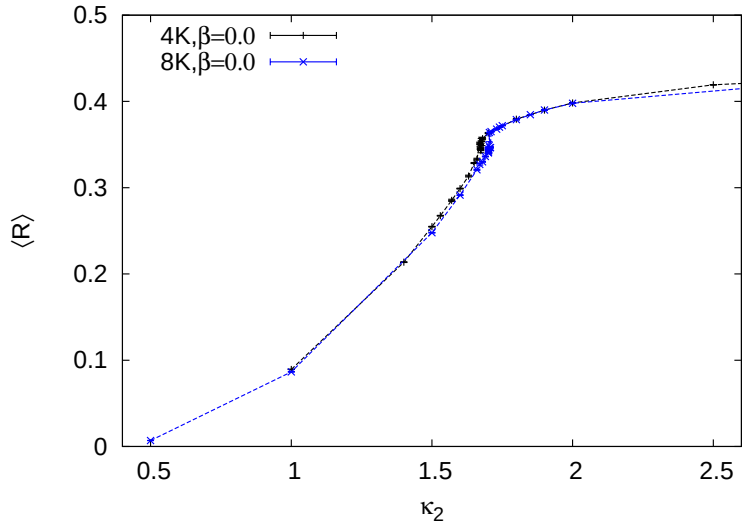

Figure 26: The average Regge curvature χ_R as a function of κ_2 for 4K and 8K simplicial volumes at $\beta = 0.0$.

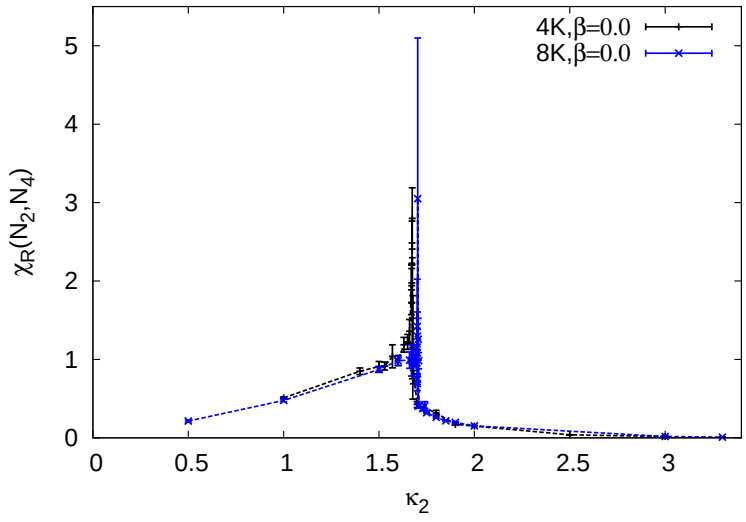

Figure 27: The curvature susceptibility χ_R as a function of κ_2 for 4K and 8K simplicial volumes at $\beta = 0.0$.

Figure 26 shows that the expectation value of the Regge curvature becomes discontinuous at some critical κ_2 value, as is the case for $\beta = 0.2$. The maximum value of the

curvature susceptibility is used to calculate the Monte Carlo time history of N_0 and the corresponding histogram. Again, the histograms of N_0/N_4 (see Fig. 29) exhibit a peak separation that is approximately constant with volume, thus indicating the existence of a first-order transition along the $\beta = 0.0$ line. Comparing the peak seperation of the histogram of N_0/N_4 via the fit functions for the 8K and 4K ensembles we find a tension of less than one standard deviation with a constant. The critical κ_2 values at which the first-order transition occurs are $\kappa_2^c(4K) = 1.672$ and $\kappa_2^c(8K) = 1.703$.

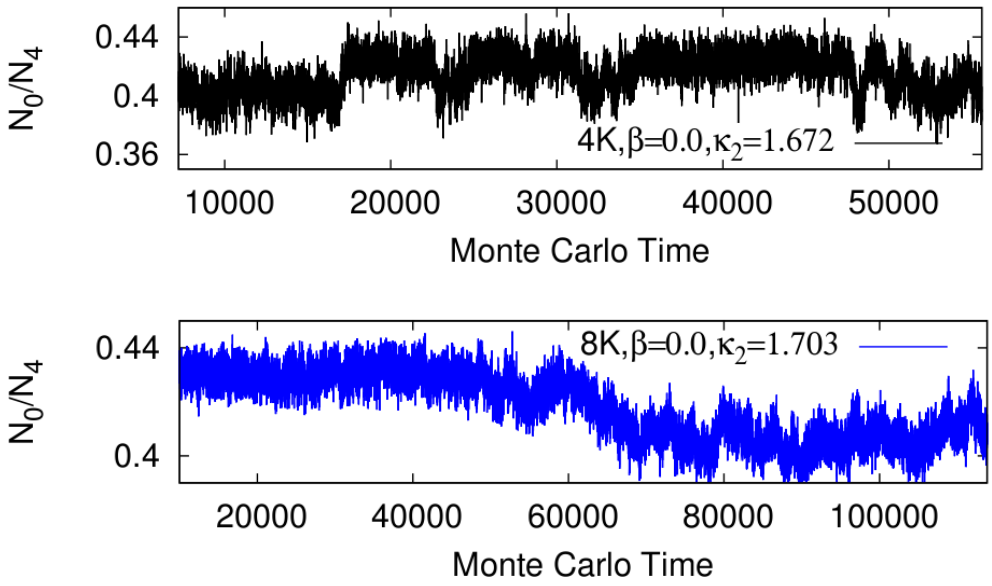

Figure 28: The Monte Carlo time history of N_0/N_4 for 4K and 8K simplicial volumes at $\beta = 0.0$. The pseudo-critical κ_2 value for the 4K ensemble (top figure) at $\beta = 0.0$ is $\kappa_2 = 1.672$, and for the 8K ensemble (bottom figure) it is $\kappa_2 = 1.703$.

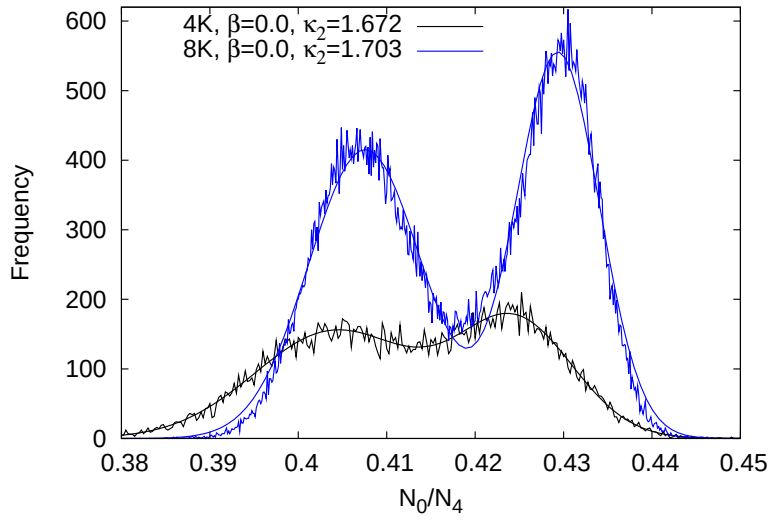

Figure 29: The histogram of N_0/N_4 including double Gaussian fits for the 4K and 8K simplicial volumes at $\beta = 0.0$.

4.2.3 $\beta = -0.2$

Although the critical κ_2 values at which a putative first-order transition for $\beta = -0.2$ have not been determined with a high enough precision to determine the order of the transition via a study of N_0 as a function of Monte Carlo time, Figs. 32 and 33 show strong evidence of discontinuous behaviour and heavily constrain the possible location of the critical κ_2 values. Based on Figs. 32 and 33 the critical κ_2 values for the 4K ensemble appear to lie in the range $\kappa_2^c = 1.863 - 1.867$, and in the range $\kappa_2^c = 1.79 - 2.0$ for the 8K ensemble.

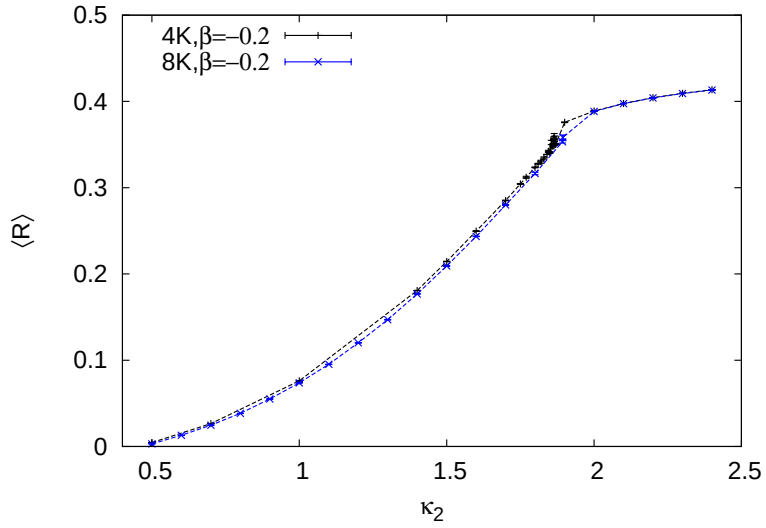

Figure 30: The curvature susceptibility χ_R as a function of κ_2 for 4K and 8K simplicial volumes at $\beta = -0.2$.

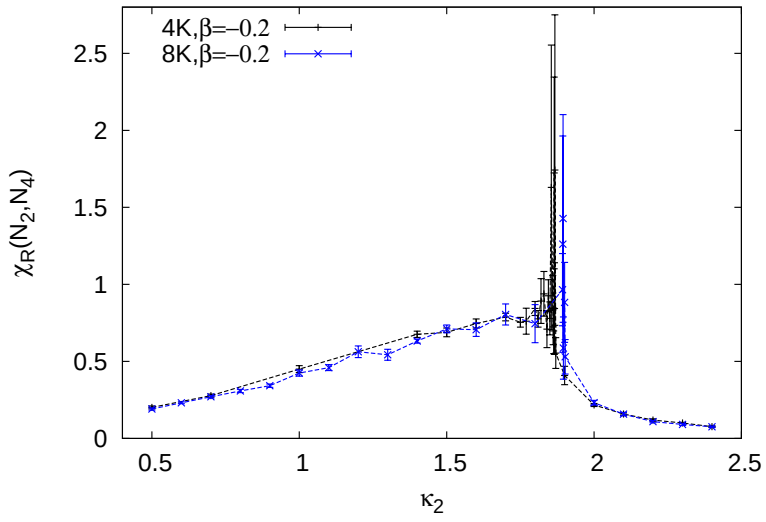

Figure 31: The curvature susceptibility χ_R as a function of κ_2 for 4K and 8K simplicial volumes at $\beta = -0.2$.

4.2.4 $\beta = -0.4$

For large negative values of β in the vicinity of the discontinuous transition the number of accepted moves becomes very low, and therefore it takes very large periods of Monte Carlo time before thermalization is achieved. This makes it difficult to accurately locate the κ_2^c values. However, we can bound their location to $\kappa_2^c(4K) = 2.070 - 2.095$ and $\kappa_2^c(8K) = 2.01 - 2.3$ based on Figs. 32 and 33.

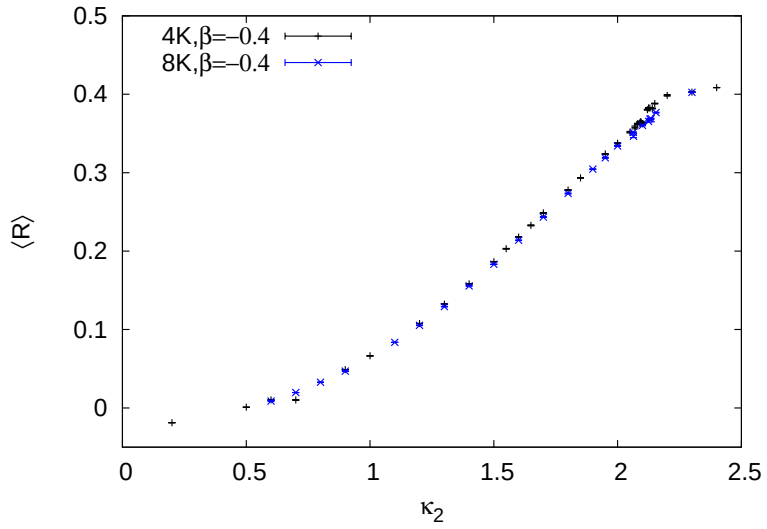

Figure 32: The average Regge curvature as a function of κ_2 for 4K and 8K simplicial volumes at $\beta = -0.4$.

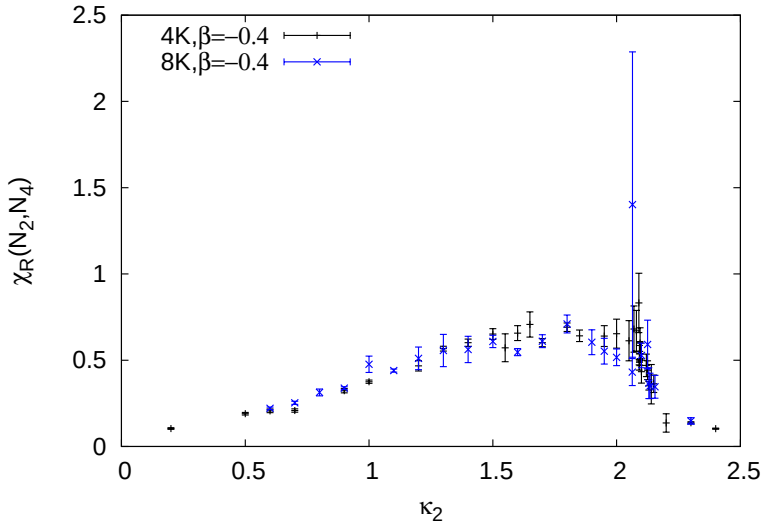

Figure 33: The curvature susceptibility χ_R as a function of κ_2 for 4K and 8K simplicial volumes at $\beta = -0.4$.

4.2.5 $\beta = -0.6$

It is difficult to establish the existence of a discontinuity at $\beta = -0.6$ by studying the order parameter $\langle R \rangle$, however the derivative of the order parameter, namely χ_R provides evidence for such a discontinuity in the region $\kappa_2 = 2.4 - 2.5$, as shown in Fig. 35.[13]

[13]Note that the order parameter and its derivative are calculated only for the 4K lattice because at present the 8K lattice for $\beta = -0.6$ has not equilibrated, as per the definition in Section 3.7. The inclusion of only one lattice volume makes it impossible to establish the order of the transition, however the discontinuous behaviour is at least suggestive.

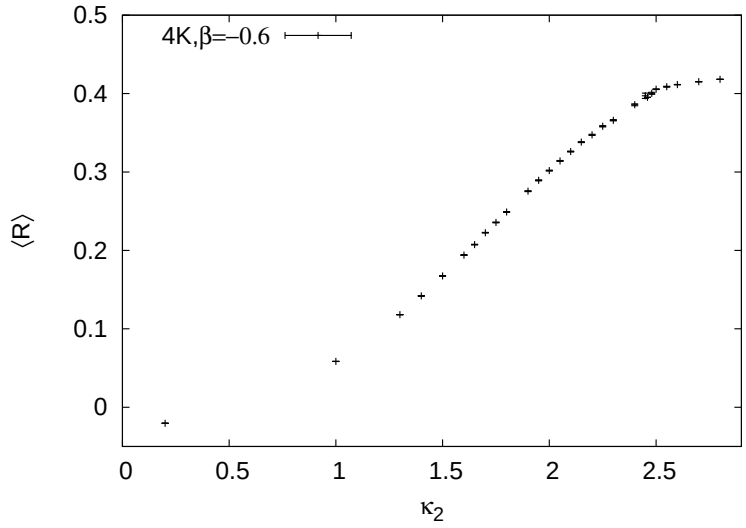

Figure 34: The average Regge curvature as a function of κ_2 for the 4K simplicial volume at $\beta = -0.6$.

For $\beta = -0.6$ the number of accepted moves is significantly lower than for larger values of β, making it difficult to easily locate the position of the critical κ_2 value at which the putative discontinuity is observed. The 8K lattice is omitted for $\beta = -0.6$ because it has not yet thermalized.

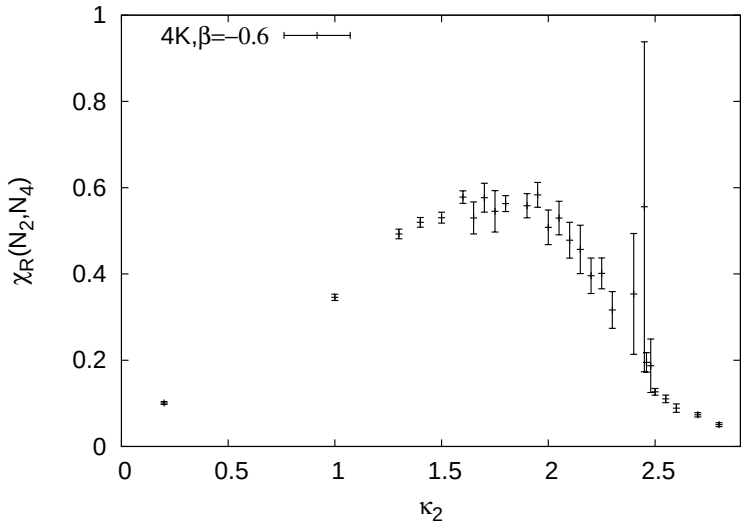

Figure 35: The curvature susceptibility χ_R as a function of κ_2 for the 4K simplicial volume at $\beta = -0.6$.

4.2.6 The Location of the Transition Line

In this section I combine all the constraints on the location of the κ_2^c values at which the order parameter exhibits discontinuous behaviour. This allows us to form a map of the location of the first-order transition in parameter space.

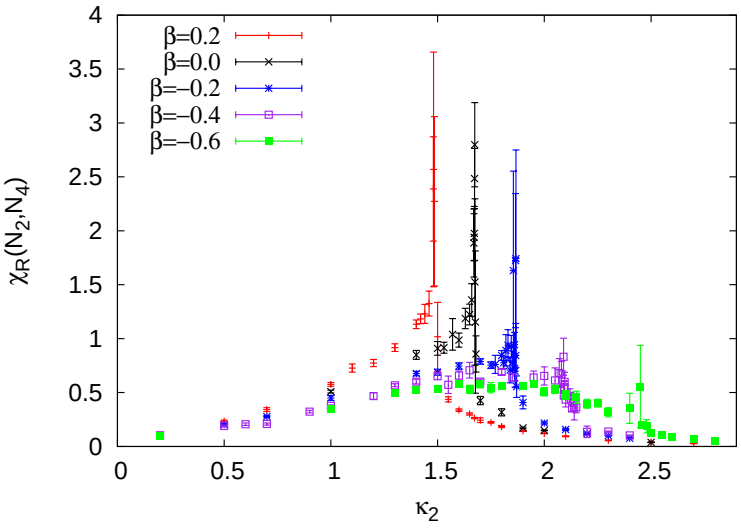

Figure 36: The curvature susceptibility χ_R as a function of κ_2 for the 4K simplicial volume at β=0.2, 0.0, -0.2, -0.4, and -0.6.

As can be seen in Fig. 36 as one decreases β the κ_2^c values, for which the curvature susceptibility behaves discontinuously, map out a first-order transition line that shifts slightly to the right. This behaviour is schematically represented in Fig. 17. Figure 37 combines the actual measurements of κ_2^c and their associated errors to constrain the location of the first-order transition within the parameter space of couplings. These measurements, however, do not include an error associated with finite-size effects.

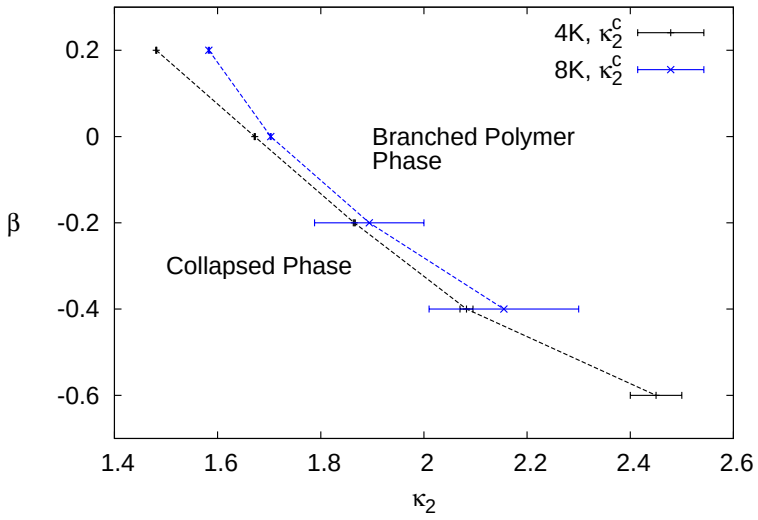

Figure 37: Constraints on the location of the first-order transition in the parameter space of EDT with a non-trivial measure term based on the critical κ_2 values for the 4K simplicial volume.

Mean field approaches, finite-size scaling, and renormalization group arguments based on the method of node decimation [125, 126] for 3-dimensional Euclidean dynamical triangulations with a nontrivial measure all support the claim that the transition line flattens out for large κ_2 values and for sufficiently negative β, and that the transition remains first-order for all negative values of β. The same mean field arguments suggest that the AB line remains first-order and turns over in four dimensions as well. Our results show a slight deviation from linearity that appears to become more pronounced with increasing simplicial volume, however, further work is needed to decide this issue.

4.3 Cross-over Transition

The behaviour of χ_R as a function of κ_2 for $\beta = -1.0$ is consistent with an analytic cross-over, or higher-order transition, as the peak in the curvature susceptibility does not appear to change with volume within errors, as shown in Fig. 39. Figure 38 shows the average Regge curvature for two different lattice volumes as a function of κ_2 for $\beta = -1.0$. It is possible that the curvature susceptibility for $\beta = -1.0$ has a discontinuous transition for some large κ_2 value, however a low acceptance rate coupled

with large finite-size effects in this region makes its existence difficult to establish. We study the first-order transition for three different simplicial volumes at $\beta = 0$ to highlight that a first-order transition can be difficult to detect if the simplicial volume is not large enough. We choose to perform this study for $\beta = 0$ because this region has significantly smaller finite-size effects and a higher acceptance rate than at $\beta = -1.0$.

Figure 40 shows that the discontinuous first-order transition observed in the curvature susceptibility at $\beta = 0.0$ is difficult to detect when the simplicial volume is too small. The curvature susceptibility is calculated along the $\beta = 0$ line for three different simplicial volumes, 0.2K, 0.5K, and 4K. The curvature susceptibility for $N_4 = 0.2$K, and $N_4 = 0.5$K exhibits similar behaviour to a crossover, or higher-order transition, and the discontinuous behaviour only becomes evident for the 4K ensemble. Finite-size effects are smaller along the $\beta = 0.0$ line than they are for $\beta = -1.0$, and so the first-order transition will only become evident at $\beta = -1.0$ for significantly larger simplicial volumes. It is possible that a first-order transition exists somewhere along the $\beta = -1.0$ line but its presence is difficult to detect for the 4K and 8K volumes shown in Fig. 39 due to large finite-size effects. This evidence is suggestive, but further studies would be needed to verify the existence of a first-order transition at $\beta = -1.0$.

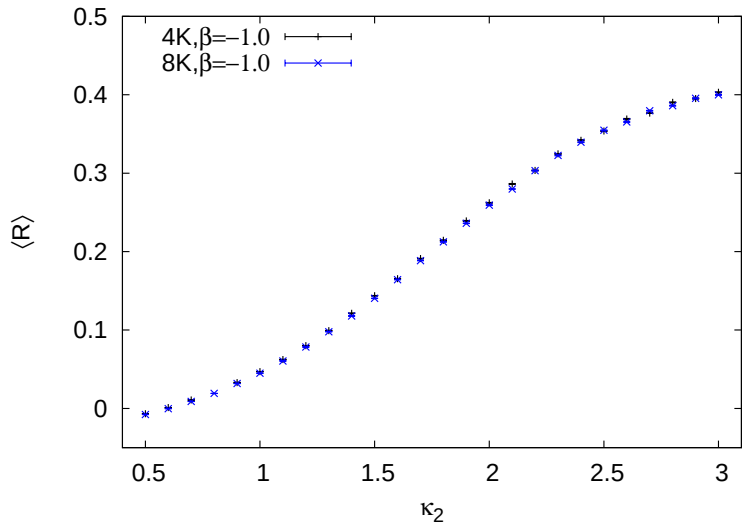

Figure 38: The average Regge curvature as a function of κ_2 for the 4K and 8K simplicial volumes at $\beta = -1.0$.

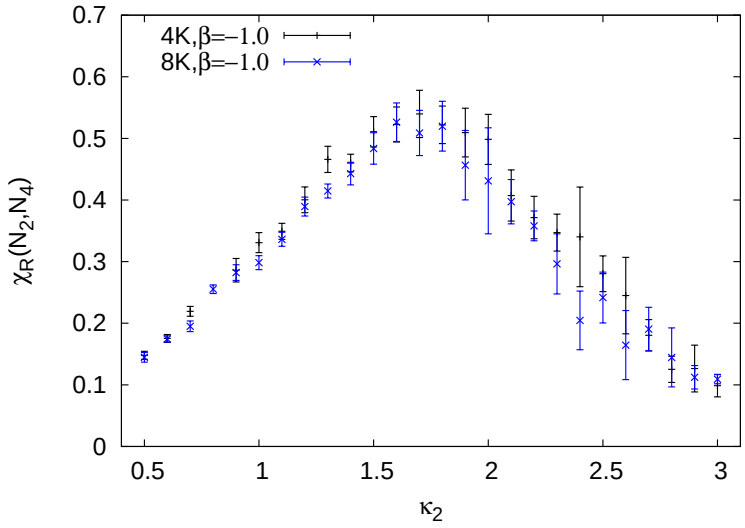

Figure 39: The curvature susceptibility χ_R as a function of κ_2 for the 4K and 8K simplicial volumes at $\beta = -1.0$.

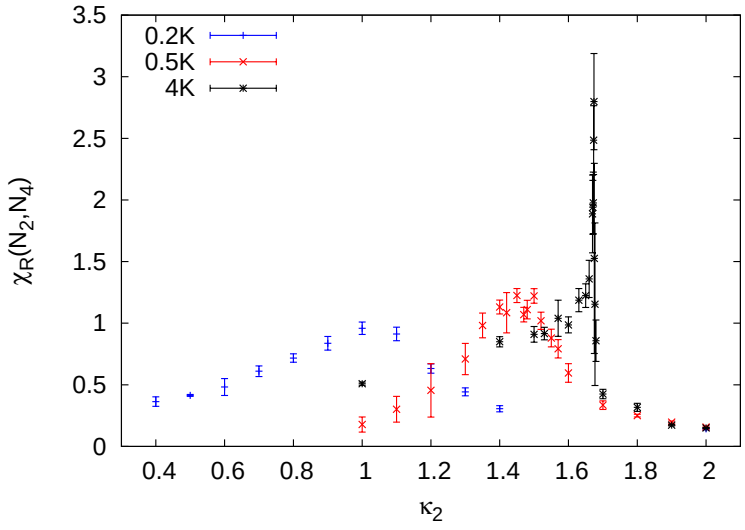

Figure 40: The curvature susceptibility χ_R as a function of κ_2 for 0.2K, 0.5K, and 4K simplicial volumes at $\beta = 0.0$. This plot shows that the order of the transition only becomes evident for sufficiently large lattice volumes.

5 The Crinkled Phase

5.1 Overview

Our aim in reviving the Euclidean version of dynamical triangulations with a non-trivial measure term is to investigate the possibility that there was a phase similar to the 4-dimensional semi-classical de Sitter phase found in Causal dynamical triangulations [102, 103]. The crinkled region of EDT is a candidate for a phase with extended 4-dimensional geometry.

In this section I present results for the volume-volume correlator and the running spectral dimension within the crinkled region of the EDT phase diagram. The results presented ultimately support the conclusion that the crinkled region behaves similar to the collapsed phase but with large finite-size effects and long autocorrelation lengths.

5.2 The volume-volume Correlator

The reader is briefly reminded of the definition of the volume-volume correlator given in Section 2.1, before results are presented and discussed for the volume-volume correlator within the crinkled phase.

We study the finite volume scaling behaviour of the volume-volume correlator similar to the one introduced in Ref. [77] to study the scaling of CDT,

$$C_{N_4}(\delta) = \sum_{\tau=1}^{t} \frac{\left\langle N_4^{\text{slice}}(\tau) N_4^{\text{slice}}(\tau+\delta) \right\rangle}{N_4^2}. \tag{58}$$

$N_4^{\text{slice}}(\tau)$ is the total number of 4-simplices in a spherical shell a geodesic distance τ from a randomly chosen simplex. N_4 is the total number of 4-simplices and the normalization of the correlator is chosen such that $\sum_{\delta=0}^{t-1} C_{N_4}(\delta) = 1$. If we rescale δ and $C_{N_4}(\delta)$, defining $x = \delta/N_4^{1/D_H}$, then the universal distribution $c_{N_4}(x)$ should be independent of the lattice volume, where $c_{N_4}(x) = N_4^{1/D_H} C_{N_4}\left(\delta/N_4^{1/D_H}\right)$. One can determine the fractal Hausdorff dimension, D_H, as the value that leaves $c_{N_4}(x)$ invariant under a change in four-volume N_4.

Figure 41 is a plot of the rescaled volume-volume correlator $c_{N_4}(x)$ as a function of x for $k_2 = 2.1$ and $\beta = -1.0$, for three different simplicial volumes 4K, 8K, and 12K. Here $c_{N_4}(x)$ is calculated with $D_H = 4.0$. The quantity $c_{N_4}(x)$ should be volume independent for a constant value of the Hausdorff dimension. However, as can be seen in Fig. 41 the peak height of $c_{N_4}(x)$ grows with volume, thus indicating that the Hausdorff dimension is inconsistent with $D_H = 4$, as is symptomatic of the collapsed phase. The crinkled

phase appears then to be similar to the collapsed phase but with larger finite-size effects and a lower acceptance rate.

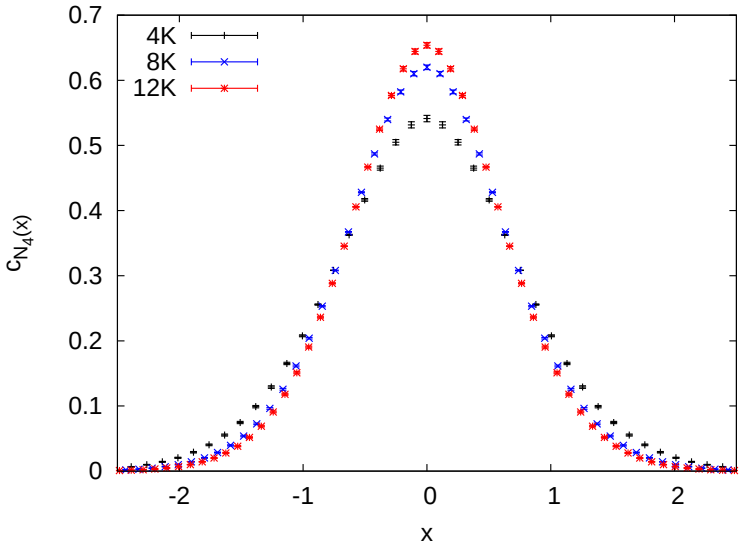

Figure 41: The volume-volume correlator as a function of the rescaled variable x for the volumes 4K, 8K, and 12K within the crinkled phase. $c_{N_x}(x)$ is calculated with a Hausdorff dimension $D_H = 4.0$. This plot suggests that the Hausdorff dimension in the crinkled phase grows with volume, or that $D_H \neq 4$, which is consistent with the collapsed phase.

5.3 The Spectral Dimension

Studies using causal dynamical triangulations [77] and independent studies using functional renormalization group methods [127] report that the spectral dimension exhibits a dimensional reduction as one probes smaller distance scales. We find that Euclidean dynamical triangulations with a non-trivial measure term in the path integral also exhibits a smooth dynamical dimensional reduction as a function of decreasing distance. We report that the spectral dimension D_S is greater than 4, and is possibly infinite in the infinite-volume limit, on large distance scales and runs to $D_S \sim 4/3$ at short distances within the crinkled phase. For negligible finite-size effects and lattice discretisation errors it is thought that the spectral dimension might have a universal functional form, which was originally suggested in Ref. [8] to be $D_s = a - \frac{b}{c+\sigma}$. The spectral dimension is determined within the crinkled phase for the 4K ensemble (Fig. 42), the 8K ensemble (Fig. 43), and the 12K ensemble (Fig. 44). The results imply that the

crinkled phase is unphysical in nature and similar to the collapsed phase, as evidenced by $D_S > 4$ in the large distance limit for all three volumes.

For the 4K ensemble we analysed $\sim 30,000$ (with the number of attempted moves set at $h = 10^8$) configurations using the average return probability given in Eq. (33). The statistical errors are determined from a single elimination jackknife procedure, as detailed in Section 3.9. The fit is to the functional form $D_s = a - \frac{b}{c+\sigma}$, where the constants a, b, and c are determined by the fit. The results of our preferred fit are $D_S(\infty) = 4.44 \pm 0.10$, and $D_S(0) = 1.471 \pm 0.014$.

For the 8K ensemble we analysed $\sim 70,000$ configurations. The fit to the 8K data gives $D_S(\infty) = 4.77 \pm 0.10$, and $D_S(0) = 1.464 \pm 0.010$.

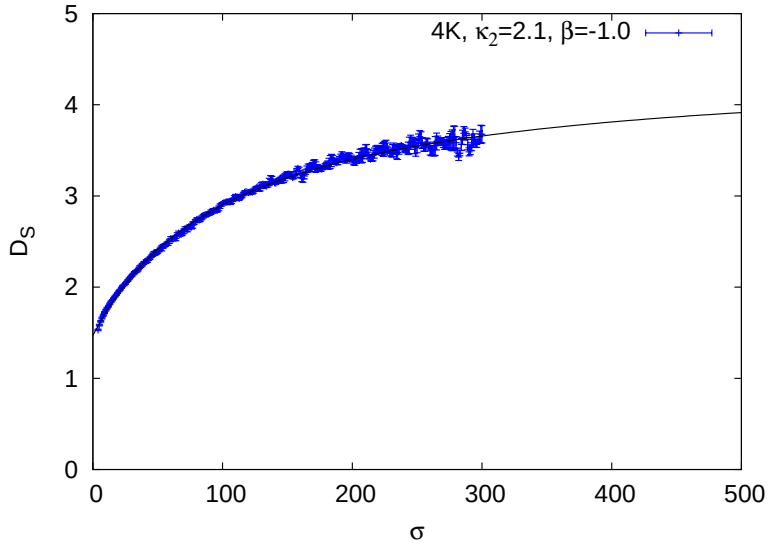

Figure 42: The spectral dimension as a function of diffusion time σ calculated for parameters $\kappa_2 = 2.1$ and $\beta = -1.0$ using an ensemble of 4,000 4-simplices.

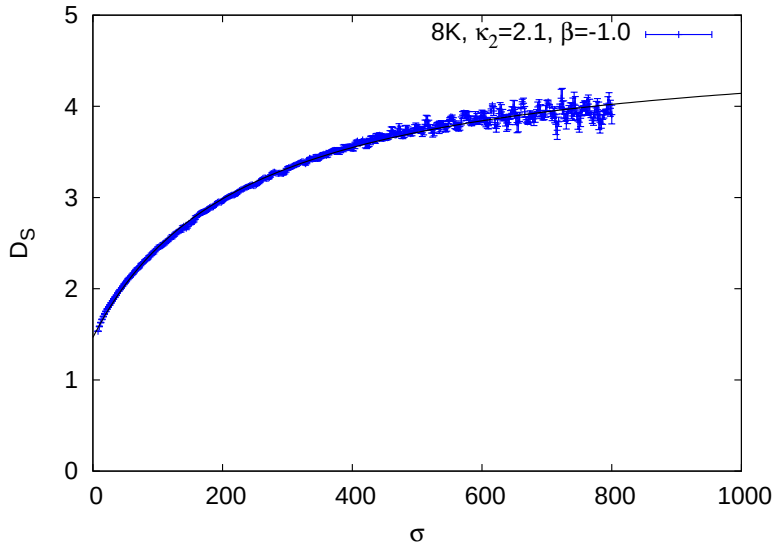

Figure 43: The spectral dimension as a function of diffusion time σ calculated for parameters $\kappa_2 = 2.1$ and $\beta = -1.0$ using an ensemble of 8,000 4-simplices.

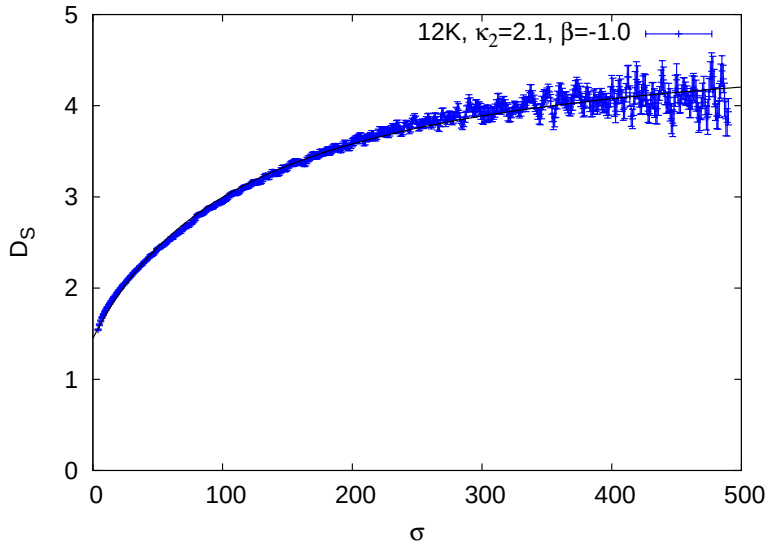

Figure 44: The spectral dimension as a function of diffusion time σ calculated for parameters $\kappa_2 = 2.1$ and $\beta = -1.0$ using an ensemble of 12,000 4-simplices.

For the 12K ensemble we analysed $\sim 40,000$ configurations. The fit to the 12K data gives $D_S(\infty) = 4.87 \pm 0.15$, and $D_S(0) = 1.464 \pm 0.024$. The errors quoted for $D_S(\sigma)$

for the 4K, 8K, and 12K simplicial volumes include estimations of the statistical error and not the systematic error.[14] The fit function assumes that the spectral dimension approaches a constant in the $\sigma \to \infty$ limit, and that $D_S(\sigma)$ is monotonic.[15]

Our conclusion in Ref. [109] that the crinkled phase of EDT is a physical semiclassical phase with 4-dimensional extended geometry, as based on our calculation of $D_S(\sigma)$ (see Fig. 47), most likely need to be revised due to improved estimates of finite-size effects and discretisation errors coming as a result of simulating with larger lattice volumes and over larger diffusion times. However, simulating with larger lattice volumes would give a clearer picture whether or not this is the case. Combining the 4K, 8K, and 12K spectral dimension curves into one plot (see Fig. 45) allows us to see that the spectral dimension increases beyond $D_S = 4$ and continues to grow with increasing lattice volume. The crinkled phase is therefore more akin to the unphysical collapsed phase than to a physical 4-dimensional phase.

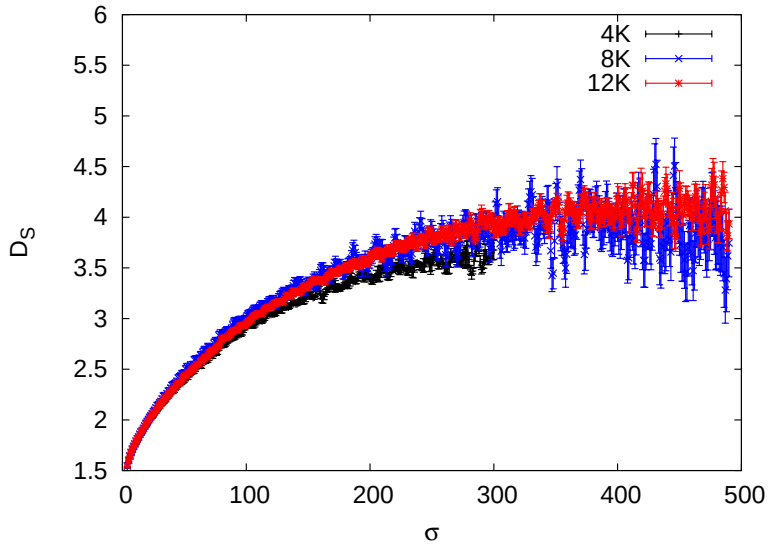

Figure 45: The spectral dimension as a function of diffusion time σ calculated for parameters $\kappa_2 = 2.1$ and $\beta = -1.0$ using 4K, 8K, and 12K 4-simplices.

In a lattice formulation of an asymptotically safe field theory, the fixed point would appear as a second-order critical point, the approach to which would define a continuum

[14] The range of σ values over which the fit function is applied is taken over the entire range of σ values and is not varied.

[15] Ref. [127] argues using renormalization group methods that there will be a long plateau at $\sim 4/3$ in D_S for small values of σ before D_S increases to 2 as $\sigma \to 0$. This finding questions the validity of the assumption that the running spectral dimension is monotonic for all σ.

limit. The divergent correlation length characteristic of a second-order phase transition would allow one to take the lattice spacing to zero while keeping observable quantities fixed in physical units. However, this is only possible within an extended semi-classical phase, which as this work shows probably does not exist for EDT with a non-trivial measure term.

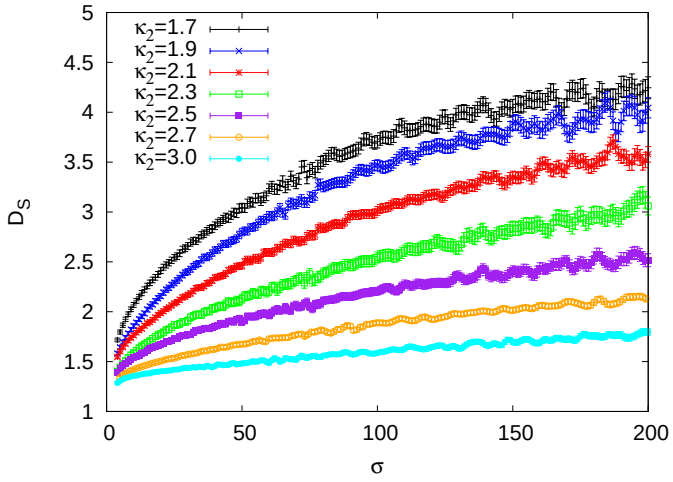

Figure 46: The spectral dimension as a function of diffusion time σ for five different values of κ_2 at $\beta = -1.0$. This data is calculated using 8,000 4-simplices.

Figure 46 shows the spectral dimension as a function of diffusion time for κ_2 =1.7, 1.9, 2.1, 2.3, 2.5, 2.7, and 3.0 with a fixed β value of -1.0. As one increases κ_2 along the $\beta = -1.0$ line the spectral dimension curves flatten out. If this were an extended phase one could conclude that increasing κ_2 means decreasing the lattice spacing a, because for larger κ_2 values it takes a greater number of diffusion steps before the same dimension is obtained. It is possible to rescale the diffusion time by a factor a until all the $D_S(\sigma)$ curves overlap.

We fit the $D_S(\sigma)$ curves for all seven κ_2 values shown in Fig. 46 to the functional form $a - \frac{b}{c+\sigma}$ first suggested in [8], where a, b, and c are determined by the fit. The small scale spectral dimension determined from the fit-function for each κ_2 value is shown in Table. 4. The errors associated with the $D_S(\sigma \to 0)$ measurements include the statistical error, with no estimation of the systematic error.[16] Table 4 suggests that the small scale spectral dimension tends to decrease as κ_2 is increased; possibly approaching

[16] Because we think the large scale spectral dimension goes to infinity in the collapsed phase it is difficult to estimate a systematic error.

κ_2	$D_S(\sigma \to 0)$
1.7	1.701 ± 0.026
1.9	1.327 ± 0.028
2.1	1.494 ± 0.010
2.3	1.510 ± 0.026
2.5	1.421 ± 0.012
2.7	1.347 ± 0.008
3.0	1.323 ± 0.009

Table 4: A table of the short distance spectral dimension $D_S(\sigma \to 0)$ for 7 different κ_2 values. $D_S(\sigma \to 0)$ is determined from a fit-function of the form $a - \frac{b}{c+\sigma}$ as first proposed in Ref. [8].

a minimum of $D_S = 4/3$ as κ_2 is taken to infinity. Figure 46 suggests that the spectral dimension curves also become weakly dependent on the diffusion time in the large κ_2 limit, approaching a constant that is consistent with $D_S \approx 4/3$. It is interesting to note that this is precisely the value of the spectral dimension of the branched polymer phase in EDT, and so it is possible that the value of the spectral dimension in the branched polymer phase acts as a lower bound for D_S within the crinkled phase. We have performed preliminary calculations using CDT that indicate that the spectral dimension in the branched polymer phase is consistent with $D_S = 3/2$[17], and so it is possible that this value could act as a lower bound on D_S in the extended phase of CDT.

[17]The value of the spectral dimension in the branched polymer phase of CDT does not necessarily have to be 4/3 because it can consist of branched polymers of a different class.

6 Asymptotic Safety and Holography

6.1 Short Distance Spectral Dimension in CDT

In four spacetime dimensions gravity is perturbatively nonrenormalizable. However, in spacetime dimensions of two or less gravity is power-counting renormalizable. If the dimensionality of spacetime were to decrease as one approaches the Planck scale one could in principle have a self-renormalizing quantum field theory of gravity.

Over the last decade a number of independent field-theoretic approaches to quantum gravity have reported a scale-dependent dimensionality. Exact renormalization group methods [79] and Hořava-Lifshitz gravity [80, 81] have both reported evidence of dynamical dimensional reduction. The two leading approaches to quantum gravity also report evidence for a dimensional reduction on short distance scales. The method of loop quantum gravity has reported a short distance scaling of the area spectrum, resulting in an effective dimension that is four-dimensional on macroscopic scales and two-dimensional on microscopic scales [82]. Atick and Witten showed in Ref. [83] that high-temperature string theory also behaves as if spacetime were two-dimensional. Furthermore, the effective graviton propagator appears to behave two-dimensionally as one approaches the Planck scale [84, 85, 79, 1]. Individually none of these independent approaches constitute substantial evidence in support of dynamical dimensional reduction; collectively however, they form a compelling argument. See Ref. [128] for an overview of theories that predict dimensional reduction on short distance scales.

The CDT approach to quantum gravity has produced some of the strongest evidence for dynamical dimensional reduction on short distance scales. The evidence in support of a scale-dependent spectral dimension from CDT is reviewed in this subsection.

In *Spectral Dimension of the Universe* Ambjorn et al. [8] present a result for the running spectral dimension using a fit to the functional form,

$$D_S(\sigma) = a - \frac{b}{c+\sigma}. \tag{59}$$

Where σ is the diffusion time, an effective measure of the distance scale probed by the diffusion process. The numerical coefficients of this fit were determined to be $a = 4.02$, $b = 119$, and $c = 54$. The physical significance of the particular fit function chosen by Ambjorn et al. (Eq. (59)) is not known from first principles, it is simply the functional form that best describes the dependence of the spectral dimension over the entire range of their data.[18] The work of Refs. [129, 130, 131, 132] have attempted to derive this

[18] The alternative fit functions considered in Ref. [8] were $a - b\mathrm{e}^{-c\sigma}$ and $a - \frac{b}{\sigma^c}$.

function from first principles using analytical methods.

The large scale spectral dimension for CDT is quoted as

$$D_S(\sigma \to \infty) = 4.02 \pm 0.10, \tag{60}$$

whilst the short distance spectral dimension is quoted as

$$D_S(\sigma \to 0) = 1.80 \pm 0.25. \tag{61}$$

The authors of [8] correctly claim that the value for $D_S(\sigma \to 0)$ is therefore consistent with the integer value two. However, large discretisation errors are typically associated with the small scale spectral dimension because for a small number of diffusion steps the behaviour of $D_S(\sigma)$ can be significantly different when considering an even or odd number of diffusion steps. This effect can be understood by considering a simplified diffusion process on a one-dimensional piecewise straight line; in this scenario it is impossible to begin and end at the origin after an odd number of diffusion steps, whereas this is not true for an even number of diffusion steps. A similar effect is present in 4-dimensional triangulations, although in this case the discrepancy between odd and even integer steps becomes negligible for sufficiently large σ values [8]. The relatively large error of Eq. (61) leaves some ambiguity in the conclusions that can be drawn from this result.

6.2 Argument Against Asymptotic Safety

There exists an argument against the possibility of asymptotic safety due to Banks [49, 50]. The argument compares the density of states at high energies expected for a theory of gravity to that of a conformal field theory. Since a renormalizable quantum field theory is a perturbation of a conformal field theory by relevant operators, a renormalizable field theory must have the same high energy asymptotic density of states as a conformal field theory. It follows from dimensional analysis, and the extensive scaling of the quantities considered, and the fact that a finite temperature conformal field theory has no dimensionful scales other than the temperature, that the entropy S and energy E scale as

$$S \sim (RT)^{d-1}, E \sim R^{d-1}T^d \tag{62}$$

where R is the radius of the spatial volume under consideration and T is the temperature. It follows that the entropy of a renormalizable theory must scale as

$$S \sim E^{\frac{d-1}{d}}. \tag{63}$$

For gravity, however, one expects that the high energy spectrum will be dominated by black holes. The 4-dimensional Schwarzschild solution in asymptotically flat spacetime has a black hole with event horizon of radius r_S given by,

$$r_S = \frac{2G_N M}{c^2}. \tag{64}$$

Extending this concept to arbitrary dimension d and defining natural units of $\hbar = c = 1$, we find that

$$r^{d-3} \sim G_N M \sim E, \tag{65}$$

where M is the mass of the black hole [19]. The Bekenstein-Hawking entropy in Planck units for a spherical (non-rotating) black hole is given by

$$S_{BH} = k_B \frac{\pi r_S^2}{l_P^2}, \tag{66}$$

and again generalising to arbitrary dimension d one obtains

$$S \sim r^{d-2}. \tag{67}$$

From equations (66) and (67) one obtains the following scaling of the entropy S as a function of the energy E,

$$S \sim E^{\frac{d-2}{d-3}}. \tag{68}$$

This scaling disagrees with that of Eq. (63) when $d = 4$. Assuming the validity of the assumptions in this argument, one is led to conclude that gravity cannot be formulated as a renormalizable quantum field theory. This is a potentially serious obstacle for the asymptotic safety programme.

Perccaci and Vacca in Ref. [73] have called into question the validity of the argument set forth by Banks [49] (see also Shomer [50]) against the possibility of the asymptotic safety scenario. They contend that because the argument of Banks and Shomer is dependent on semiclassical assumptions, particularly the assumptions regarding the semiclassical treatment of black holes, that a full quantum mechanical treatment in

[19] An interesting link between the functional renormalization group procedure for gravity in 4-dimensions and the 5-dimensional holographic renormalization group has been suggested in Ref. [133]

a regime where semiclassical arguments are not valid may lead to either significant corrections or to the complete invalidation of the argument.

Falls and Litim in Ref. [72] also critique the argument set forth by Banks and Shomer [49, 50]. They argue that the scaling relations of Eqs. (63) and (68) are incorrect for the class of black hole considered, due to the fact that R depends on the energy E of the black hole, whereas to obtain Eqs. (63) and (68) R must be treated as a constant. This leads to the entropy and energy density relation

$$\frac{S}{R^{d-1}} \sim \left(\frac{E}{R^{d-1}}\right)^{\nu}. \tag{69}$$

For a conformal field theory one then obtains the scaling behaviour

$$\nu_{CFT} = \frac{d-1}{d}. \tag{70}$$

Which is in disagreement with the scaling behaviour $S \sim E^{\frac{d-1}{d}}$ reported by Banks and Shomer [49, 50].[20]

We wish to highlight the fact that Eqs. (63) and (68) agree if, and only if, the spacetime dimension d is equal to 3/2. It is interesting to note that the short distance spectral dimension determined in Ref. [8] to be $D_S(\sigma \to 0) = 1.80 \pm 0.25$ is also consistent with 3/2, with the result being only 1.2 standard deviations from 3/2.[21] We have performed an independent preliminary calculation using CDT, which indicates that the short-distance spectral dimension of CDT is more consistent with $D_S(0) = 3/2$ than with $D_S(0) = 2$. If this result is confirmed it may resolve a long-standing argument against the possibility of the asymptotic safety scenario.

6.3 Short Distance Spectral Dimension in EDT

In our earlier work (Ref. [109]) we presented a result for the running spectral dimension of EDT in the crinkled phase of the EDT model we have been considering (see Fig. 47).

[20] For a semiclassical black hole one also obtains the scaling behaviour $\nu_{BH} = \frac{1}{2}$ for any dimension. This shows that semiclassical blackholes do not behave as conformal field theories, which can be seen from the fact that the Schwarzschild solution depends on the dimensionful quantity G_N. However, $\nu_{BH} = \nu_{CFT}$ precisely when G_N becomes dimensionless, i.e. at $d = 2$ [72].

[21] This counter-argument relies on the plausible assumption that the relevant dimension in the holographic scaling argument is also the spectral dimension, which was later shown to be valid in Ref. [134].

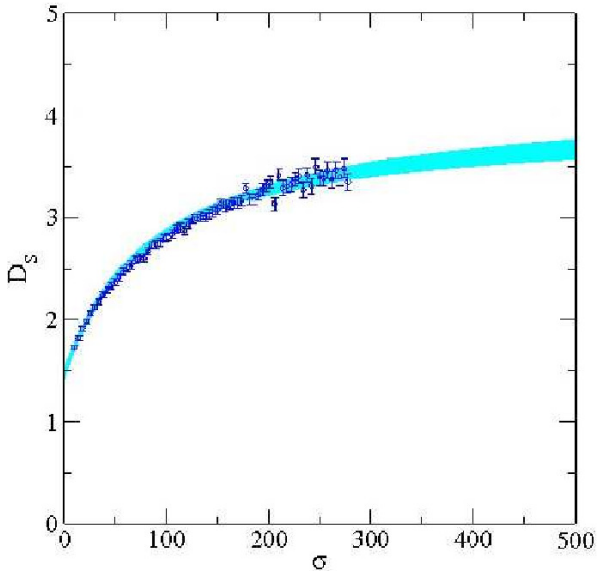

Figure 47: The spectral dimension as a function of diffusion time σ for $\kappa_2 = 2.1$ and $\beta = -1.0$ using 4,000 4-simplices. The plot includes a fit to Eq. (71). The width of the band shows the statistical error in the fit.

We obtained this result from an ensemble of degenerate triangulations with a volume of 4000 four-simplices. The simulation was performed for the bare parameters $\kappa_2 = 2.1$ and $\beta = -1.0$. We analysed ~ 1000 configurations using the average return probability of Eq. (33). The errors are determined from a single elimination jackknife procedure, as described in Subsection 3.9. Fluctuations were reduced by histogramming the data into bin sizes of two from $\sigma = 2 - 80$ and in bin sizes of four from $\sigma = 80 - 288$. The fit is to the same functional form suggested in Ref. [8], namely

$$D_S(\sigma) = a - \frac{b}{c + \sigma}, \tag{71}$$

with a, b, and c determined by the fit. The fit uses the full covariance matrix in the estimate of χ^2 with σ ranging from 10 to 146 in increments of 4, giving a $\chi^2/dof = 35/32$ and a confidence level (corrected for finite sample size) of CL=0.37. Variations of the fit function were used to estimate a systematic error on the asymptotic value of D_S, based on the assumptions that $D_S(\sigma)$ is a monotonic function.[22]

The results of our preferred fit in the earlier publication [109] are $D_S(\infty) = 4.04 \pm 0.26$, and $D_S(0) = 1.457 \pm 0.064$, where the errors include both the statistical error and

[22] Reuter and Saueressig in Ref. [127] use renormalization group methods to show that the spectral dimension should exhibit a long plateau at $\sim 4/3$ for small values of the diffusion time σ, and that as $\sigma \to 0$ the spectral dimension will increase again to $D_S = 2$, therefore predicting that the behaviour of the spectral dimension as a function of diffusion time is not monotonic, although this prediction may not be correct due to the truncation that is used.

a systematic error associated with varying the fit function and the fit range added in quadrature.[23] Calculations of the spectral dimension with combinatorial triangulations gave similar results, but required significantly larger lattice volumes.

New results for the spectral dimension at the same point in parameter space are presented in Section 5.3 for the 4K, 8K, and 12K ensembles. Extending our original calculation of the spectral dimension to include larger lattice volumes and simulating over longer periods of Monte Carlo time we observe that this point in parameter space has a macroscopic spectral dimension that is inconsistent with the integer 4, as discussed in Section 5.3. Furthermore, the Hausdorff dimension at this point is observed to increase beyond $D_H = 4$ with increasing simplicial volume, as shown in Fig. 41. This suggests that the crinkled phase is unphysical in nature and exhibits similar behaviour to the collapsed phase.

Since the version of EDT considered here does not appear to have a phase with a good semiclassical limit, it no longer makes sense to interpret the spectral dimension result as being physical. Section 5.3 presents results for $\kappa_2 = 2.1$ and $\beta = -1.0$ that give a short distance spectral dimension of $D_S(\sigma \to 0) \approx 3/2$ for the 4K, 8K, and 12K simplicial volumes, however $D_S(\sigma \to 0)$ can be made as small as $4/3$ in our EDT model by taking κ_2 large, as discussed in Section 5.3. Our argument that $D_S(\sigma \to 0) = 3/2$ would resolve the tension between asymptotic safety and the holographic principle is dependent on the existence of a physical phase[24], and not on our particular implementation of EDT, and so it is interesting to ask what the result for $D_S(\sigma \to 0)$ is in the CDT model; an approach that is known to have a physical phase.

If a suitable modification of EDT could be found that would lead to a semiclassical phase then an accurate determination of the short distance spectral dimension in this phase may have something concrete to say about the possibility of realising the asymptotic safety scenario. Furthermore, a study using CDT for finer lattices would resolve the debate over whether the short distance spectral dimension in the extended phase is more consistent with $D_S = 3/2$, or with the result claimed by the CDT group $D_S = 2$ [8].

[23] The alternative fit functions considered are those suggested in Ref. [8], namely $a - b\mathrm{e}^{-c\sigma}$ and $a - \frac{b}{\sigma^c}$.

[24] And on the assumption that R is a constant, see Ref. [72].

7 Summary and Conclusions

7.1 Summary

The main focus of this thesis is the phase structure and geometric properties of the parameter space of couplings defined via Euclidean dynamical triangulations with a non-trivial measure term included in the gravitational path integral.

In Section 1 the reader is introduced to the field of quantum gravity, explaining what quantum gravity is and some of the challenges that arise when trying to formulate such a theory. A possible solution is presented in the form of nonperturbative quantum gravity as defined via the asymptotic safety scenario. The simplicial approach to quantum gravity is then naturally motivated because of the possibility of testing the asymptotic safety scenario in a controlled and systematic way.

Simplicial quantum gravity is a viable candidate for a theory of quantum gravity. The geometrical observables in simplicial quantum gravity are introduced in Chapter 2, including the determination of the simplicial volume, the spectral dimension, and the Hausdorff dimension. Chapter 2 then focuses on Euclidean dynamical triangulations (EDT), which is also the central focus of this thesis. The approach of EDT is introduced via the Euclidean path integral and simplicial Einstein-Regge action, where the inclusion of a non-trivial measure term in our model is motivated. Some of the difficulties encountered in EDT are discussed before introducing causal dynamical triangulations (CDT) as a possible resolution. The essentials of CDT are introduced and the phase diagram discussed. The chapter ends with a brief discussion about generalising the approach of simplicial gravity to 4-dimensions.

Chapter 3 is devoted to the numerical implementation of EDT. The chapter discusses the Metropolis algorithm and the set of local update moves that update the simplicial geometry. The set of degenerate and combinatorial triangulations are introduced and their relative merits are discussed. The average Regge curvature is introduced as an order parameter for studying the phase diagram of EDT. An important aspect of any type of numerical implementation is checks of the code and testing the data output. Quantitative tests of our code against the literature are presented in Chapter 3, along with a discussion and analysis of how we check that our ensembles are thermalized. Sources of systematic and statistical errors are also discussed.

Chapter 4 focuses on the phase diagram of EDT, presenting evidence for the existence of a collapsed phase and branched polymer phase via a calculation of the volume-volume correlator and the running spectral dimension. For the point $\kappa_2 = 1.0$ and

$\beta = 0.0$ in parameter space the Hausdorff dimension and spectral dimension are found to increase beyond four as the simplicial volume increases, thus supporting the conclusion that this point lies within the collapsed phase of EDT. The Hausdorff dimension and the spectral dimension are also studied for $\kappa_2 = 3.0$ and $\beta = 0.2$; the results are consistent with the theoretically predicted values of the branched polymer phase. The first-order transition separating the branched polymer phase from the collapsed phase is studied by varying κ_2 for five different values of β. The existence of a first-order transition is demonstrated for $\beta = 0.2$ and $\beta = 0.0$, and evidence of a phase transition is also reported for 3 additional β values. This work is the first to demonstrate the existence of a first-order transition for $\beta \neq 0$ using degenerate triangulations in 4-dimensional EDT. In this work we also present the first ever constraints on the location of the first-order transition line in 4-dimensional EDT with a nontrivial measure. For sufficiently negative β the first-order transition line is seen to have a slight deviation from linearity for the 4K ensemble, which appears to become more pronounced with the larger 8K simplicial volume. Evidence for the existence of a crossover, or higher-order transition, separating the collapsed phase from the crinkled phase is presented, with the transition appearing to be a cross-over at $\beta = -1.0$.

Chapter 5 explores the crinkled phase of EDT. The volume-volume correlator and spectral dimension are calculated for the point $\kappa_2 = 2.1$ and $\beta = -1.0$, where D_H appears to grow with increasing volume, as does the spectral dimension. This indicates that the crinkled phase is unlikely to be a semiclassical phase with extended 4-dimensional geometry, and is more akin to the collapsed phase but with larger finite-size effects. However, it is difficult to determine whether or not this is the case because of large finite-size effects.

Chapter 6 focuses on a possible resolution of the argument by Banks [49] against the possibility of the asymptotic safety scenario. We argue that the tension between asymptotic safety and the holographic principle may be resolved by the dynamical dimensional reduction of the spectral dimension to 3/2 on small distance scales.

7.2 Conclusions

We have presented evidence that EDT with a non-trivial measure term has three phases; the branched polymer phase, the collapsed phase, and the crinkled phase. The branched polymer phase of EDT is found to have a spectral dimension that is consistent with $D_S = 4/3$ and a Hausdorff dimension that is consistent with $D_H = 2$. The collapsed phase of EDT is found to be consistent with $D_S \to \infty$ and $D_H \to \infty$ in the infinite

volume limit. The crinkled phase also appears consistent with $D_S \to \infty$ and $D_H \to \infty$ in the infinite volume limit, only in this phase the finite-size effects are significantly greater and it is therefore harder to demonstrate that this is the case.

This work constitutes the first detailed study of the phase diagram of EDT with a non-trivial measure term using degenerate triangulations. From this study we have demonstrated that EDT with a non-trivial measure does not contain a semiclassical phase with 4-dimensional extended geometry similar to that of CDT.

We have demonstrated the existence of a first-order phase transition for EDT with a non-trivial measure term using degenerate triangulations. Prior to this work no one has observed a first-order transition in EDT for $\beta \neq 0$ using degenerate triangulations.

We have presented an original resolution to the argument put forward by Banks and Shomer against the possibility of the asymptotic safety scenario, by noting that the tension between holographic entropy scaling and asymptotic safety is resolved if the spectral dimension undergoes a dynamical reduction to 3/2 on short distance scales. Although our EDT results are no longer compatible with this, preliminary results suggest that CDT may be.

This work demonstrates that EDT with a non-trivial measure does not contain a semiclassical 4-dimensional extended phase. However, such a phase does exist in CDT. It is therefore tempting to attribute the emergence of an extended phase to the causality condition itself. However, we ask whether there exists an alternative way of removing the unphysical degrees of freedom present in EDT? Or is there something unique about the causality condition? Unphysical degrees of freedom can typically be removed by introducing fictitious fields, called ghost fields [135, 136]. It is at least possible that EDT contains unphysical degrees of freedom that can be removed via the introduction of such ghost terms. The ghost terms may constrain the unphysical geometries presently observed in EDT in such a way as to allow an extended semiclassical phase to emerge. We emphasise that this is highly speculative, and that significant amounts of work are necessary to decide this issue.

8 Appendices

8.1 Code to Calculate χ_R and $< R >$ and Errors

The order parameter $< R >$ and its derivative χ_R are dependent on the variables N_2 and N_4 (see Eqs. (54) and (55)). The first step in the numerical calculation of $< R >$ and χ_R is to extract N_2 and N_4 for each sweep (where a sweep is defined as 10^8 attempted update moves), and send them to the respective arrays `N2sus[m]` and `N4sus[m]`.

```
infile input1(file[nfiles-1]);
for(int j(initConfig[nfiles-1]); j<finalConfig; j++)
 {if(j==initConfig[nfiles-1])
  {input1.find("update");}
  input1 >> N4sus[m];
  input1 >> N2sus[m];
  m++;}
```

The ratio of N_2 to N_4 (`Ravg[sus]`) and its square `R2avg[sus]` are then determined.

```
for(int j(initConfig[0]); j<nConfig + initConfig[0]; j++)
 {int sus(j-initConfig[0]);
  R2avg[sus] = (N2sus[sus]/N4sus[sus])*(N2sus[sus]/N4sus[sus]);
  Ravg[sus] = N2sus[sus]/N4sus[sus];}
```

In order to accurately estimate the statistical errors associated with a measurement we block the data to reduce statistical correlations and then apply a jackknife to the data via an imported library.

```
for(int j(0); j<nConfig/block; j++)
 {for(int lblock(0); lblock<block; lblock++)
  {R2avg_b[j] += R2avg[block*j+lblock];
   Ravg_b[j] += Ravg[block*j+lblock];}
  R2avg_b[j] = R2avg_b[j]/block;
  Ravg_b[j] = Ravg_b[j]/block;}
jackknife(R2avg_b);
jackknife(Ravg_b);
```

The average Regge curvature `R[sus]` and the curvature susceptibility `Suscept[sus]` are then calculated via,

```
R[sus] = 0.47668*Ravg_b[sus]-1.0;
Suscept[sus]=N4f*(R2avg_b[sus]-(Ravg_b[sus])*(Ravg_b[sus]));
```

where the multiplicative constant factor in the expression is just $\frac{1}{\rho}$ as defined by Eq. (54), and `N4f` is the number of 4-simplices.

As discussed in Section 3.9 the data is blocked into bins of size N/n, where N is the total number of configurations and n is some positive integer greater than or equal to 2, thus giving the factors of N. It is necessary to calculate $< R >$ and χ_R for all possible factors of N so as to determine the block size at which the statistical error is maximised, meaning that the correlation between blocks of data is minimised. To achieve this I determine the difference between the final configuration number `finalConfigNoP` and the initial configuration number `startnofrst` and divide by an integer `n` that is incrementally increased inside a while loop.[25]

```
frst=$(head -n22 /scratch/tenon/dcoumbe/logfiles_${volume}_k${k2}_h${k6}/logdeg_$
filefrst=${frst%.*}
startnofrst=${filefrst#*:}
block=$((($finalConfigNoP-$startnofrst)/(1+$n)))
echo "${block}" > Block.dat
```

For each blocking value a different value of $< R >$ and χ_R are output by the code. The value of $< R >$ and χ_R for which the statistical error is maximised is accepted as the value with the most reliable estimate of the statistical error.

8.2 Code to Determine Histogram and Monte Carlo Evolution of N_0

A useful procedure in determining the order of a phase transition in dynamical triangulations is to determine how the number of vertices changes as a function of Monte Carlo time t_{MC}. A discontinuous transition between two metastable phases, for example, is characterised by the discontinuous transition between two values of N_0. For a first-order transition these meta-stable transitions lead to a double Gaussian in the histogram of N_0 whose peak separation grows with volume. This section discusses the code that is used to determine $N_0(t_{MC})$ and its histogram.

[25] The code determining the blocking factor N/n is a shell script written in the bash programming language. This shell script enables the extraction and insertion of parameters into the C++ script without the need for recompiling and is thus faster to implement.

Firstly, N_0 is extracted from the generated lattice configuration, and sent to an array `N0(nConfig)`.

```
for(int j(initConfig); j<nConfig + initConfig; j++)
 {input1 >> dumb1;
  for(int i(0); i<9; i++)
   {input1 >> dumb2;}
  input1 >> N0[j-initConfig];
 }
```

For a first-order transition the peak separation should grow approximately linearly with simplicial volume. Therefore, by dividing the number of vertices N_0 by the number of 4-simplices N_4 the peak separation should remain constant as a function of volume if a first-order transition is present. A for-loop is implemented to cycle over the entire number of configurations `nConfig` and the ratio of the number of vertices `N0[j]` to the simplicial volume `Vol` is output as a function of configuration number.

```
for(int j(0); j<nConfig; j++)
 {outdat1 << j+initConfig << " " << N0[j]/Vol << endl;}
```

The histogram of N_0 is determined by first defining an array of bins `bin[i]` with a number of elements equal to the total number of configurations to be analysed, thus giving a bin size of unity. The extracted values of N_0 are cycled through in a for-loop and the frequency with which each value of N_0 appears is counted by incrementing the array `bin[i]`.

```
for (int i=nBinsMin; i<nBins; i++)
 {for(int z(initConfig); z<nConfig + initConfig; z++)
  {if(N0[z-initConfig]==i)
   {bin[i]+=1;}}
 }
```

For a first-order transition the peak separation in the histogrammed data should grow approximately linearly with simplicial volume, therefore by dividing the number of vertices N_0 by the number of 4-simplices N_4 the peak separation should remain constant as a function of volume if a first-order transition is present. A for-loop is implemented to cycle over the entire number of configurations `nConfig` and the frequency with which the particular value of N_0 appears `bin[i]` is output along with the ratio of the number of vertices to the simplicial volume `z/Vol`.

```
for(int z=nBinsMin, i=nBinsMin ; z<nBinsMin + nConfig + initConfig
&& i<nBins; z++, i++ )
 {outdat1<<z/Vol<<" "<<bin[i]<<endl;}
```

8.3 Conformal Instability of the Euclidean Action

One of the major obstacles to formulating a Euclidean theory of quantum gravity is that the Euclidean action for Einstein gravity is unbounded from below. This section will outline this problem and discuss some of the ideas that have been proposed to resolve this issue.

To motivate the desire to Euclideanize the Lorentzian Einstein action and to highlight the fact that it is unbound from below we take a simple interacting scalar field theory as an example. The expectation value of an observable O for a scalar field theory is given by the path integral

$$\langle O \rangle = \frac{1}{Z} \int O[\phi] e^{iS[\phi]} [d\phi] \tag{72}$$

Where the action is the functional

$$S[\phi] = \int dt \int d^3x \left(\left(\frac{\partial \phi}{\partial t} \right)^2 - (\nabla \phi)^2 - V(\phi) \right). \tag{73}$$

When performing computations it is not clear how one would directly evaluate the observable O numerically using the path integral of Eq. (72) because it contains complex oscillatory factors e^{iS}. In order to make computations tractable one typically performs a change of variables of the type $t \to -i\tau$ such that the Lorentzian action transforms into the Euclidean action,

$$S_{Eucl}[\phi] = \int d\tau \int d^3x \left(\left(\frac{\partial \phi}{\partial \tau} \right)^2 + (\nabla \phi)^2 + V(\phi) \right). \tag{74}$$

The oscillatory factor e^{iS} appearing in the path integral is then transformed into e^{-S_E}, giving a path integral that is damped as opposed to being oscillatory, in addition to being amenable to numerical simulations. The Euclidean action given in Eq. (74) is positive definite for positive definite interaction potentials $V(\phi)$ [137]. However, the problem arises due to the gravitational interaction potential being negative in general relativity. The reason is that although gravitational waves have a positive energy, the gravitational potential is always negative because gravity is always attractive [138].

The fundamental degrees of freedom in general relativity are given by the metric $g_{\mu\nu}$. General relativity is diffeomorphism invariant and so one is free to transform the metric $g_{\mu\nu}$ via a conformal transformation. Any two metrics $g_{\mu\nu}$ and $h_{\mu\nu}$ are said to be conformally equivalent if $g_{\mu\nu} = \Omega h_{\mu\nu}$ where Ω is some positive conformal factor. Following Ref. [138] we make a conformal transformation $g_{\mu\nu} = \Omega^2 h_{\mu\nu}$, where once again Ω is some positive conformal factor. The Einstein action then becomes

$$S_E\left(h_{\mu\nu}\right) = -\frac{1}{16\pi G}\int d^4x\sqrt{\det\left(\mathrm{g}_{\mu\nu}\right)}\left(\Omega^2 R + 6g^{\mu\nu}\partial_\mu\Omega\partial_\nu\Omega\right). \tag{75}$$

One can see from Eq. (75) that the Einstein action can be made arbitrarily negative if the conformal factor Ω is rapidly varying.

This means that the Euclidean Einstein action is unbounded from below and that the path integral of Eq. (75) could be divergent, depending on the behaviour of the gravitational measure in the strong field limit and in the regime of rapidly varying conformal factors Ω [139].

The *positive energy conjecture* outlined in Refs. [140, 141] seems to suggest that the total energy of an asymptotically flat gravitational field as measured at infinity is always positive, and that the formation of black holes in regions of arbitrarily negative potentials prevents such scenarios from being physically realised [138]. If Euclidean general relativity is to accurately describe reality one would need to mathematically prevent the conformal instability appearing in the Euclidean action. A number of possible solutions to the unboundedness problem of the gravitational action have been put forward, most notably those of Gibbons, Hawking and Perry [142, 143]. The conformal instability of the Euclidean gravitational action was shown in Refs. [144, 145] to cancel, at least to one-loop in perturbation theory [139], and possibly nonperturbatively [140].

Because the Euclidean path integral is unbounded from below one may ask whether Euclidean dynamical triangulations is a well defined theory at all. This is a legitimate concern because the partition function can become dominated by lattice configurations with arbitrarily large curvature. However, the hope is that by introducing an appropriate measure term into the Euclidean action one can suppress the contributions coming from configurations with arbitrarily large curvature, thus making the gravitational path integral convergent.

9 References

References

[1] Daniel F. Litim. Fixed points of quantum gravity. *Phys.Rev.Lett.*, 92:201301, 2004.

[2] O. Lauscher and M. Reuter. Ultraviolet fixed point and generalized flow equation of quantum gravity. *Phys.Rev.*, D65:025013, 2002.

[3] Wataru Souma. Nontrivial ultraviolet fixed point in quantum gravity. *Prog.Theor.Phys.*, 102:181–195, 1999.

[4] Max Niedermaier and Martin Reuter. The asymptotic safety scenario in quantum gravity. *Living Reviews in Relativity*, 9(5), 2006.

[5] Jan Ambjorn, S. Jordan, J. Jurkiewicz, and R. Loll. Second- and First-Order Phase Transitions in CDT. *Phys.Rev.*, D85:124044, 2012.

[6] J. Ambjorn, A. Goerlich, J. Jurkiewicz, and R. Loll. Nonperturbative Quantum Gravity. *Phys.Rept.*, 519:127–210, 2012.

[7] Bas V. de Bakker and Jan Smit. Curvature and scaling in 4-d dynamical triangulation. *Nucl.Phys.*, B439:239–258, 1995.

[8] J. Ambjorn, J. Jurkiewicz, and R. Loll. Spectral dimension of the universe. *Phys.Rev.Lett.*, 95:171301, 2005.

[9] Albert Einstein. On the General Theory of Relativity. *Sitzungsber.Preuss.Akad.Wiss.Berlin (Math.Phys.)*, 1915:778–786, 1915.

[10] S.W. Hawking and W. Israel. General Relativity, an Einstein Centenary Survey. pages 1–23, 1979.

[11] M. Kramer, Ingrid H. Stairs, R.N. Manchester, M.A. McLaughlin, A.G. Lyne, et al. Tests of general relativity from timing the double pulsar. *Science*, 314:97–102, 2006.

[12] M. Chaichian and A. Demichev. Path Integrals in Physics. *Institute of Physics, Series in Mathematical and Computational Physics*, page 688, 2001.

[13] P.A.M. Dirac. The Lagrangian in Quantum Mechanics. *Physikalische Zeitschrift der Sowjetunion* **3**, pages 64–72, 1933.

[14] R.P. Feynman and A.R. Hibbs. Quantum Mechanics and Path Integrals. *New York: McGraw-Hill*, 1965.

[15] Jan Ambjorn, J. Jurkiewicz, and R. Loll. A Nonperturbative Lorentzian path integral for gravity. *Phys.Rev.Lett.*, 85:924–927, 2000.

[16] D. Hanneke, S. Fogwell Hoogerheide, and G. Gabrielse. Cavity Control of a Single-Electron Quantum Cyclotron: Measuring the Electron Magnetic Moment. 2010.

[17] T. Aoyama, M. Hayakawa, T. Kinoshita, and M. Nio. Revised value of the eighth-order QED contribution to the anomalous magnetic moment of the electron. *Phys.Rev.*, D77:053012, 2008.

[18] Carlo Rovelli. Notes for a brief history of quantum gravity. pages 742–768, (arXiv:gr-qc/0006061), 2000.

[19] E. Einstein. Naeherungsweise Integration der Feldgleichungen der Gravitation. *Preussische Akademie der Wissenschaften (Berlin) Sitzungsberichte*, page 688, 1916.

[20] O. Klein. Zur funfdimensionalen Darstellung der Relativitaetstheorie. *Zeitscrift feur Physik 46*, (1927)188.

[21] M. Fierz and W. Pauli. *Hel Phys Acta 12*, (1939)297.

[22] W. Pauli and M. Fierz. On Relativistic Field Equations of Particles with Arbitrary Spin in an Electromagnetic Field. *Helv.Phys.Acta*, 12:297–300, 1939.

[23] D.I. Blokhintsev and F.M. Gal'perin. Pod znamenem marxisma 6. (1934)147.

[24] W. Heisenberg. *Z Physik 110*, (1938)251.

[25] Charles W. Misner. Feynman quantization of general relativity. *Rev.Mod.Phys.*, 29:497–509, 1957.

[26] Bryce S. DeWitt. Quantum Theory of Gravity. 1. The Canonical Theory. *Phys.Rev.*, 160:1113–1148, 1967.

[27] S.W. Hawking. Particle Creation by Black Holes. *Commun.Math.Phys.*, 43:199–220, 1975.

[28] S.A. Fulling. Nonuniqueness of Canonical Field Quantization in Riemannian Space-Time. *Phys.Rev.*, D7:2850, 1973.

[29] P.C.W. Davies. Scalar particle production in Schwarzschild and Rindler metrics. *J.Phys.*, A8:609–616, 1975.

[30] W.G. Unruh. Notes on black hole evaporation. *Phys.Rev.*, D14:870, 1976.

[31] John F. Donoghue. Introduction to the effective field theory description of gravity. 1995.

[32] Marc H. Goroff and Augusto Sagnotti. The Ultraviolet Behavior of Einstein Gravity. *Nucl.Phys.*, B266:709, 1986.

[33] John Donoghue. Perturbative dynamics of quantum general relativity. pages 26–39, 1997.

[34] Steven Weinberg. General Relativity, an Einstein Centenary Survey. 1997.

[35] K.S. Stelle. Renormalization of Higher-Derivative Quantum Gravity. *Phys.Rev.*, D16:953–969, 1977.

[36] Stephen P. Martin. A Supersymmetry primer. *Perspectives on sypersymmetry 2*, 1-153.

[37] Peter Van. Nieuwenhuizen. Supergravity. *North-Holland Publishing Company*, (1981).

[38] Horatiu Nastase. Introduction to Supergravity. (arXiv:hep-th/1112.3502), 2011.

[39] Schwarz J. H. Witten E. Green, M. B. Superstring Theory. *Cambridge University Press*, page Vol.1 and 2, 1987.

[40] J. Polchinski. String Theory. *Cambridge University Press*, 1987.

[41] Andrew Strominger and Cumrun Vafa. Microscopic origin of the Bekenstein-Hawking entropy. *Phys.Lett.*, B379:99–104, 1996.

[42] Gary T. Horowitz. Quantum states of black holes. (arXiv:gr-qc/9704072), 1996.

[43] Amanda W. Peet. TASI lectures on black holes in string theory. pages 353–433, 2000.

[44] Juan Martin Maldacena and Andrew Strominger. Black hole grey body factors and d-brane spectroscopy. *Phys.Rev.*, D55:861–870, 1997.

[45] Lee Smolin. How far are we from the quantum theory of gravity? (arXiv:hep-th/0303185), 2003.

[46] Joseph Polchinski. Quantum gravity at the Planck length. *eConf*, C9808031:08, 1998.

[47] Ernesto Frodden, Amit Ghosh, and Alejandro Perez. Black hole entropy in LQG: Recent developments. *AIP Conf.Proc.*, 1458:100–115, 2011.

[48] Eugenio Bianchi, Leonardo Modesto, Carlo Rovelli, and Simone Speziale. Graviton propagator in loop quantum gravity. *Class.Quant.Grav.*, 23:6989–7028, 2006.

[49] Tom Banks. TASI Lectures on Holographic Space-Time, SUSY and Gravitational Effective Field Theory. 2010.

[50] Assaf Shomer. A Pedagogical explanation for the non-renormalizability of gravity. 2007, arXiv/0709.3555.

[51] K. G. Wilson. Confinement of quarks. *prd*, 10:2445–2459, oct 1974.

[52] Rajan Gupta. Introduction to lattice QCD: Course. pages 83–219, 1997.

[53] Rajan Gupta. Lattice QCD. *AIP Conf.Proc.*, 490:3–9, 1999.

[54] S. Hashimoto, J. Laiho, and S.R. Sharpe. Lattice Quantum Chromodynamics. *Particle Data Group*, 17, 2011.

[55] Simon Catterall. Supersymmetric lattices. 2010, hep-lat/1005.5346.

[56] Biagio Lucini. Strongly Interacting Dynamics beyond the Standard Model on a Spacetime Lattice. *Phil.Trans.Roy.Soc.Lond.*, A368:3657–3670, 2010.

[57] E. Stueckelberg and A. Petermann. La renormalisation des constants dans la theorie de quanta. *Helv. Phys. Acta 26, 499*, (1953).

[58] M. Gell-Mann and F.E. Low. Quantum Electrodynamics at Small Distances. *Physical Review*, 95:1300–1312, 1954.

[59] Roberto Percacci. Asymptotic Safety. 2007, hep-th/0709.3851.

[60] Marianne Heilmann, Daniel F. Litim, Franziska Synatschke-Czerwonka, and Andreas Wipf. Phases of supersymmetric O(N) theories. *Phys.Rev.*, D86:105006, 2012.

[61] Daniel F. Litim, Marianne C. Mastaler, Franziska Synatschke-Czerwonka, and Andreas Wipf. Critical behavior of supersymmetric O(N) models in the large-N limit. *Phys.Rev.*, D84:125009, 2011.

[62] R. Percacci and A. Eichhorn. What is asymptotic safety. *www.percacci.it/roberto/physics/as/faq.html*, 2012.

[63] Alessandro Codello, Roberto Percacci, and Christoph Rahmede. Ultraviolet properties of f(R)-gravity. *Int.J.Mod.Phys.*, A23:143–150, 2008.

[64] Alessandro Codello, Roberto Percacci, and Christoph Rahmede. Investigating the Ultraviolet Properties of Gravity with a Wilsonian Renormalization Group Equation. *Annals Phys.*, 324:414–469, 2009.

[65] Dario Benedetti, Pedro F. Machado, and Frank Saueressig. Asymptotic safety in higher-derivative gravity. *Mod.Phys.Lett.*, A24:2233–2241, 2009.

[66] K. Falls, D.F. Litim, K. Nikolakopoulos, and C. Rahmede. A bootstrap towards asymptotic safety. 2013.

[67] Daniel F. Litim. Renormalisation group and the Planck scale. *Phil.Trans.Roy.Soc.Lond.*, A369:2759–2778, 2011.

[68] Daniel F. Litim and Dario Zappala. Ising exponents from the functional renormalisation group. *Phys.Rev.*, D83:085009, 2011.

[69] Daniel F. Litim. Optimized renormalization group flows. *Phys.Rev.*, D64:105007, 2001.

[70] Peter Fischer and Daniel F. Litim. Fixed points of quantum gravity in extra dimensions. *Phys.Lett.*, B638:497–502, 2006.

[71] Jan Ambjorn, B. Durhuus, and T. Jonsson. Quantum geometry. A statistical field theory approach. 1997.

[72] Kevin Falls and Daniel F. Litim. Black hole thermodynamics under the microscope. 2012.

[73] Roberto Percacci and Gian Paolo Vacca. Asymptotic Safety, Emergence and Minimal Length. *Class.Quant.Grav.*, 27:245026, 2010.

[74] T. Regge. General Relativity Without Coordinates. *Nuovo Cim.*, 19:558–571, 1961.

[75] Sarp Akcay and Richard A. Matzner. Kerr-de Sitter Universe. *Class.Quant.Grav.*, 28:085012, 2011.

[76] F. Hausdorff. Dimension und ueres Ma. *Mathematische Annalen 79 (1-2)*, page 157179, 1919.

[77] J. Ambjorn, J. Jurkiewicz, and R. Loll. Reconstructing the universe. *Phys.Rev.*, D72:064014, 2005.

[78] Dario Benedetti and Joe Henson. Spectral geometry as a probe of quantum spacetime. *Phys.Rev.*, D80:124036, 2009.

[79] O. Lauscher and M. Reuter. Fractal spacetime structure in asymptotically safe gravity. *JHEP*, 0510:050, 2005.

[80] J. Ambjorn, A. Gorlich, S. Jordan, J. Jurkiewicz, and R. Loll. CDT meets Hořava-Lifshitz gravity. *Phys.Lett.*, B690:413–419, 2010.

[81] Petr Hořava. Spectral Dimension of the Universe in Quantum Gravity at a Lifshitz Point. *Phys.Rev.Lett.*, 102:161301, 2009.

[82] Leonardo Modesto. Fractal Structure of Loop Quantum Gravity. *Class.Quant.Grav.*, 26:242002, 2009.

[83] Joseph J. Atick and Edward Witten. The Hagedorn Transition and the Number of Degrees of Freedom of String Theory. *Nucl.Phys.*, B310:291–334, 1988.

[84] M. Niedermaier. The Asymptotic safety scenario in quantum gravity: An Introduction. *Class.Quant.Grav.*, 24:R171–230, 2007.

[85] M. Reuter and Frank Saueressig. Renormalization group flow of quantum gravity in the Einstein-Hilbert truncation. *Phys.Rev.*, D65:065016, 2002.

[86] Jan Ambjorn, B. Durhuus, and J. Frohlich. Diseases of Triangulated Random Surface Models, and Possible Cures. *Nucl.Phys.*, B257:433, 1985.

[87] V.A. Kazakov, Alexander A. Migdal, and I.K. Kostov. Critical Properties of Randomly Triangulated Planar Random Surfaces. *Phys.Lett.*, B157:295–300, 1985.

[88] Jan Ambjorn. Strings, quantum gravity and noncommutative geometry on the lattice. *Nucl.Phys.Proc.Suppl.*, 106:62–70, 2002.

[89] Jan Ambjorn and Steen Varsted. Three-dimensional simplicial quantum gravity. *Nucl.Phys.*, B373:557–580, 1992.

[90] M.E. Agishtein and Alexander A. Migdal. Three-dimensional quantum gravity as dynamical triangulation. *Mod.Phys.Lett.*, A6:1863–1884, 1991.

[91] D.V. Boulatov and A. Krzywicki. On the phase diagram of three-dimensional simplicial quantum gravity. *Mod.Phys.Lett.*, A6:3005–3014, 1991.

[92] Jan Ambjorn and Jerzy Jurkiewicz. Four-dimensional simplicial quantum gravity. *Phys.Lett.*, B278:42–50, 1992.

[93] M.E. Agishtein and Alexander A. Migdal. Simulations of four-dimensional simplicial quantum gravity. *Mod.Phys.Lett.*, A7:1039–1062, 1992.

[94] Jan Ambjorn and J. Jurkiewicz. Scaling in four-dimensional quantum gravity. *Nucl.Phys.*, B451:643–676, 1995.

[95] S. Catterall, John B. Kogut, and R. Renken. Phase structure of four-dimensional simplicial quantum gravity. *Phys.Lett.*, B328:277–283, 1994.

[96] H.S. Egawa, T. Hotta, T. Izubuchi, N. Tsuda, and T. Yukawa. Scaling behavior in 4-D simplicial quantum gravity. *Prog.Theor.Phys.*, 97:539–552, 1997.

[97] Bas V. de Bakker. Further evidence that the transition of 4-D dynamical triangulation is first order. *Phys.Lett.*, B389:238–242, 1996.

[98] P. Bialas, Z. Burda, A. Krzywicki, and B. Petersson. Focusing on the fixed point of 4-D simplicial gravity. *Nucl.Phys.*, B472:293–308, 1996.

[99] Bernd Bruegmann and Enzo Marinari. 4-d simplicial quantum gravity with a nontrivial measure. *Phys.Rev.Lett.*, 70:1908–1911, 1993.

[100] S. Bilke, Z. Burda, A. Krzywicki, B. Petersson, J. Tabaczek, et al. 4-D simplicial quantum gravity: Matter fields and the corresponding effective action. *Phys.Lett.*, B432:279–286, 1998.

[101] Bas V. De Bakker and Jan Smit. Volume dependence of the phase boundary in 4-D dynamical triangulation. *Phys.Lett.*, B334:304–308, 1994.

[102] Jan Ambjorn and R. Loll. Nonperturbative Lorentzian quantum gravity, causality and topology change. *Nucl.Phys.*, B536:407–434, 1998.

[103] J. Ambjorn, A. Gorlich, J. Jurkiewicz, and R. Loll. The Nonperturbative Quantum de Sitter Universe. *Phys.Rev.*, D78:063544, 2008.

[104] J. Ambjorn, A. Gorlich, J. Jurkiewicz, and R. Loll. Planckian Birth of the Quantum de Sitter Universe. *Phys.Rev.Lett.*, 100:091304, 2008.

[105] Hildegard Meyer-Ortmanns. Phase transitions in quantum chromodynamics. *Rev.Mod.Phys.*, 68:473–598, 1996.

[106] Petr Hořava. Quantum Gravity at a Lifshitz Point. *Phys.Rev.*, D79:084008, 2009.

[107] Jan Ambjorn, Lisa Glaser, Yuki Sato, and Yoshiyuki Watabiki. 2d CDT is 2d Hořava-Lifshitz quantum gravity. 2013.

[108] Fotini Markopoulou and Lee Smolin. Gauge fixing in causal dynamical triangulations. *Nucl.Phys.*, B739:120–130, 2006.

[109] J. Laiho and D. Coumbe. Evidence for Asymptotic Safety from Lattice Quantum Gravity. *Phys.Rev.Lett.*, 107:161301, 2011.

[110] Jack Laiho and Daniel Coumbe. Asymptotic safety and lattice quantum gravity. *PoS*, LATTICE2011:005, 2011.

[111] Daniel Coumbe and Jack Laiho. Exploring the Phase Diagram of Lattice Quantum Gravity. *PoS*, LATTICE2011:334, 2011.

[112] Sergio Caracciolo and Andrea Pelissetto. Analysis of the Critical Behavior of de Sitter Quantum Gravity on a Hypercubic Lattice. *Phys.Lett.*, B193:237, 1987.

[113] Alun George. Five-dimensional dynamical triangulations. *Ph.D thesis*, (arXiv:hep-lat/9909033), 1999.

[114] Jan Ambjorn and Timothy G. Budd. Trees and spatial topology change in CDT. 2013.

[115] Jan Ambjorn, J. Jurkiewicz, and R. Loll. Lorentzian and Euclidean quantum gravity: Analytical and numerical results. 1999.

[116] L. Thorlacius and T. Jonsson. M-Theory and Quantum Geometry. *NATO Science Series C*, pages 415–416.

[117] Sven Bilke and Gudmar Thorleifsson. Simulating four-dimensional simplicial gravity using degenerate triangulations. *Phys.Rev.*, D59:124008, 1999.

[118] S.J. Blundell and K.M. Blundell. Concepts in Thermal Physics. *Oxford University Press*, 2008.

[119] Y. Aoki, G. Endrodi, Z. Fodor, S.D. Katz, and K.K. Szabo. The Order of the quantum chromodynamics transition predicted by the standard model of particle physics. *Nature*, 443:675–678, 2006.

[120] Thordur Jonsson and John F. Wheater. The Spectral dimension of the branched polymer phase of two-dimensional quantum gravity. *Nucl.Phys.*, B515:549–574, 1998.

[121] Jan Ambjorn, Dimitrij Boulatov, Jakob L. Nielsen, Juri Rolf, and Yoshiyuki Watabiki. The Spectral dimension of 2-D quantum gravity. *JHEP*, 9802:010, 1998.

[122] M.E.J. Newman and G.T. Barkema. *Monte Carlo Methods in Statistical Physics*. Oxford University Press, 1999.

[123] J. Ambjorn, S. Jordan, J. Jurkiewicz, and R. Loll. A Second-order phase transition in CDT. *Phys.Rev.Lett.*, 107:211303, 2011.

[124] Gudmar Thorleifsson. Three-dimensional simplicial gravity and degenerate triangulations. *Nucl.Phys.*, B538:278–294, 1999.

[125] S. Warner, S. Catterall, and R. Renken. Phase structure of 3-D dynamical triangulations with a boundary. 1998.

[126] Ray L. Renken, Simon M. Catterall, and John B. Kogut. Phase structure of dynamical triangulation models in three-dimensions. *Nucl.Phys.*, B523:553–568, 1998.

[127] Martin Reuter and Frank Saueressig. Fractal space-times under the microscope: A Renormalization Group view on Monte Carlo data. *JHEP*, 1112:012, 2011.

[128] Steven Carlip. Spontaneous Dimensional Reduction in Short-Distance Quantum Gravity? 2009.

[129] Bergfinnur Durhuus, Thordur Jonsson, and John F. Wheater. Random walks on combs. *J.Phys.*, A39:1009–1038, 2006.

[130] Bergfinnur Durhuus, Thordur Jonsson, and John F. Wheater. On the spectral dimension of causal triangulations. 2009.

[131] Georgios Giasemidis, John F. Wheater, and Stefan Zohren. Dynamical dimensional reduction in toy models of 4D causal quantum gravity. *Phys.Rev.*, D86:081503, 2012.

[132] Georgios Giasemidis, John F. Wheater, and Stefan Zohren. Aspects of dynamical dimensional reduction in multigraph ensembles of CDT. *J.Phys.Conf.Ser.*, 410:012154, 2013.

[133] Daniel F. Litim, Roberto Percacci, and Leslaw Rachwal. Scale-dependent Planck mass and Higgs VEV from holography and functional renormalization. *Phys.Lett.*, B710:472–477, 2012.

[134] S. Carlip and D. Grumiller. Lower bound on the spectral dimension near a black hole. *Phys.Rev.*, D84:084029, 2011.

[135] L.D. Faddeev and V.N. Popov. Feynman Diagrams for the Yang-Mills Field. *Phys.Lett.*, B25:29–30, 1967.

[136] L.D. Faddeev. Feynman integral for singular Lagrangians. *Theor.Math.Phys.*, 1:1–13, 1969.

[137] Eric Myers. The Unbounded action and the density of states in nonperturbative quantum gravity. *Class.Quant.Grav.*, 9:405–412, 1992.

[138] Stephen Hawking. General Relativity, an Einstein Centenary Survey. pages 746–789, 1979.

[139] H. Hamber. *Quantum Gravitation: The Feynman Path Integral Approach*. Springer-Verlag, Berlin, 2009.

[140] D.R. Brill and Stanley Deser. Variational methods and positive energy in general relativity. *Annals Phys.*, 50:548–570, 1968.

[141] Robert P. Geroch. Structure of the gravitational field at spatial infinity. *J.Math.Phys.*, 13:956–968, 1972.

[142] G.W. Gibbons and S.W. Hawking. Cosmological Event Horizons, Thermodynamics, and Particle Creation. *Phys.Rev.*, D15:2738–2751, 1977.

[143] G.W. Gibbons, S.W. Hawking, and M.J. Perry. Path Integrals and the Indefiniteness of the Gravitational Action. *Nucl.Phys.*, B138:141, 1978.

[144] Pawel O. Mazur and Emil Mottola. The Gravitational Measure, Solution of the Conformal Factor Problem and Stability of the Ground State of Quantum Gravity. *Nucl.Phys.*, B341:187–212, 1990.

[145] A. Dasgupta and R. Loll. A Proper time cure for the conformal sickness in quantum gravity. *Nucl.Phys.*, B606:357–379, 2001.